E.3.6 Downstream Debris Sampling

Three sampling ports are installed in the flume recirculation flow loop downstream of the pressure taps used to measure strainer head loss. Each port is connected to a valve in a three-valve array. Two pumps (main sampling pump and a back-up pump) are calibrated to a desired flow such that the flow velocity in the three ports is representative of the velocity in the recirculation flow loop. Samples are drawn during debris testing as required by procedure. Samples are collected at a location downstream of the test strainer and miniflow line tap and upstream of the main recirculation pump. Therefore, the debris load collected in the bypass samples is representative of the test fluid that would bypass the strainer and enter the ECCS. Prior to drawing a sample, the sampling lines are flushed to remove any residual debris from the previous sample.

E.3.7 Water Management

The water management system functions to control and maintain a prototypical test water level by adding and removing water from the test flume. The flume water volume increases as the wetted debris is added to the flume. To maintain the prototypical strainer submergence, an overflow weir is built into the rear wall of the test flume. The overflow weir captures the debris laden water mix and filters out the debris with 10 micron bag filters located behind the rear wall of the flume. The debris captured by the bag filters is periodically flushed and the captured debris is added back into the test flume. Figure E.3-11 depicts the overflow weir and Figure E.3-12 depicts the micron bag filters.

Figure E.3-11 Overflow Weir

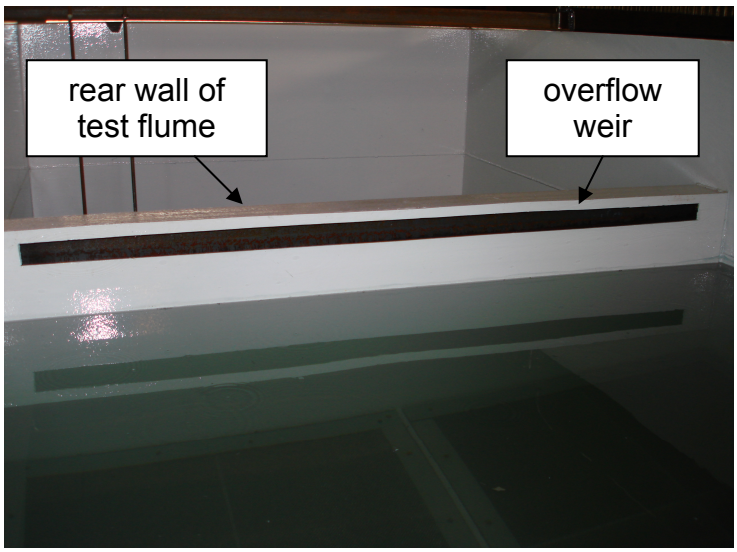

Figure E.3-12 10 Micron Bag Filters

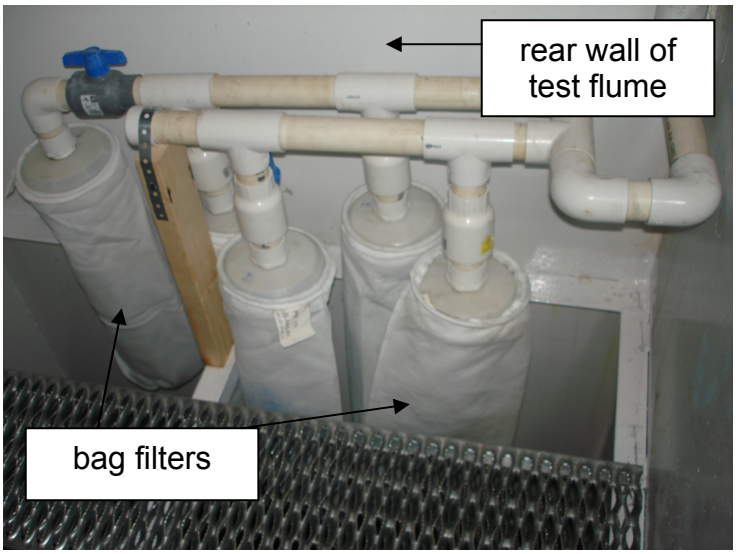

The water addition system utilizes a make-up water tank to add water to the test flume as necessary. As the debris bed forms and clogs the retaining basket, the water level in the basket area increases above the water level surrounding the strainer. The water volume increase in the retaining basket area decreases the available volume of water

around the strainer. As the water volume in the strainer area begins to decrease below the prototypical level, a make-up water pump adds water in front of the retaining basket to restore the normal prototypical water level surrounding the strainer. The make-up pump is controlled by float switches that monitor changes in the flume water level.

E.3.8 Strainer Scaling Methodology

The test strainer is prototypical of the U.S. EPR design. The strainer configuration used for Phase 1 and Phase 2 testing is the same. Table E.3-1 and Table E.3-2 provide the strainer scaling summary for Phase 1 and Phase 2 testing, respectively.

The basic geometry of the ECCS strainer is preserved for testing. Figure E.3-13 shows the strainer drawing with the outline of the modeled portion. Dimensions B and C are unchanged from the plant configuration. A small 0.75 ft portion on the bottom of the strainer is comprised of skirt and support feet. This portion is not considered an active screen area and is not included in the test strainer design. To maintain proper water submergence above the strainer, the modeled IRWST water level in the test flume is reduced from 10 ft to 9.25 ft. Dimension A is based on conservatively modeling the sump exit location with respect to the strainer faces.

Figure E.3-13 Modeled Portion of Strainer

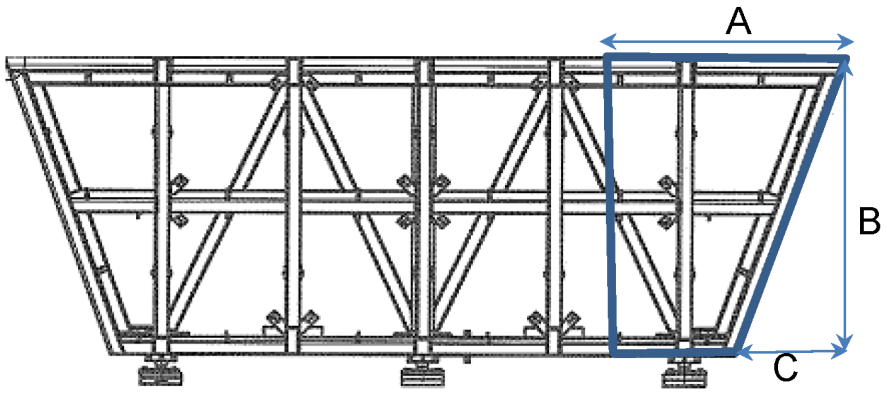

Figure E.3-14 shows the layout of the strainer supports with respect to the strainer sump cover. To conservatively represent the flow within the strainer, the test facility

represents the strainer face with the minimum clearance from the sump to the face of the strainer. Dimension A is therefore determined by matching the distance from the strainer face directly to the leading edge of the sump cover. The sump cover size is scaled by flow area to the flow rate of the test flume.

Figure E.3-14 Strainer Support and Sump Cover (overhead view)

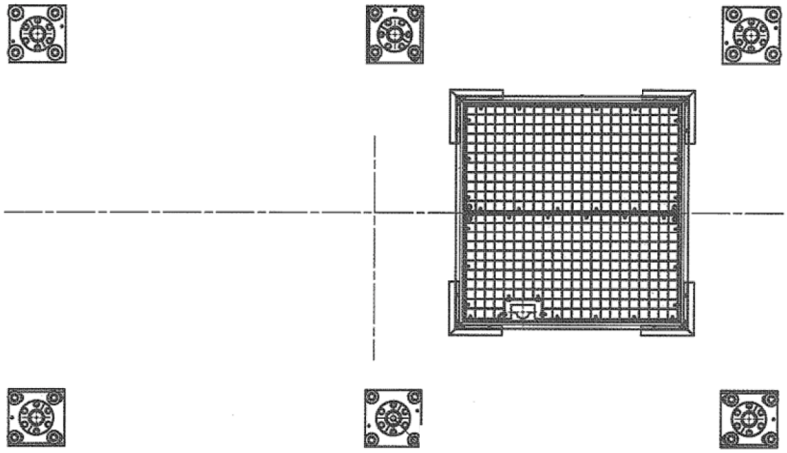

E.3.9 Retaining Basket Scaling Methodology

Two different retaining basket models were used for ECCS strainer performance testing. Phase 1 testing uses a retaining basket modeled in accordance with the scaling summary of Table E.3-1. Phase 2 testing uses a retaining basket modeled in accordance with the scaling summary of Table E.3-2.

Retaining Basket Scaling Methodology - Phase 1 Testing

The U.S. EPR design utilizes four retaining baskets consisting of two single compartment retaining baskets and two double compartment retaining baskets. A scaled single compartment basket was used for Phase 1 testing. For the retaining basket, a reference flow per unit area of wetted screen was determined. The flow per

unit area of screen is determined using the minimum wetted surface area of the single compartment retention basket. The flow rate scale factor of approximately 9.37% was applied to the postulated conservative flow scenario of 100% of the break flow entering a single retaining basket. The flow rate together with the flow per unit wetted screen area determines the retaining basket modeled screen area. Conservatively, the retaining basket is modeled to only be open on the side of the facility that is facing the strainer. Arranging the test facility in this manner allows debris to travel freely from the retention basket to the strainer. The test basket frontal area mesh consists of 0.083" (2.1mm) openings, which is consistent with the U.S. EPR single and double compartment basket design. Both the retaining basket and the strainer are elevated in the plant. In the test flume these heights are not considered. This results in a conservative scenario of debris transport to the active strainer and retaining basket filtering surfaces. For the retaining basket, a low velocity area under the basket floor is not represented resulting in less debris settling. For the strainer, lowering the strainer face to the floor exposes the strainer to more floor transported tumbling debris.

The test facility retaining basket volume scaled by approximately 9.4%, matching the conservative plant flow per unit volume described above. Dividing the scaled retaining basket volume by the screened retaining basket area yields the test flume retaining basket depth.

Retaining Basket Scaling Methodology – Phase 2 Testing

The U.S. EPR utilizes two retaining basket designs in the IRWST. These designs consist of the single and double compartment retaining basket arrangements. The scaled large compartment of the double compartment retaining basket was used for Phase 2 testing. The double compartment retaining basket is separated into a large and small compartment. The small compartment basket is designed to capture any debris laden water that may enter the IRWST from the annular area of containment. The large compartment basket receives flow from the heavy floor opening. The screened area of the large compartment of the double compartment retaining basket

contains less screened surface area than the single compartment retaining basket. Therefore, it is conservative to model the large compartment of the double compartment basket in the test apparatus. The portions of screened area that are scaled for the test apparatus include the large compartment's left, right, front, and bottom surfaces. For conservatism, the area between the large and small compartment of the double compartment basket is not modeled.

Table E.3-3, Retaining Basket (RB) Scaling Summary and Modeled Parameters provides the retaining basket scaling summary and modeled parameters for the large compartment of the double compartment retaining basket. The scaled volume ensures that the retaining basket receives a prototypical flow per unit volume. The double compartment retaining basket is positioned on pedestals 0.66 feet above the IRWST floor. The bottom surface area of the basket is covered with a meshed screen of the same perforation size as the remainder of the basket. Consistent with the retaining basket design, the test basket is raised above the test floor with the bottom area screened and scaled approximately 9.37%. Subtracting the scaled bottom portion of the retaining basket from the scaled total surface area of the retaining basket provides the scaled vertical portion of the test basket. Based on the test apparatus maintaining 1:1 vertical scale, the test basket is designed and constructed to reach 16.57 feet above the test apparatus floor which is consistent with the plant design. The test basket width is determined by dividing the 'scaled vertical surface area' by the 'RB screened vertical height' in the test apparatus (excluding the pedestal height). The test apparatus retaining basket length (screened basket front face to back wall) is determined by dividing the 'scaled RB volume' by the 'RB screened height' and the 'test apparatus RB width'.

Table E.3-3 Retaining Basket (RB) Scaling Summary and Modeled Parameters

Description	Value[2]	Unit
Scale	9.37	%
Total RB Surface Area	642.00	ft^2
Scaled Total RB Surface Area	60.17	ft^2
RB Floor Surface Area	120.38	ft^2
Scaled RB Floor Surface Area	11.28	ft^2
Plant Vertical RB Surface Area	521.62	ft^2
Test Apparatus Vertical Surface Area	48.89	ft^2
RB Vertical Height	16.57	ft
RB Pedestal Height	0.66	ft
RB Screened Vertical Height	15.91	ft
Test Apparatus RB Width	3.07	ft
Plant RB Volume	2024.00	ft^3
Scaled RB Volume	189.71	ft^3
Test Apparatus RB Length[1]	3.88	ft

Note[1]: A retaining basket length of 3.7 feet is used instead of 3.88 feet. This length creates the correct scaling for the surface area of the retaining basket bottom.

Note[2]: Only surface areas and volumes are scaled.

E.3.10 Flume Vertical Flow Water Management

The majority of the water flow downstream of the strainer was re-introduced to the test flume with a nozzle delivery system. This was accomplished to represent the LOCA return flow onto the heavy floor and into one of four retaining baskets through the heavy floor openings. The plant design provides approximately 15.3 feet of water free-fall before the water reaches the surface of the IRWST pool. The test flume represents an adjusted 1:1 vertical scale of the U.S. EPR IRWST design. To conserve the vertical scale in the test facility, the momentum produced by the water free-fall must be preserved. The test facility ceiling limits the free-fall of water to approximately 8 feet.

Therefore, the velocity of the water exiting the nozzles above the flume pool is increased to represent the plant's actual water free-fall conditions.

E.4 Debris Description

Debris types for strainer performance testing consist of non-chemical and chemical debris. The non-chemical debris types and amounts are based on the Debris Generation Evaluation for the U.S. EPR (Appendix C). The chemical debris types and amounts are based on the Chemical Effects Evaluation for the U.S EPR (Appendix D). The following sections discuss the debris types used for testing. Specific debris types, quantities, and surrogate materials used in testing are documented in the debris allocation tables in Section E.5.

E.4.1 Reflective Metallic Insulation (RMI)

During the Debris Transport Test conducted in December 2009, RMI debris pieces of 2 mil thickness and various sizes from 0.25 inch x 0.25 inch up to 4 inch x 4 inch were shown to sink and settle on the bottom of the retaining basket. Due to the non-transport characteristics of RMI under design flow conditions, RMI was not included in subsequent tests. Removing RMI from subsequent tests also prevents the possibility of RMI debris trapping fibrous debris in the retaining basket, thus resulting in less conservative test conditions. Figure E.4-1 depicts typical RMI test debris.

Figure E.4-1 RMI Test Debris

E.4.2 Coatings

For the U.S EPR containment strainer testing, coatings are categorized into two debris types:

- coating chips
- coatings as particulate

During the debris transport test performed in December 2009, a small amount of coating chips were introduced to the test apparatus. The majority of chips, when viewed with an underwater camera, appeared to cover the top 12 inches of submerged retaining basket screen where a higher velocity flow towards the strainer appeared to exist. Chips that were not caught in the initial current near the water surface appeared to sink to the floor of the retaining basket. Due to these observations, it was determined that the qualified epoxy coatings would be tested in both particulate and chip form for conservatism. This conservatively increased the total epoxy coating source term by 34%. The qualified epoxy coatings are represented as “acylic powder or walnut shell powder.” This amount

of particulate coating was weighed and added to the flume. The same amount of coating chips were weighed and added to the flume.

For coatings acting as particulate debris, acrylic powder was used as a surrogate material for epoxy coatings and tin powder was used as a surrogate material for inorganic zinc coatings. The acrylic powder has an average density of approximately 77.4 lb_m/ft^3. The acrylic coatings have a similar density, size and shape characteristics to plant containment coatings and are a suitable surrogate material. The tin powder has a particle density of 445.3 lb_m/ft^3 as compared to 457 lb_m/ft^3 for inorganic zinc. Since inorganic zinc is considered a hazardous material, tin powder was used as the surrogate material. Figure E.4-2 depicts examples of coating chips used for testing. Figure E.4-3 and Figure E.4-4 depict examples of the acrylic powder and tin powder used in testing, respectively.

Figure E.4-2 Coating Chips

Figure E.4-3 Acrylic Powder

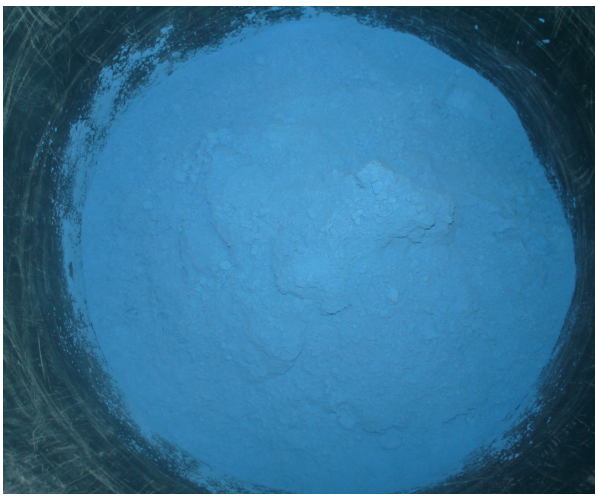

Figure E.4-4 Tin Powder

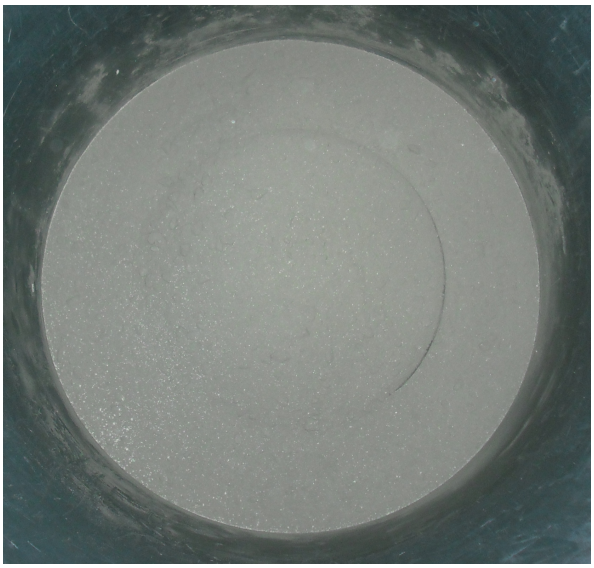

E.4.3 Fiber

Fiber material used for testing is NUKON fiber. NUKON fiber was tested as fines and shredded into fines using a debris shredder. Figure E.4-5 depicts an example of the NUKON fines fiber used for testing.

Figure E.4-5 NUKON Fines Fiber

E.4.4 Particulate

The particulate debris used for testing is comprised of:

- latent dirt and dust mix (prepared by Performance Contracting Incorporated)
- coatings (particulate)
- microtherm

Figure E.4-6 depicts a sample of the latent dirt and dust mix. Figure E.4-7 depicts a sample of microtherm.

Figure E.4-6 Latent Dirt and Dust Mix

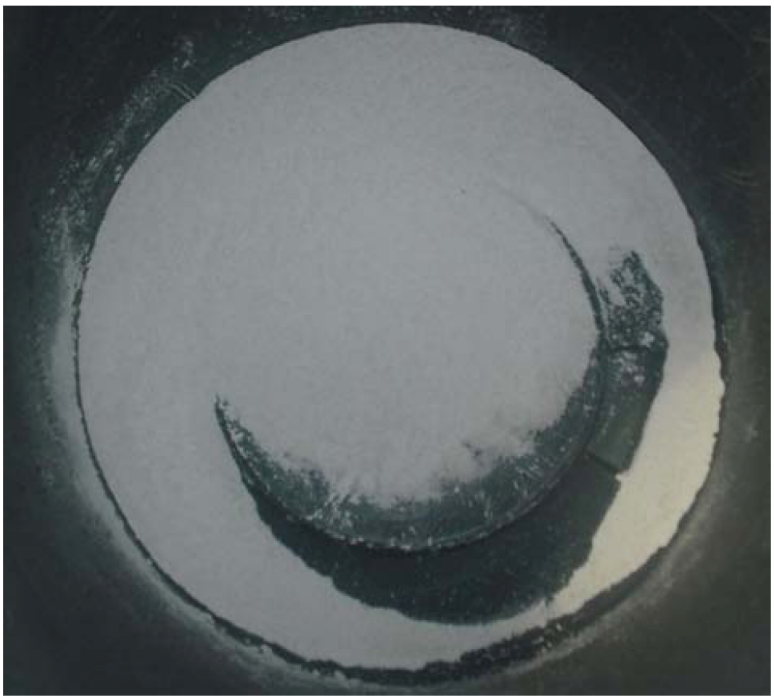

Figure E.4-7 Microtherm

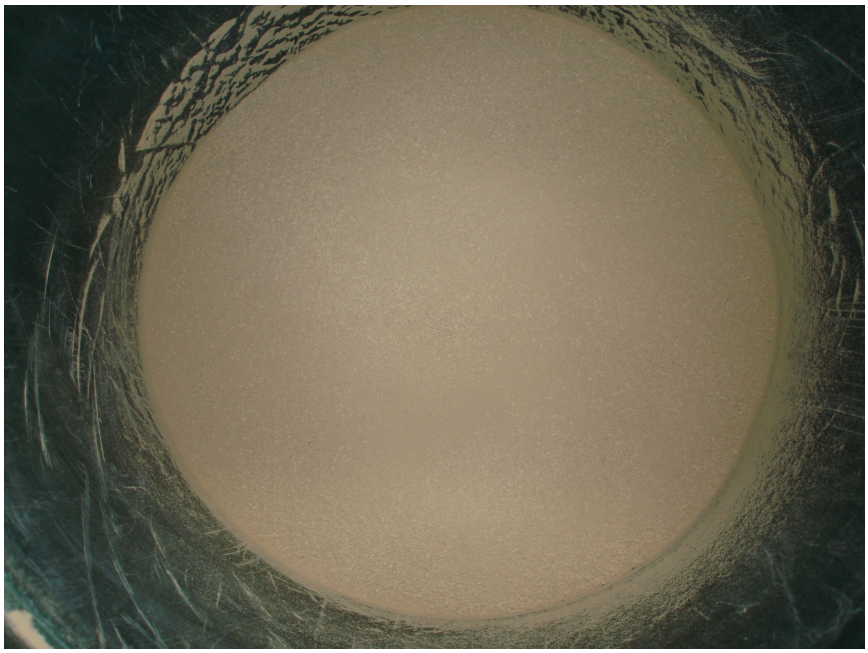

E.4.5 Miscellaneous Debris

During the Debris Transport Test conducted in December 2009, miscellaneous debris materials were added to the flume to document how these items responded to the test flow conditions. The miscellaneous debris consists of various debris items expected to be found in containment. The specific miscellaneous debris used for testing is listed in Section E.5.

E.4.6 Chemical Debris

The predicted chemical precipitates generated after a postulated LOCA in the U.S. EPR containment are calcium phosphate ($Ca_3(PO_4)_2$) and sodium aluminum silicate ($NaAlSi_3O_8$). Since $NaAlSi_3O_8$ is considered hazardous, aluminum oxyhydroxide (ALOOH) is used as a surrogate. Because the characteristics of $NaAlSi_3O_8$ are similar to AlOOH, ALOOH is used for testing in lieu of $NaAlSi_3O_8$.

E.5 Debris Quantities and Introduction Sequence

E.5.1 Phase 1 Testing - Debris Transport Test No. 1

For the Debris Transport Test, debris was manually added to the fume flow above the retaining basket. Table E.5-1 provides the debris allocation and flume flow rate for the Debris Transport Test. The following is the list of debris and approximate sizes introduced into the flume during the Debris Transport Test.

- leather work glove
- plastic glove
- caution tag (6 inch x 3 inch plastic material)
- caution label (yellow ribbon 2.5 feet in length)
- white cloth (1 foot x 1.5 feet)
- 2 plastic tie wraps (1 foot and 2 feet long)
- ¾ inch nylon rope (2 feet long)

- plastic chain link (1.5 feet long)
- plastic bag (1foot x 2 feet)
- ear plugs (1 set connected with an elastic string)
- ear plugs (1 set in a plastic bag)
- ¼ inch x ¼ inch RMI
- ½ inch x ½ inch RMI
- 4 inch x 4 inch RMI
- coating chips (5/8 inches and smaller)

Table E.5-1 Debris Allocation and Flume Flow Rate for the Debris Transport Test

Scaling Factor 9.37%			Wt Conversions	Debris Scaled		
Debris Type	**U/M**	**Quantity**	**(lbs / ft^3 or ft^2)**	**(lbm)**	**Units**	**Debris Form / (Surrogate)**
Fibers (Design Basis)						
NUKON (Small Fines)	ft^3	n/a	2.4	n/a	lbm	Shredded Fiber (Binder Burned Out)
Latent Fibers	lbm	n/a	n/a	n/a	lbm	Shredded Fiber
			Total Fibrous Debris	**0.0**		
RMI						
Total RMI	ft^2	2098.87				
RMI (1/4" x 1/4")	ft^2	111.24	0.0813	0.85	lbm	
RMI (1/2" x 1/2")	ft^2	444.96	0.0813	3.39	lbm	
RMI (1" & 2")	ft^2	1017.95	0.0813	7.76	lbm	
RMI Larges (4" and 6") (Limited to 25% RMI total)	ft^2	524.72	0.0813	4.00	lbm	
			Total RMI Debris	**15.99**		
Particulates						
Latent Particulate; Dirt & Dust	lbm	n/a	n/a	n/a	lbm	PCI PWR Dirt Mix (85% of Latent Debris)
Microtherm	ft^3	n/a	15.0	n/a	lbm	Microtherm® Free Flow
Coatings (lbs)						
Qualified Coatings	lbm	459.82	94	43.10	lbm	Acrylic Paint Chips (5/8" and smaller)
Qualified Coatings	lbm	n/a	457	n/a	lbm	IOZ Powder (Tin Powder)
Unqualified Coatings	lbm	n/a	94	n/a	lbm	Acrylic Powder or Walnut Shell Powder
			Total Particulate Debris	**43.10**		
Chemical Debris Concentrations						
Sodium Aluminum Silicate (Unknown)	lbm	n/a	n/a	n/a	lbm	Chemical Surrogate - AlOOH
Calcium Phosphate (Unknown)	lbm	n/a	n/a	n/a	lbm	Chemical Surrogate - $Ca_3(PO_4)_2$
Aluminum Oxyhydroxide (Unknown)	lbm	n/a	n/a	n/a	lbm	Chemical Surrogate - AlOOH
			Total Surrogate Debris	**0.0**	lbm	
Miscellaneous Debris						
Labels, Stickers, Tape, Placards, Tags	ft^2	100.00	n/a	note 1	ft^2	Miscellaneous Debris

Flume Water Level	ft	9.25	
Scaling Factor	%	9.37%	
Target Flume Flow	gpm	307.81	

note 1: scaled miscellaneous debris is provided as a combination of various debris items

E.5.2 Phase 2 Testing - Clean Strainer Head Loss Test No. 1

For the Clean Strainer Head Loss Test, no debris was added into the test flume. Table E.5-2 lists the five (5) flume flow rates for the Clean Strainer Head Loss Test.

Table E.5-2 Flume Flow Rates for the Clean Strainer Head Loss Test

Scaling Factor 9.37%			Wt Conversions	Debris Scaled		
Debris Type	U/M	Quantity	(lbs / ft^3 or ft^2)[4]	(lbm)	Units	Debris Form / (Surrogate)
Fibers (Design Basis)						
NUKON (Small Fines)	ft^3	n/a	2.4	n/a	lbm	Shredded Fiber (Binder Burned Out)
Latent Fibers	lbm	n/a	n/a	n/a	lbm	Shredded Fiber (Binder Burned Out)
			Total Fibrous Debris	0.0		
RMI						
Total RMI	ft^2	n/a				
RMI (1/4" x 1/4")	ft^2	n/a	0.0813	n/a	lbm	
RMI (1/2" x 1/2")	ft^2	n/a	0.0813	n/a	lbm	
RMI (1" & 2")	ft^2	n/a	0.0813	n/a	lbm	
RMI Larges (4" and 6") (Limited to 25% RMI total)	ft^2	n/a	0.0813	n/a	lbm	
			Total RMI Debris	0.0		
Particulates						
Latent Particulate; Dirt & Dust	lbm	n/a	n/a	n/a	lbm	PCI PWR Dirt Mix (85% of Latent Debris)
Microtherm	ft^3	n/a	15.0	n/a	lbm	Microtherm® Free Flow
Coatings (lbs)						
Qualified Coatings	lbm	n/a	94	n/a	lbm	Acrylic Chips (5/8" and smaller)
Qualified Coatings	lbm	n/a	457	n/a	lbm	IOZ Powder (Tin Powder)
Unqualified Coatings	lbm	n/a	94	n/a	lbm	Acrylic Powder or Walnut Shell Powder
			Total Particulate Debris	0.0		
Chemical Debris Concentrations						
Sodium Aluminum Silicate	lbm	n/a	n/a	n/a	lbm	Chemical Surrogate - AlOOH
Calcium Phosphate	lbm	n/a	n/a	n/a	lbm	Chemical Surrogate - $Ca_3(PO_4)_2$
Aluminum Oxyhydroxide	lbm	n/a	n/a	n/a	lbm	Chemical Surrogate - AlOOH
			Total Surrogate Debris	0.0	lbm	
Miscellaneous Debris						
Labels, Stickers, Tape, Placards, Tags	ft^2	n/a	n/a	n/a	ft^2	Miscellaneous Debris

Flume Water Level	ft	9.25	
Scaling Factor	%	9.37%	
25% Below Target Flow	gpm	230.85	
12.5% Below Target Flow	gpm	269.33	
Target Flume Flow	gpm	307.81	
12.5% Above Target Flow	gpm	346.28	
25% Above Target Flow	gpm	384.76	

E.5.3 Phase 2 Testing - Design Basis Debris Loaded Strainer Head Loss Test No. 2

For the Design Basis Debris Loaded Strainer Head Loss Test, debris introduction started by first adding the particulate debris to the flume. The particulate debris

introduction sequence was based on the most transportable particulate added first, followed by the next most transportable debris. Particulate debris was added into the flume via the debris introduction locations shown in Figure E.3-8 and Figure E.3-10. Table E.5-3 and Table E.5-4 provide the debris allocation and flume flow rate for Test No. 2. The sequence for debris introduction and amounts is as follows:

Fine Particulate Debris

Batch 1: 100% of Microtherm (1.55 lb_m)

Batch 2: 100% of acrylic powder particulate debris (35.40 lb_m)

Batch 3: 105.5% of dirt & dust (21.10 lb_m)

Batch 4: 100% of tin powder particulate debris (90.00 lb_m)

Note: An additional 5% of dirt and dust was added to the test flume to account for any particulate debris lost in transit.

Fine Fibrous Debris

Batch 5: approximately 10% of the total fine NUKON fibers (0.5 lb_m)

Batch 6: approximately 90% of the total fine NUKON fibers (4.60 lb_m)

Note: Batch 5 was added to the test flume directly between the retaining basket and strainer. Batch 6 debris introductions consisted of approximately 0.5 lb_m of fibrous debris per 33 gallon container to prevent fibrous debris agglomeration.

Coating Chips Debris

Batch 7: 100% of the qualified epoxy coatings – chips (12.00 lb_m)

Note: Based on the results of a debris transport test conducted in December 2009 it was observed that coating chips attached to the retaining basket screen near the surface of the flume. For conservatism, the qualified coatings debris source term was added to the flume in both particulate and chips form, essentially doubling that debris source term.

Chemical Precipitate Debris

Aluminum oxyhydroxide (AlOOH) and calcium phosphate (Ca3(PO4)2) were introduced to the flume over a 13 hour period. The first three batches of ALOOH were added to the flume in approximately 5.8 gallon amounts. The first three batches of Ca3(PO4)2 were added to the flume in approximately 13.4 gallon amounts. After the first three batches of each chemical precipitant were added to the flume, the flume reached its prototypical chemical concentration. After the first three batches, the ALOOH and Ca3(PO4)2 were added to the flume in approximately 4.4 and 10.2 gallon amounts, respectively, until 100% of the scaled quantity by mass of chemical was introduced into the test flume. The purpose of the chemical batching was to prevent the flume from becoming overly concentrated with chemical debris and possibly causing the chemical to settle quicker to the flume floor. Refer to Table E.5-4 for the chemical batching volumes.

The chemical addition was comprised of approximately 40 total batches of each chemical precipitate until 100% of the chemical debris source term was introduced to the flume. The batching process comprised of one ALOOH batch introduction followed by one Ca3(PO4)2 batch introduction, with a five minute interval in between the two precipitates. One flume turnover (14 minutes) was allotted before the next batch of AlOOH was introduced to the test flume.

The following observations were made during the Design Basis Debris Loaded Strainer Head Loss Test:

- Visual observation of the strainer area at various times during the design basis test showed no signs of vortexing around the strainer.

- With a fiber bed restricting flow on the wetted retaining basket, the coating chips were propelled directly to the open retaining basket screen. The chips quickly created a bed on the retaining basket as the water level increased leading to basket overflow.
- During the initial basket overflow, some coating chips flowed into the strainer area. The strainer head loss did not change from this occurrence.
- The retaining basket successfully retained debris and prevented any change in strainer head loss.
- Following the testing, drain down of the test apparatus revealed little debris at the strainer.

Table E.5-3 Debris Allocation and Flume Flow Rate for the Design Basis Debris Loaded Strainer Head Loss Test

Scaling Factor 9.37%			Wt Conversions	Debris Scaled		
Debris Type	U/M	Quantity	(lbs / ft^3 or ft^2)	(lbm)	Units	Debris Form / (Surrogate)
Fibers (Design Basis)						
NUKON (Small Fines)	ft^3	6.62	2.4	1.49	lbm	Shredded Fiber (Binder Burned Out)
Latent Fibers	lbm	37.50	n/a	3.51	lbm	Shredded Fiber (Binder Burned Out)
			Total Fibrous Debris	5.00		
RMI						
Total RMI	ft^2	2098.87				
RMI (1/4" x 1/4")	ft^2	111.24	0.0813	0.85	lbm	
RMI (1/2" x 1/2")	ft^2	444.96	0.0813	3.39	lbm	
RMI (1" & 2")	ft^2	1017.95	0.0813	7.76	lbm	
RMI Larges (4" and 6") (Limited to 25% RMI total)	ft^2	524.72	0.0813	4.00	lbm	
			Total RMI Debris	15.99		
Particulates						
Latent Particulate; Dirt & Dust	lbm	212.50	n/a	19.92	lbm	PCI PWR Dirt Mix (85% of Latent Debris)
Microtherm	ft^3	1.00	15.0	1.41	lbm	Microtherm® Free Flow
Coatings (lbs)						
Qualified Coatings	lbm	126.50	94	11.86	lbm	Acrylic Powder or Walnut Shell Powder
Qualified Coatings	lbm	958.70	457	89.86	lbm	IOZ Powder (Tin Powder)
Unqualified Coatings	lbm	250.00	94	23.43	lbm	Acrylic Powder or Walnut Shell Powder
			Total Particulate Debris	146.47		
Chemical Debris Concentrations						
Sodium Aluminum Silicate	kg	77.0	(2.2 lbs/kg)	15.91	lbm	Chemical Surrogate - AlOOH
Calcium Phosphate	kg	81.0	(2.2 lbs/kg)	16.74	lbm	Chemical Surrogate - $Ca_3(PO_4)_2$
Aluminum Oxyhydroxide	kg	0.00	(2.2 lbs/kg)	0.00	lbm	Chemical Surrogate - AlOOH
			Total Surrogate Debris	32.65	lbm	
Miscellaneous Debris						
Labels, Stickers, Tape, Placards, Tags	ft^2	100.00	n/a	n/a	ft^2	Miscellaneous Debris

Flume Water Level	ft	9.25
Scaling Factor	%	9.37%
Target Flume Flow	gpm	307.81

Table E.5-4 Chemical Debris Additions and Flume Flow Rate for the Design Basis Debris Loaded Strainer Head Loss Test

Pump Flow Rate During Chem. Batching	Pump Flow (gpm)	Pump Flow (ft^3 / sec)	Flume Depth (ft)	Flume Volume (cu ft @ 9.25')	Pipe Volume (cu ft)	Total Volume (cu ft)	Total Volume (gal)	Flume Flow (cfs)	One flume cycle (sec)	1 Flume Turn Over FTO (min)	2 Flume Turn Over FTO (min)
	307.81	0.686	9.25	519.39	31.60	550.99	4,121.70	0.686	803.44	14.0	28.0

Chemical Debris Concentrations	U/M	Quantity	(lbs / ft^3 or ft^3)	Scaled Quantity	Qty w/ Bump Ups	U/M
Chemical Bump Up Added for Soluability	%	1.0%		9.37%		
Chemical Bump Up to Eliminate Bag Filters	%	1.4%				
Sodium Aluminum Silicate	max lbm	169.75		15.91	16.30	lbm
Aluminum Oxyhydroxide	max lbm	0.00		0.00	0.00	lbm
Calcium Phosphate	max lbm	178.60		16.74	17.15	lbm
			Total Surrogate Debris	32.65	33.45	lbm

	Plant Calculated lbm	Scaled Test lbm	Chemicals	Plant Conc	Flume Conc	U/M	lbs = Plant Conc	lbs / batch to start; 1 PTO in between	lbs / batch thereafter; 1 PTO in between	Est No. of PTO's Req'd	EST Minutes to Introduce Chemicals
Aluminum Oxyhydroxide	169.75	16.30	ALOOH	0.000392	0.003955	lbs/gal	1.61	0.5329	0.4037	39.40	552
Calcium Phosphate	178.60	17.15	Cal Phos	0.000412	0.004161	lbs/gal	1.70	0.5607	0.4248	39.40	197
Totals	348.35	33.45	Totals	0.000804	0.008116	lbs/gal	3.31	1.0936	0.8285	39.40	749
				433,242	4,121.7	gal		Batch Sizes			
				57,916	551.0	ft^3		33.00%	25.00%		12.48

Conversion of "grams / liter" to "lbs / gallon"				
	1 gram	=	0.0022	lbs
	1 liter	=	0.26417	gallons
	1 g / l	=	0.00835	lbs / gallon
	11 g / l	=	0.0918	lbs / gallon
	5 g / l	=	0.04173	lbs / gallon

Batch Volumes				
33% Batches @	0.53 lbm	=	5.81	gal of ALOOH mix
25% Batches @	0.40 lbm	=	4.40	gal of ALOOH mix
33% Batches @	0.56 lbm	=	13.44	gal of Cal Phosphate mix
25% Batches @	0.42 lbm	=	10.18	gal of Cal Phosphate mix

E.5.4 Phase 2 Testing - Fibrous Debris Only Sample Bypass Test No. 3 and 3A

For Test No. 3, the fiber was introduced to the flume in two batches. The first batch consisted of the mass of fiber that could potentially create a thin bed on the retaining basket and strainer surface. This first batch amount is 3.3 lb_m. The second batch consisted of the remaining fibrous debris. Two flume turnovers totaling 28 minutes were allotted between fiber batch introductions. The first 0.5 lb_m of batch 1 was introduced between retaining basket and the front of the strainer. All other batches were added to the flume via the debris introduction tank and debris pump. Strainer head loss was negligible throughout the entire test. Table E.5-5 provides the debris allocation and flume flow rate for Test No. 3 and 3A. The sequence for debris introduction and amounts is as follows:

Fibrous Debris

Batch 1: (3.4 lb_m for Test No. 3 and 3.3 lb_m for Test No. 3A).

Batch 2: Fine NUKON fibers (1.7 lb_m for Test No. 3 and 1.8 lb_m for Test No. 3A).

After Test No. 3 was complete, the water in the test flume was slowly drained. A visual inspection of the strainer showed no fibrous debris on the strainer screen.

Test No. 3A was performed using the same procedure and debris amounts used for Test No. 3. Strainer head loss was negligible throughout Test No. 3A and visual observations after the test showed the strainer was free of debris.

Table E.5-5 Debris Allocation and Flume Flow Rate for the Fibrous Debris Only Sample Bypass Test

Scaling Factor 9.37%			Wt Conversions	Debris Scaled		
Debris Type	U/M	Quantity	(lbs / ft^3 or ft^2)	(lbm)	Units	Debris Form / (Surrogate)
Fibers (Design Basis)						
NUKON (Small Fines)	ft^3	6.62	2.4	1.49	lbm	Shredded Fiber (Binder Burned Out)
Latent Fibers	lbm	37.50	n/a	3.51	lbm	Shredded Fiber (Binder Burned Out)
			Total Fibrous Debris	5.00		
RMI						
Total RMI	ft^2	2098.87				
RMI (1/4" x 1/4")	ft^2	111.24	0.0813	n/a	lbm	
RMI (1/2" x 1/2")	ft^2	444.96	0.0813	n/a	lbm	
RMI (1" & 2")	ft^2	1017.95	0.0813	n/a	lbm	
RMI Larges (4" and 6") (Limited to 25% RMI total)	ft^2	524.72	0.0813	n/a	lbm	
			Total RMI Debris	0.0		
Particulates						
Latent Particulate; Dirt & Dust	lbm	n/a	n/a	n/a	lbm	PCI PWR Dirt Mix (85% of Latent Debris)
Microtherm	ft^3	n/a	15.0	n/a	lbm	Microtherm® Free Flow
Coatings (lbs)						
Qualified Coatings	lbm	n/a	94	n/a	lbm	Acrylic Powder or Walnut Shell Powder
Qualified Coatings	lbm	n/a	457	n/a	lbm	IOZ Powder (Tin Powder)
Unqualified Coatings	lbm	n/a	94	n/a	lbm	Acrylic Powder or Walnut Shell Powder
			Total Particulate Debris	0.0		
Chemical Debris Concentrations						
Sodium Aluminum Silicate	lbm	n/a	n/a	n/a	lbm	Chemical Surrogate - AlOOH
Calcium Phosphate	lbm	n/a	n/a	n/a	lbm	Chemical Surrogate - $Ca_3(PO_4)_2$
Aluminum Oxyhydroxide	lbm	n/a	n/a	n/a	lbm	Chemical Surrogate - AlOOH
			Total Surrogate Debris	0.0	lbm	
Miscellaneous Debris						
Labels, Stickers, Tape, Placards, Tags	ft^2	100.00	n/a	n/a	ft^2	Miscellaneous Debris

Flume Water Level	ft	9.25
Scaling Factor	%	9.37%
Target Flume Flow	gpm	307.81
Strainer and Basket Surface Area	ft^2	130.77
Thin Bed Size	ft	0.010
Required Fiber for 1/8" Bed	ft^3	1.36
Required Fiber for 1/8" Bed @ 2.4 lbm/ft^3	lbm	3.27
Total Fibrous Debris	lbm	5.00
Thin Bed Batches	#	1.53

E.5.5 Phase 2 Testing - Debris Loaded Strainer Head Loss Thin Bed Test No. 4

For Test No. 4, the particulate debris introduction sequencing was based on the most transportable particulate added first, followed by the next most transportable debris. The Microtherm and acrylic powder particulate debris was added to the flume with the debris introduction tank and trash pump. The 'dirt and dust' and tin powder were added through the observation window using the debris introduction chute. Next, the first thin bed batch was introduced through the debris introduction tank and trash pump. The first thin bed batch corresponded to the fiber amount that may potentially lead to a thin bed on the strainer and the retaining basket. The second batch of fiber was added to the test flume 1 hour and 2 minutes after the completion of the first batch once the retaining basket measured head loss stabilized. Table E.5-6 and Table E.5-7 provides the debris allocation and flume flowrate for Test No. 4. The sequence for debris introduction and amounts is as follows:

Fine Particulate Debris

Batch 1: 100% of Microtherm (1.55 lb_m)

Batch 2: 100% of acrylic powder particulate debris (35.40 lb_m).

Batch 3: 105.5% of dirt & dust (21.10 lb_m)

Batch 4: 100% of tin powder particulate debris (90.00 lb_m)

Fine Fibrous Debris

Batch 5A: approx. 10% of total fine NUKON fibers (0.5 lb_m)

Batch 5B: approx. 57% of total fine NUKON fibers (2.9 lb_m)

Batch 6: approx. 33% of total fine NUKON fibers (1.7 lb_m)

Note: Batch 5A was added to the test flume between the retaining basket and strainer. Batch 6 debris introductions consisted of approximately 0.5 lb_m of fibrous debris per 33 gallon container to prevent fibrous debris agglomeration.

Coating Chip Debris

Batch 7: 100% of the U.S. EPR Qualified Epoxy Coatings – Chips (12.00 lb_m)

Note: Based on the results of the debris transport test conducted in December 2009, it was observed that coating chips attached to the retaining basket screen near the surface of the flume. For conservatism, the qualified coatings debris source term was added to the flume in both particulate and chips form, essentially doubling that debris source term.

Chemical Precipitate Debris

Aluminum oxyhydroxide (AlOOH) and calcium phosphate (Ca3(PO4)2) were introduced to the test flume over a 9 hour period. The first three batches of ALOOH were added to the flume in approximately 5.8 gallon amounts. The first three batched of Ca3(PO4)2 were added to the flume in approximately 13.4 gallon amounts. After the first three batches of each chemical precipitant were added to the flume, the flume reached its prototypical chemical concentration. After the first three batches, the ALOOH and Ca3(PO4)2 were added to in approximately 4.4 and 10.2 gallon amounts, respectively, until 100% of the scaled quantity by mass of chemical was introduced into the test flume. The purpose of the chemical batching was to prevent the flume from becoming overly concentrated with chemical debris, thus causing the chemical to settle quicker to the flume floor. Refer to Table E.5-7 for the chemical batching volumes.

Approximately 40 total batches of each chemical precipitate were added to the test flume until 100% of the chemical debris source term was introduced to the flume. The batching process comprised of an ALOOH introduction followed by a Ca3(PO4)2

introduction, with a five minute interval in between the two precipitates. One flume turnover (14 minutes) was allotted before the next batch of AlOOH was introduced to the test flume. However, the batching process was expedited after the first 15 total batches. The batch timing changed to 3 minute intervals between chemicals and only ½ flume turnover (7 minutes) between batches.

The following observations were made during Test No. 4:

- Visual observation of the strainer area showed no signs of vortexing around the strainer.
- The fiber bed created by the first batch alone created a greater head loss across the basket. The second fiber batch addition brought the basket to within one foot of overflow.
- The chips rapidly created the overflow condition of the retaining basket. A large quantity of chips overflowed to the strainer area. The strainer head loss remained stable.
- After the test, flume drain down showed little debris on the strainer screen.

Table E.5-6 Debris Allocation and Flume Flow Rate for the Thin Bed Test

Scaling Factor 9.37%			Wt Conversions	Debris Scaled		
Debris Type	U/M	Quantity[2,3]	(lbs / ft^3 or ft^2)	(lbm)	Units	Debris Form / (Surrogate)
Fibers (Design Basis)						
NUKON (Small Fines)	ft^3	6.62	2.4	1.49	lbm	Shredded Fiber (Binder Burned Out)
Latent Fibers	lbm	37.50	n/a	3.51	lbm	Shredded Fiber (Binder Burned Out)
			Total Fibrous Debris	5.00		
RMI						
Total RMI	ft^2	2098.87				
RMI (1/4" x 1/4")	ft^2	111.24	0.0813	0.85	lbm	
RMI (1/2" x 1/2")	ft^2	444.96	0.0813	3.39	lbm	
RMI (1" & 2")	ft^2	1017.95	0.0813	7.76	lbm	
RMI Larges (4" and 6") (Limited to 25% RMI total)	ft^2	524.72	0.0813	4.00	lbm	
			Total RMI Debris	15.99		
Particulates						
Latent Particulate; Dirt & Dust	lbm	212.50	n/a	19.92	lbm	PCI PWR Dirt Mix (85% of Latent Debris)
Microtherm	ft^3	1.00	15.0	1.41	lbm	Microtherm® Free Flow
Coatings (lbs)						
Qualified Coatings	lbm	126.50	94	11.86	lbm	Acrylic Powder or Walnut Shell Powder
Qualified Coatings	lbm	958.70	457	89.86	lbm	IOZ Powder (Tin Powder)
Unqualified Coatings	lbm	250.00	94	23.43	lbm	Acrylic Powder or Walnut Shell Powder
			Total Particulate Debris	146.47		
Chemical Debris Concentrations						
Sodium Aluminum Silicate	kg	77.0	(2.2 lbs/kg)	15.91	lbm	Chemical Surrogate - AlOOH
Calcium Phosphate	kg	81.0	(2.2 lbs/kg)	16.74	lbm	Chemical Surrogate - $Ca_3(PO_4)_2$
Aluminum Oxyhydroxide	kg	0.00	(2.2 lbs/kg)	0.00	lbm	Chemical Surrogate - AlOOH
			Total Surrogate Debris	32.65	lbm	
Miscellaneous Debris						
Labels, Stickers, Tape, Placards, Tags	ft^2	100.00	n/a	n/a	ft^2	Miscellaneous Debris

Flume Water Level	ft	9.25
Scaling Factor	%	9.37%
Target Flume Flow	gpm	307.81
Strainer and Basket Surface Area	ft^2	130.77
Thin Bed Size	ft	0.010
Required Fiber for 1/8" Bed	ft^3	1.36
Required Fiber for 1/8" Bed @ 2.4 lbm/ft^3	lbm	3.27
Total Fibrous Debris	lbm	5.00
Thin Bed Batches	#	1.53

Table E.5-7 Chemical Debris Additions and Flume Flow Rate for the Thin Bed Test

Pump Flow Rate During Chem. Batching	Pump Flow (gpm)	Pump Flow (ft^3 / sec)	Flume Depth (ft)	Flume Volume (cu ft @ 9.25')	Pipe Volume (cu ft)	Total Volume (cu ft)	Total Volume (gal)	Flume Flow (cfs)	One flume cycle (sec)	1 Flume Turn Over FTO (min)	2 Flume Turn Over FTO (min)
	307.81	0.686	9.25	519.39	31.60	550.99	4,121.70	0.686	803.44	14.0	28.0

Chemical Debris Concentrations	U/M	Quantity	(lbs / ft^3 or ft^3)	Scaled Quantity	Qty w/ Bump Ups	U/M
Chemical Bump Up Added for Soluability	%	1.0%		9.37%		
Chemical Bump Up to Eliminate Bag Filters	%	1.4%				
Sodium Aluminum Silicate	max lbm	169.75		15.91	16.30	lbm
Aluminum Oxyhydroxide	max lbm	0.00		0.00	0.00	lbm
Calcium Phosphate	max lbm	178.60		16.74	17.15	lbm
			Total Surrogate Debris	32.65	33.45	lbm

	Plant Calculated lbm	Scaled Test lbm	Chemicals	Plant Conc	Flume Conc	U/M	lbs = Plant Conc	lbs / batch to start; 1 PTO in between	lbs / batch thereafter; 1 PTO in between	Est No. of PTO's Req'd	EST Minutes to Introduce Chemicals
Aluminum Oxyhydroxide	169.75	16.30	ALOOH	0.000392	0.003955	lbs/gal	1.61	0.5329	0.4037	39.40	552
Calcium Phosphate	178.60	17.15	Cal Phos	0.000412	0.004161	lbs/gal	1.70	0.5607	0.4248	39.40	197
Totals	348.35	33.45	Totals	0.000804	0.008116	lbs/gal	3.31	1.0936	0.8285	39.40	749
				433,242	4,121.7	gal		Batch Sizes			
				57,916	551.0	ft^3		33.00%	25.00%		12.48

Conversion of "grams / liter" to "lbs / gallon"

1 gram	=	0.0022	lbs
1 liter	=	0.26417	gallons
1 g / l	=	0.00835	lbs / gallon
11 g / l	=	0.0918	lbs / gallon
5 g / l	=	0.04173	lbs / gallon

Batch Volumes				
33% Batches @	0.53 lbm	=	5.81	gal of ALOOH mix
25% Batches @	0.40 lbm	=	4.40	gal of ALOOH mix
33% Batches @	0.56 lbm	=	13.44	gal of Cal Phosphate mix
25% Batches @	0.42 lbm	=	10.18	gal of Cal Phosphate mix

E.6 Test Results

E.6.1 Debris Transport Test

The Debris Transport Test determines the transportability of reflective metallic insulation (RMI), coatings (in the form of paint chips), and miscellaneous debris including other miscellaneous debris. Section E.5.1 lists the debris types used for the Debris Transport Test. The test results conclude the debris was captured and contained within the retaining basket. Table E.6-1 details the Debris Transport Test results.

Table E.6-1 Debris Transport Test Results

Debris Type	Debris Transport Response
leather work glove	* floated on the surface of the water
plastic glove	* floated on the surface of the water
caution tag (6 inch x 3 inch plastic material)	settled on retaining basket floor
caution label (yellow ribbon 2.5 feet in length)	* floated on the surface of the water
white cloth (1 foot x 1.5 feet)	* floated on the surface of the water
2 plastic tie wraps (1 foot and 2 feet long)	settled on retaining basket floor
¾ inch nylon rope (2 feet long)	settled on retaining basket floor
plastic chain link (1.5 feet long)	* floated on the surface of the water
plastic bag (1 foot x 2 feet)	* floated on the surface of the water
ear plugs (1 set connected with an elastic string)	* floated on the surface of the water
ear plugs (1 set in a plastic bag)	* floated on the surface of the water
¼ inch x ¼ inch RMI	settled on retaining basket floor
½ inch x ½ inch RMI	settled on retaining basket floor
4 inch x 4 inch RMI	settled on retaining basket floor
coating chips (5/8 inches and smaller)	* most floated on the surface

* These debris items were observed to float on the surface of the water and lay against the retaining basket screen due to the direction of the test flume flow.

E.6.2 Clean Strainer Head Loss Test

The Clean Strainer Head Loss Test determines the head loss of the clean strainer for five different flume flow rates. For this test, the measured flow rates, head losses, and water temperatures were averaged over the test duration once the desired flow rate was achieved. Table E.6-2 summarizes the clean strainer head loss results for the target flow rates. Figure E.6-1 provides a plot of the measured clean strainer head loss versus the average total flow rates for the Clean Strainer Head Loss Test.

Table E.6-2 Clean Strainer Head Loss Test Results

Target Flow (gpm)	Measured Basket Flow (gpm)	Measured Mini-Flow (gpm)	Measured Total Flow (gpm)	Temperature (°F)	Measured Strainer Head Loss (ft. H_2O)
230.9	204.8	28.9	233.7	116.2	0.246
269.3	247.6	28.9	276.5	118.1	0.313
307.8	286.9	28.8	315.7	119.3	0.385
346.3	326.5	28.8	355.3	120.7	0.464
384.8	363.4	28.4	391.8	119.9	0.539

Figure E.6-1 Clean Strainer Measured Head Loss vs. the Average Total Flow Rates

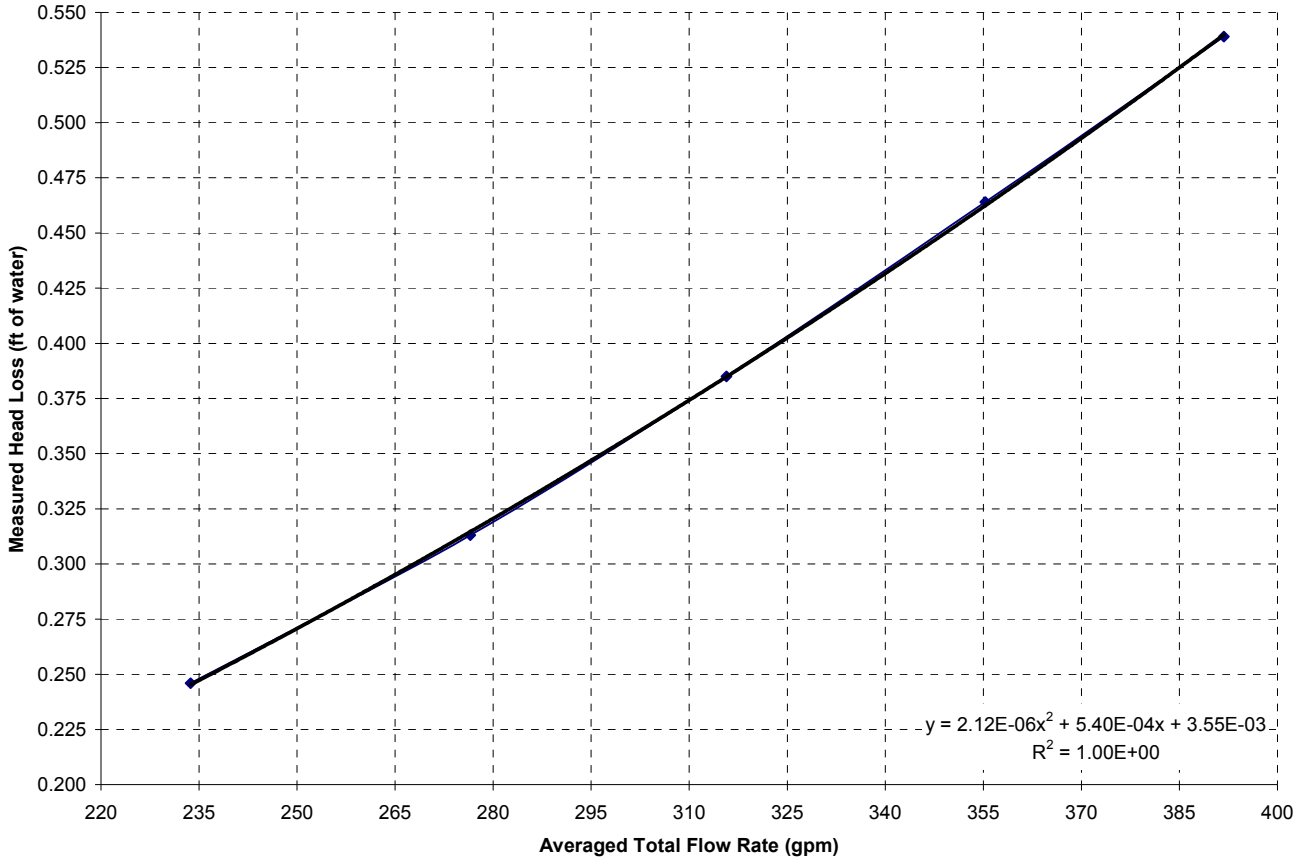

E.6.3 Design Basis Debris Loaded Strainer Head Loss Test

The Design Basis Debris Loaded Strainer Head Loss Test determines the debris bed head loss for the U.S. EPR design basis accident. The maximum and average measured head losses recorded during the test period are presented in Table E.6-3. During this test, the maximum head loss occurred prior to the completion of particulate addition and before fiber and chemicals were added to the test apparatus.

Table E.6-3 Maximum and Average Measured Head Loss for the Design Basis Debris Loaded Strainer Head Loss Test

	Hour	Total Flow (gpm)	Temp (°F)	Measured Basket Head Loss (ft. of water)	Strainer Head Loss (ft. of water)
Average	N/A	316.8	115.9	6.27	0.377
Maximum	00.13	328.0	118.2	0	0.414

The strainer and retaining basket head loss data recorded during Test No. 2 is graphed in Figure E.6-2. As indicated in Figure E.6-2, the strainer head loss remains constant throughout the test. The retaining basket overflows after the addition of coating chips, and then remains constant until the final batch of chemical debris is added to the test flume. Following the final batch of chemical debris, an approximate 1.3 inch measured increase in retaining basket head loss occurs over a period of 3.6 hours. Towards the end of the test there was a slight increase in the recorded retaining basket head loss caused by evaporation of water in the test apparatus. Following the test, the flume was drained revealing an essentially clean strainer screen. Figure E.6-3 shows the strainer screen following flume drain down.

Figure E.6-2 Strainer and Retaining Basket Head loss Data for the Design Basis Debris Loaded Strainer Head Loss Test

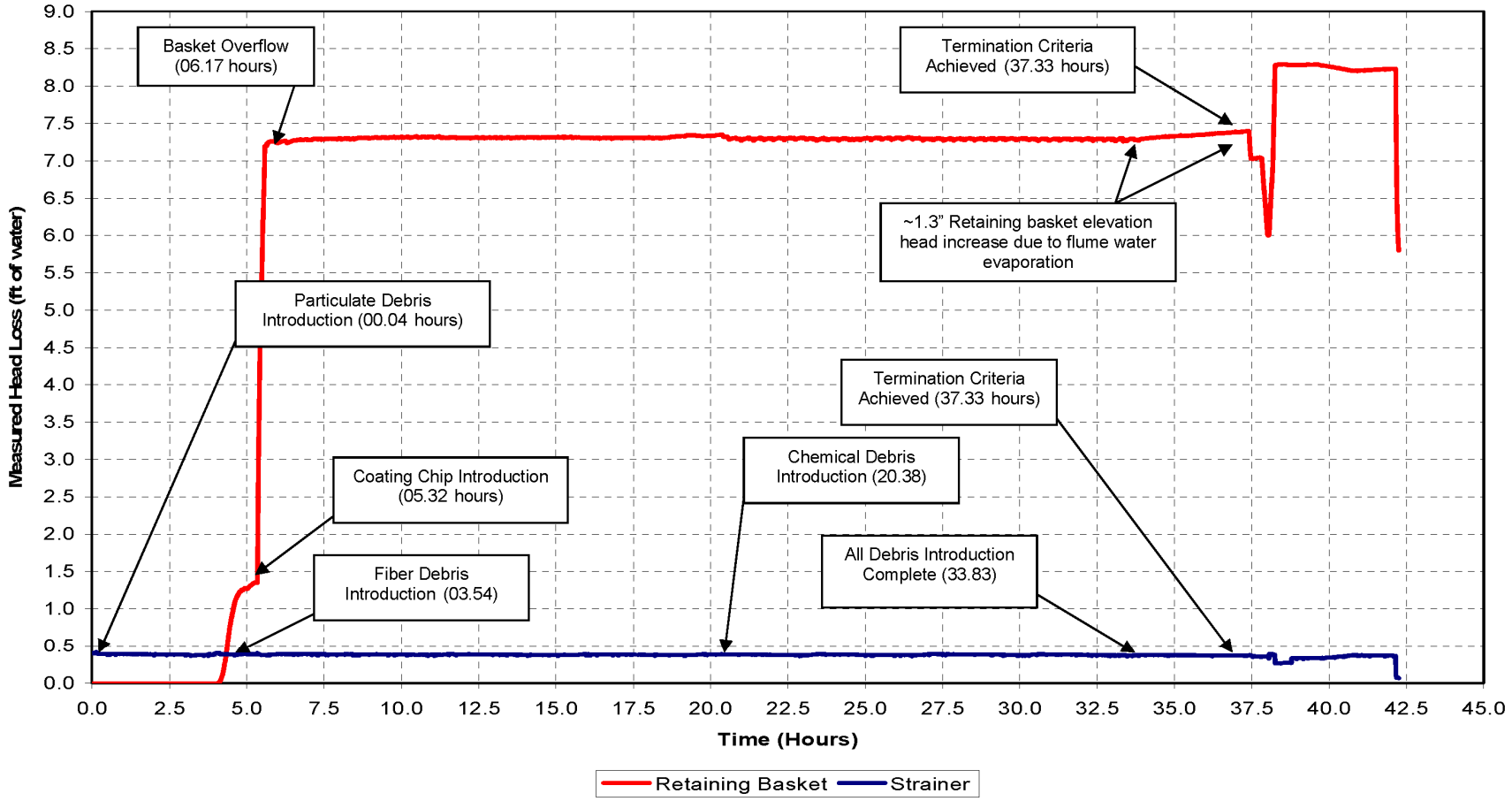

Figure E.6-3 Strainer Screen After Flume Drain Down Following the Design Basis Debris Loaded Strainer Head Loss Test

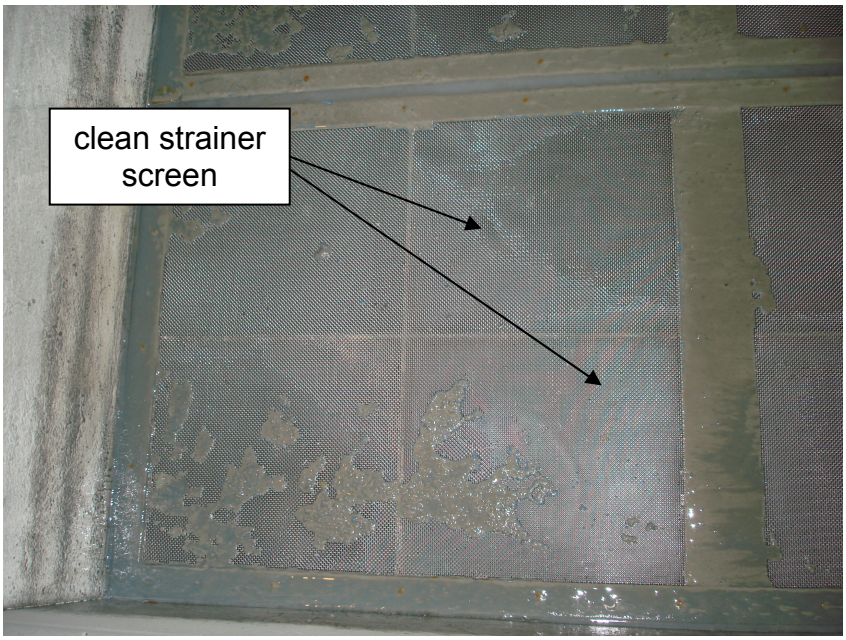

E.6.4 Fibrous Debris Only Sample Bypass Test

The Fibrous Debris Only Sample Bypass Test establishes the transport characteristics of fibers introduced incrementally up through the maximum design basis fiber load. This test also evaluates how a fibrous debris bed forms on the retaining basket and strainer. Debris bypass testing was performed during this type test to provide debris bypass results for downstream analysis.

The Fibrous Debris Only Sample Bypass Test was originally performed as Test No. 3. After Test No. 3 was terminated, the debris introduction pump was dismantled and a small amount of fibrous debris was found within the pump's internals. For this reason, Test No. 3 was invalidated and the test was repeated as Test No. 3A.

Test No. 3A used the same procedures used in Test No. 3. The head loss data measured during the Fiber Debris Only Sample Bypass Test No. 3A is shown in Table

E.6-4. The debris loaded head loss shown for Test 3A is not used as a design basis head loss since only one debris constituent was introduced for the test and chemical effects were not present. After all of the fibrous debris was introduced to the test flume, the debris introduction pump was dismantled to verify remnants of fiber did not remain in the pump internals. A small amount of debris was discovered and re-introduced to the test flume through the observation window after the pump was dismantled.

Table E.6-4 Head Loss Data for Fibrous Debris Only Sample Bypass Test No. 3A

Time	Procedure Action	Total Flow (gpm)	Temp (°F)	Measured Basket Head Loss (ft. of water)	Strainer Head Loss (ft. of water)
09:02:42	1st batch of fiber added	318	114	0.0	0.375
09:20:18	1st batch completed	317	113	0.0	0.376
09:48:21	2nd batch of fiber added	314	115	0.001	0.388
09:51:39	2nd batch completed	319	115	0.015	0.385
13:21:56	test termination	312	120	0.091	0.391

Fiber bypass sampling was conducted during Test 3A. These samples are analyzed for percent bypass and used for downstream effects analysis. A total of thirteen samples were drawn and analyzed. The results of the analysis quantify the amount of fibrous debris that penetrated the strainer during testing. Table E.6-5 provides a summary of the bypass test results. Results of testing and analysis conclude a total fibrous debris bypass percentage of 34.4%.

Table E.6-5 Bypass Test Results

TEST 3A			LENGTH						Diameter			Flow Rate	Smpl Size
Sample	Time (min)	Fibers (per smpl)	Long (%)	Med (%)	Short (%)	Long (μm)	Med (μm)	Short (μm)	Thick (μm)	Med (μm)	Thin (μm)	(gpm)	(mL)
B	N/A	94	8%	52%	40%	900	300	80	10	6	3	280.9	25
1	0	90	16%	66%	18%	1200	350	80	10	7	3	285.4	25
2	4	1501	8%	61%	31%	1100	300	90	12	7	4	290.4	25
4	14	11150	3%	53%	44%	1200	250	90	11	7	3	281.9	25
5	19	22360	2%	54%	44%	850	250	90	10	6	3	288.3	25
6	24	20707	2%	49%	49%	1100	250	90	10	7	3	287.6	25
9	39	10747	4%	48%	48%	950	300	80	12	7	3	288.1	25
10	44	10467	2%	47%	51%	850	250	90	10	6	4	285.0	25
11	49	9300	2%	46%	52%	1100	250	80	11	7	3	288.6	25
12	54	8080	2%	40%	58%	850	300	80	10	7	3	291.0	25
17	106	137	4%	52%	44%	1300	250	90	12	7	3	290.9	25
22	176	108	3%	65%	32%	950	250	80	11	7	3	287.0	25
27	246	163	8%	59%	33%	900	250	80	11	7	3	288.5	25

E.6.5 Debris Loaded Strainer Head Loss Thin Bed Test

The Debris Loaded Strainer Head Loss Thin Bed Test determines if a higher head loss is possible with a thin bed of fibers, particulate, and chemical debris present, rather than with the design basis quantity of debris. For the Debris Loaded Strainer Head Loss Thin Bed Test, a plot of the strainer and retaining basket head loss is presented in Figure E.6-4. Based on results of testing, there was no formation of a thin bed on the strainer. Upon draining the flume after test termination, the strainer screen appeared nearly free of debris. Figure E.6-5 shows the strainer screen following the flume drain down.

Figure E.6-4 Strainer and Retaining Basket Head Loss Data for the Thin Bed Test

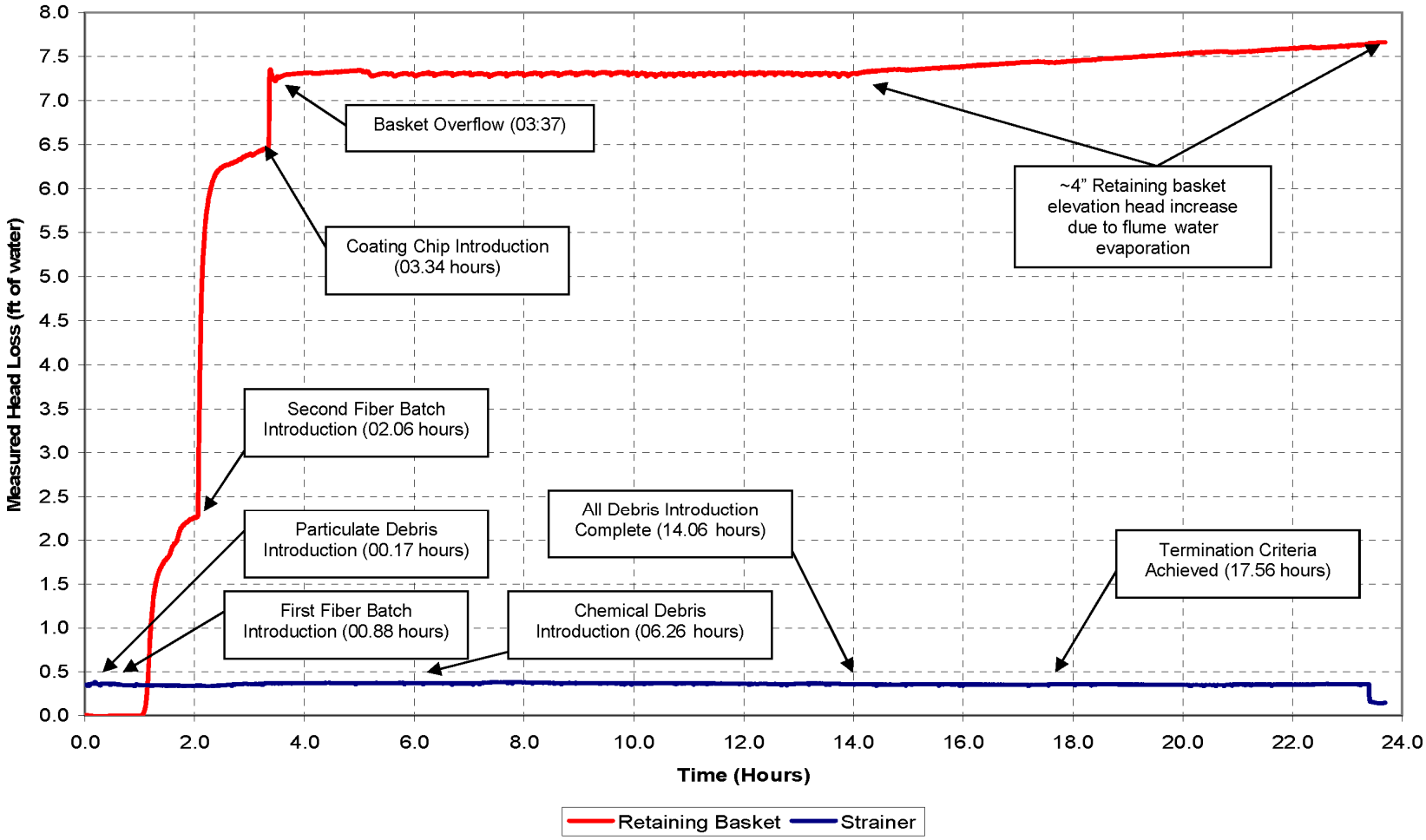

Figure E.6-5 Strainer Screen After the Flume Drain Down Following the Thin Bed Test

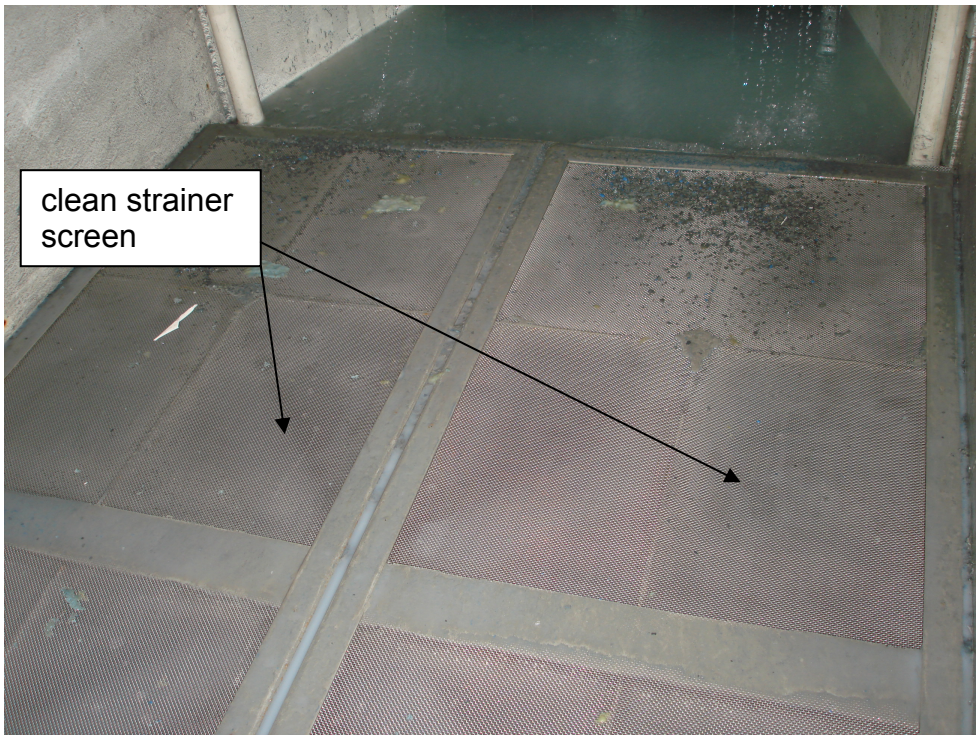

E.7 Conclusions

A total of five type tests were performed to evaluate and confirm the ECCS strainer performance. The following conclusions are provided.

E.7.1 Debris Transport Test

The results of the Debris Transport Test are provided in Section E.6.1. The test results demonstrate that the test debris was entirely captured and contained within the retaining basket. Therefore, it is concluded that there are no adverse effects to the ECCS strainer operation.

E.7.2 Clean Strainer Head Loss Test

The Clean Strainer Head Loss Test results are presented in Table E.6-2. A plot of the measured clean strainer head loss versus the measured testing target flow rates

presented in Figure E.6-1. The test results demonstrate that the clean strainer has minimal head loss. The strainer head loss associated with the scaled design basis test flow of 307.8 gpm is approximately 0.385 feet. During this test, the strainer showed no visual observations of vortexing.

E.7.3 Design Basis Debris Loaded Strainer Head Loss Test

The Design Basis Debris Loaded Srainer Head Loss Test results are presented in Table E.6-3 and Figure E.6-2. Based on Table E.6-3, the maximum strainer head loss was 0.414 feet of water as compared to the clean strainer head loss of 0.385 feet. During testing, the retaining basket was challenged with the design basis debris source term and effectively prevented the fibrous debris from reaching the strainer. Following the test, the flume was slowly drained of water to reveal an essentially clean strainer. The design basis test debris load had a negligible impact on the ECCS strainer head loss.

E.7.4 Fibrous Debris Only Sample Bypass Test

The Fibrous Debris Only Sample Bypass Test was performed as Test No. 3A. The maximum measured retaining basket and strainer head losses for Test No. 3A are presented in Table E.6-4. The test results demonstrated that the strainer head loss was negligible. Bypass samples were taken during Test 3A to analyze the percent bypass fraction for downstream effects analysis. Table E.6-5 details the bypass test results. Results of testing and analysis yield a total fibrous debris bypass percentage of 34.4%.

E.7.5 Debris Loaded Strainer Head Loss Thin Bed Test

The results of the Debris Loaded Strainer Head Loss Thin Bed Test are similar to the test results of the Design Basis Debris Loaded Strainer Head Loss Test. A plot of the strainer and retaining basket head loss is presented in Figure E.6-4. The retaining basket successfully protected the strainer from fibrous debris. With the absence of fiber at the strainer, it was not possible for a thin bed to form on the strainer. Following the test, drain down of the flume revealed a strainer screen that was nearly free of debris.

In summary, the ECCS strainer performance testing demonstrates the effective and reliable performance of the U.S. EPR design for GSI-191. The retaining basket effectively functions to limit and prevent most debris from reaching the ECCS strainer. The strainer design, complemented by the design mitigation features of the retaining basket, provides significant head loss margin for the ECCS strainer. Testing demonstrates that the strainer head loss is conservatively less than 0.5 feet of water as compared to a strainer design head loss of approximately 5.0 feet.

ECCS strainer testing conservatively challenged the “defense in depth” design of the U.S. EPR with the addition of over 100% of the design basis debris source term to one of the four sets of retaining basket/strainer combinations in the U.S. EPR design.

E.8 References

1. NEI 04-07 Vol. 1 (Methodology), “Pressurized Water Reactor Sump Performance Evaluation Methodology,” December 2004.

2. NEI 04-07 Vol. 2 (Safety Evaluation), “Pressurized Water Reactor Sump Performance Evaluation Methodology,” December 2004.

3. “NRC Staff Review Guidance Regarding Generic Letter 2004-02 Closure in the Area of Strainer Head Loss and Vortexing” March 2008.

Appendix F
Downstream Effects Evaluation for the U.S. EPR

F.1 Introduction

Pressurized Water Reactor (PWR) containment buildings are designed to both contain radioactive materials releases and facilitate core cooling in the event of a postulated loss-of-coolant accident (LOCA). The cooling process requires water discharged from the break to be collected in the in-containment refueling water storage tank (IRWST) for recirculation by the emergency core cooling system (ECCS). The IRWST contains numerous devices (weirs, strainer baskets, and screens) that protect the components of the ECCS from debris that could be washed into the IRWST. Fibrous debris could form a mat on either the basket screen or the strainer that would collect particulates, keeping them from being ingested into the ECCS. However, while the fiber bed is forming, or if the fiber bed does not completely cover the screens, particulates and some fibrous material may be ingested into the ECCS and subsequently flow into the reactor coolant system (RCS).

Concerns have been raised about the potential for debris ingested into the ECCS to affect long-term core cooling when recirculating coolant from the containment sump (NRC Generic Letter 2004-02 [1]). The fuel assembly bottom nozzles are designed with flow passages that provide coolant flow from the reactor vessel lower plenum into the region of the fuel rods. During operation of the ECCS to recirculate coolant from the IRWST, debris in the recirculating fluid that passes through the sump screen may collect on the bottom surface of the fuel assembly bottom nozzle, causing resistance to flow through this path. The collection of sufficient debris on the fuel assembly bottom nozzle is postulated to impede flow into the fuel assemblies and core. Other concerns have been raised with respect to the collection of debris and post-accident chemical products within the core itself. Specifically, the debris has been postulated to form blockages at intermediate spacer grids, thereby reducing the ability of the coolant to remove decay heat from the core. Similarly, chemical precipitants have been postulated to plate-out on fuel cladding, again resulting in a reduction of the ability of the coolant to remove decay heat from the core.

AREVA undertook a program to provide analyses and data on the effect of debris and chemical products on core cooling for the U.S. EPR plant when the ECCS is actuated. The objective of the program was to demonstrate reasonable assurance that sufficient LTCC is achieved for U.S. EPR plant to satisfy the requirements of 10 CFR 50.46(b)(5) with debris and chemical products that might be transported to the reactor vessel and core by the coolant recirculating from the IRWST. The debris composition includes particulate and fiber debris, as well as post-accident chemical products. This evaluation considered the design of the U.S. EPR plant, the design of the open-lattice fuel, the design and tested performance of the strainer baskets and sump screens, the tested performance of materials inside containment, and the tested performance of fuel assemblies in the presence of debris. Specific areas addressed in this evaluation include:

- Collection of debris on fuel assembly bottom nozzle or intermediate spacer grids,
- Production and deposition of chemical precipitants and debris on the fuel rod cladding.

To address the collection of debris in the fuel assembly bottom nozzle or at the spacer grids, fuel assembly testing was performed. The purpose of this testing, described in Section F.3, was to determine the mass of debris that can be deposited at the core entrance or spacer grids and not impede long-term core cooling flows to the core. These acceptance criteria will be used in part to demonstrate adequate flow for long-term decay heat removal.

An evaluation of the deposition of chemical precipitates and debris on the fuel rods was performed by applying U.S. EPR-specific design parameters to the U.S. EPR LOCA Deposition Analysis Model (EPRDM). This calculation, described in Section F.4, provides a conservative evaluation of (1) deposition thicknesses on fuel rod surfaces due to chemical and debris deposition and (2) to determine the cladding temperatures under the buildup for up to 30 days following a LOCA.

F.2 Background

Immediately after the break opens, the RCS fluid is expelled as a jet to containment. The energy from this jet impacts structures near the break and generates debris through destruction of coatings and insulation. The amount of debris generated depends on the break location and size. The limiting amount of debris is generated by a full-area pipe break (refer to Section C.6.5). Therefore, the discussion and transient descriptions in this document focus on large break LOCAs. The results presented bound smaller breaks, since less debris would be generated. The debris falls to the heavy floor and, depending on the size and density, transports to one of four holes in the heavy floor where it passes over the weirs around the openings, through the trash racks, to the retention baskets, and possibly into the IRWST.

Within the first minute following the break, the ECCS will begin. The medium head safety injection (MHSI) and low head safety injection (LHSI) begin to draw suction from the bottom of the IRWST. This ECCS flow in combination with the accumulator flow replaces the RCS liquid lost through the break and arrests any clad heatup. Shortly after the ECCS injection begins, the core level is recovered and the RCS is refilled to the break location. For any RCS pipe break, the two-phase mixture level is above the top of the core. The core decay heat is removed by ECCS injection. The core flow and vessel level depend on the break location, ECCS injection rate and configuration, and RCS cold leg liquid levels.

The ECCS in the U.S. EPR design operates in two configurations: (1) cold side injection and (2) simultaneous hot and cold side injection. Each configuration introduces debris to the core region at different locations and at different rates depending on the break location. The specifics are discussed in Sections F.2.1 and F.2.2.

F.2.1 Cold Side Injection

During cold side injection, MHSI and LHSI only inject into the cold legs. For cold leg pump discharge (CLPD) breaks (Figure F.2-1 and Figure F.2-2), the pumped ECCS injected into the intact cold legs provides liquid to make up for core boil-off. The ECCS liquid keeps the downcomer full to at least the bottom of the cold leg nozzles; any excess ECCS flows out of the broken cold leg through the break and back into the containment sump. The core mixture level is controlled by the manometric balance between the downcomer liquid level, the core

level, and RCS pressure drop needed to pass the core generated steam to the break location. The net ECCS flow into the core is the flow required to make up for core boil-off that removes the decay heat. The situation is similar for cold leg pump suction (CLPS) breaks, although the downcomer liquid level may be higher depending on the relationship of the pump spillover elevation to the bottom of the CLPD piping.

For a break in the hot leg (Figure F.2-3), all the ECCS flow must pass through the core to exit the break. The core mixture level will be at least to the hot leg nozzle elevation, and the core flow rate will equal the ECCS flow rate.

In either case, debris that enters the RCS will approach the core from the downcomer and RV lower plenum. Further, in order for the debris to transport through the RCS, it must be fairly well mixed in the ECCS fluid and be close to neutrally buoyant. Therefore, the debris is homogeneously mixed with the ECCS fluid such that the fraction of debris reaching the core inlet is proportional to the fraction of flow reaching the core inlet to the total ECCS flow rate.

F.2.2 Simultaneous Injection

Sixty minutes after the break, the operator realigns the operating LHSI trains from injecting solely into the cold legs to the hot leg injection mode, in which most of the LHSI water is injected into respective hot legs. This realignment mitigates the possible build up of boric acid in the core. In this configuration, MHSI and a portion of LHSI continue to inject into the cold legs. Consequently, ECCS is provided simultaneously to the cold and hot legs. This mode of operation is also known as hot leg injection (HLI). The core flow patterns for this injection configuration are illustrated in Figure F.2-4.

An assessment of fluid mixing in the reactor during HLI shows the following: with the initiation of HLI, the cold ECC water mixes with the steam-water mixture in the RV upper plenum and in the hot legs and flows down into the core region. If the RV mixture level is lower than the bottom of the hot leg, the cold water will interact with the steam in the upper plenum and in the hot leg resulting in substantial steam condensation. If the mixture level is in the hot leg and the stratified liquid level height is above the centerline of the hot leg then the ECC water jet has less chance for steam-water interaction. In either case, as the water falls into the upper plenum, it spreads on top of 15 to 20 percent of the fuel assemblies per hot leg injection

location and mixes with the re-circulating hot water and flows downwards. As the water flows down into the core region through the relatively low power periphery fuel assemblies, it suppresses the boiling in these fuel bundles as well as provides cross flows into the neighboring bundles. The cross flow in a liquid downflow bundle is primarily radially or inwards, since the fluid in the bundles on either side of the bundles (in the theta-direction) is also subcooled (except in the plume periphery). As the steam production in the next cross flow bundle reduces, the momentum of the 2-phase mixture that is entering the upper plenum reduces and this results in the migration of the cold water over the top of this bundle. Thus the down flowing liquid region continues to grow until the steam production in all the bundles eventually ceases.

Following a cold leg break, the initiation of HLI at 60 minutes induces a reverse flow in the downcomer such that ECCS injected to the cold legs flows directly to the break. The only flow to the core is from the top via HLI. Debris that reaches the RCS will approach the core from the top.

Following a hot leg break, the HLI from the intact hot leg(s) mixes with steam and flow into the core as described above. The flow in the broken loop exits the break in the hot leg before reaching the core. Therefore, the net ECCS flow to the top of the core will be less than that seen for the cold leg break, where all of the HLI reaches the top of the core. At the same time, the ECCS injected to the cold legs can enter the core in the usual core flow direction. Debris that reaches the RCS will approach the core from both the top and bottom.

In both cases, in order for the debris to transport through the RCS, it must be fairly well mixed in the ECCS fluid and be close to neutrally buoyant. Therefore, the debris is homogeneously mixed with the ECCS fluid such that the fraction of debris reaching the core inlet or exit is proportional to the fraction of flow reaching the core inlet or exit to the total ECCS flow rate.

Figure F.2-1: Core Flow Patterns Following a Cold Leg Break During Cold Side Injection

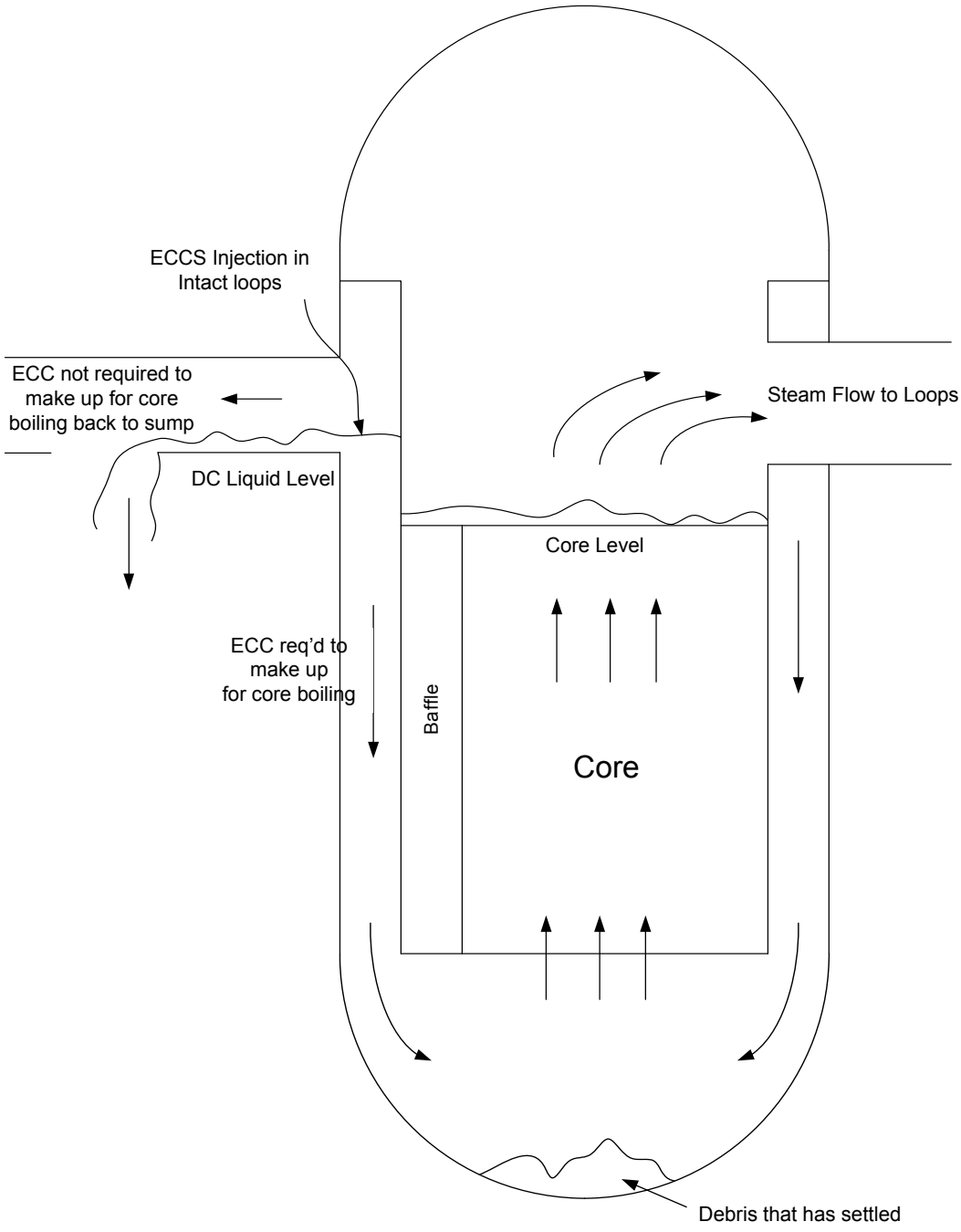

Figure F.2-2: Core Flow Patterns Following a Cold Leg Break During Cold Side Injection

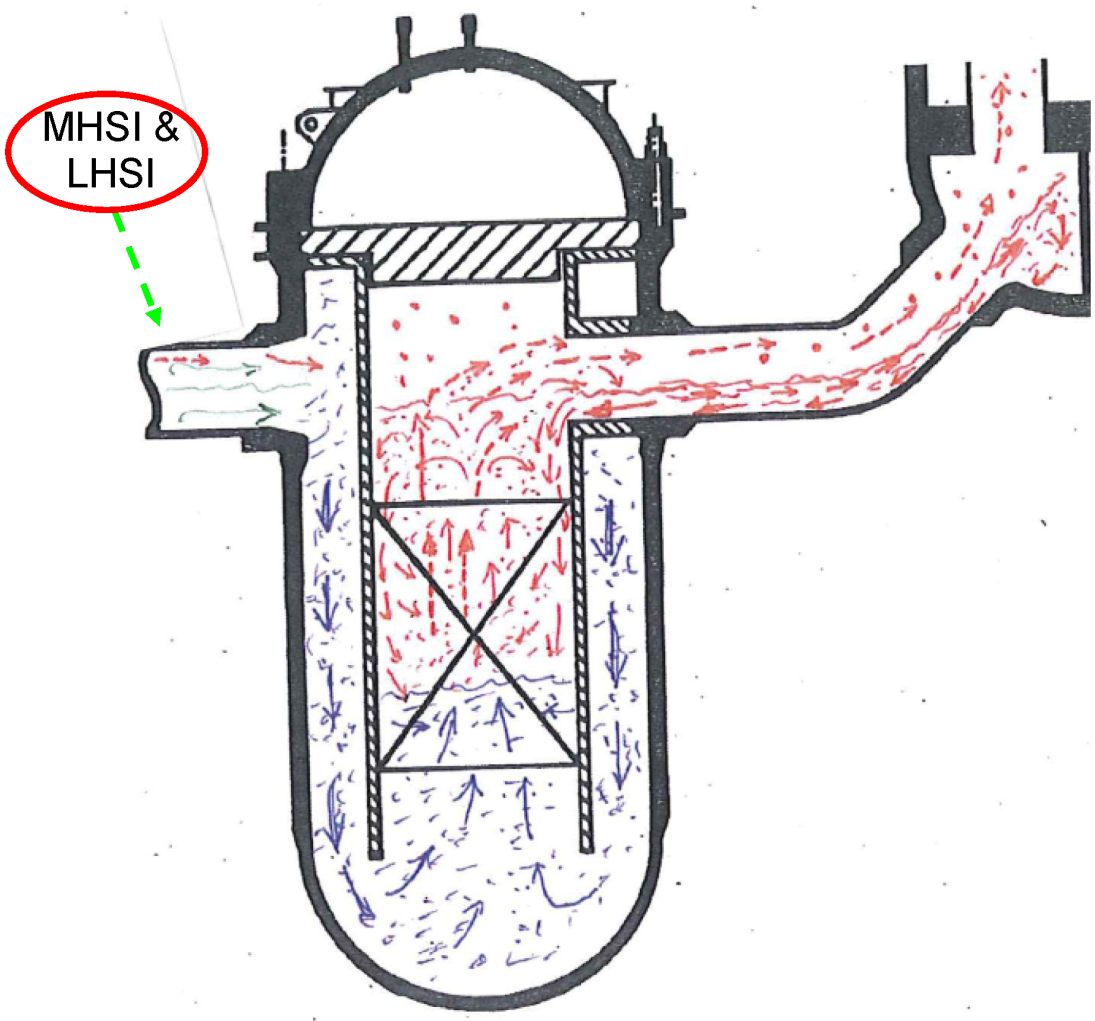

Figure F.2-3: Core Flow Patterns Following a Hot Leg Break During Cold Side Injection

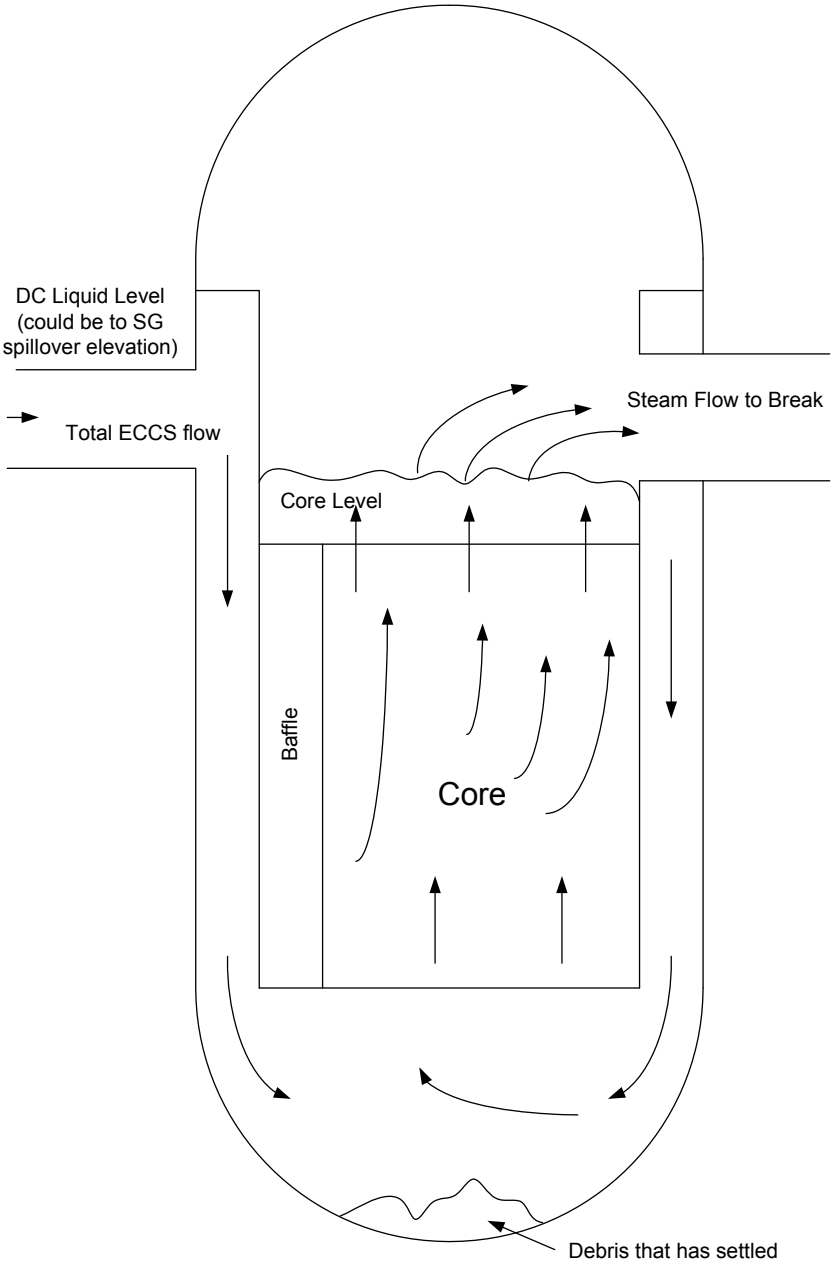

Figure F.2-4 Core Flow Patterns Following a Cold Leg Break During Simultaneous Injection

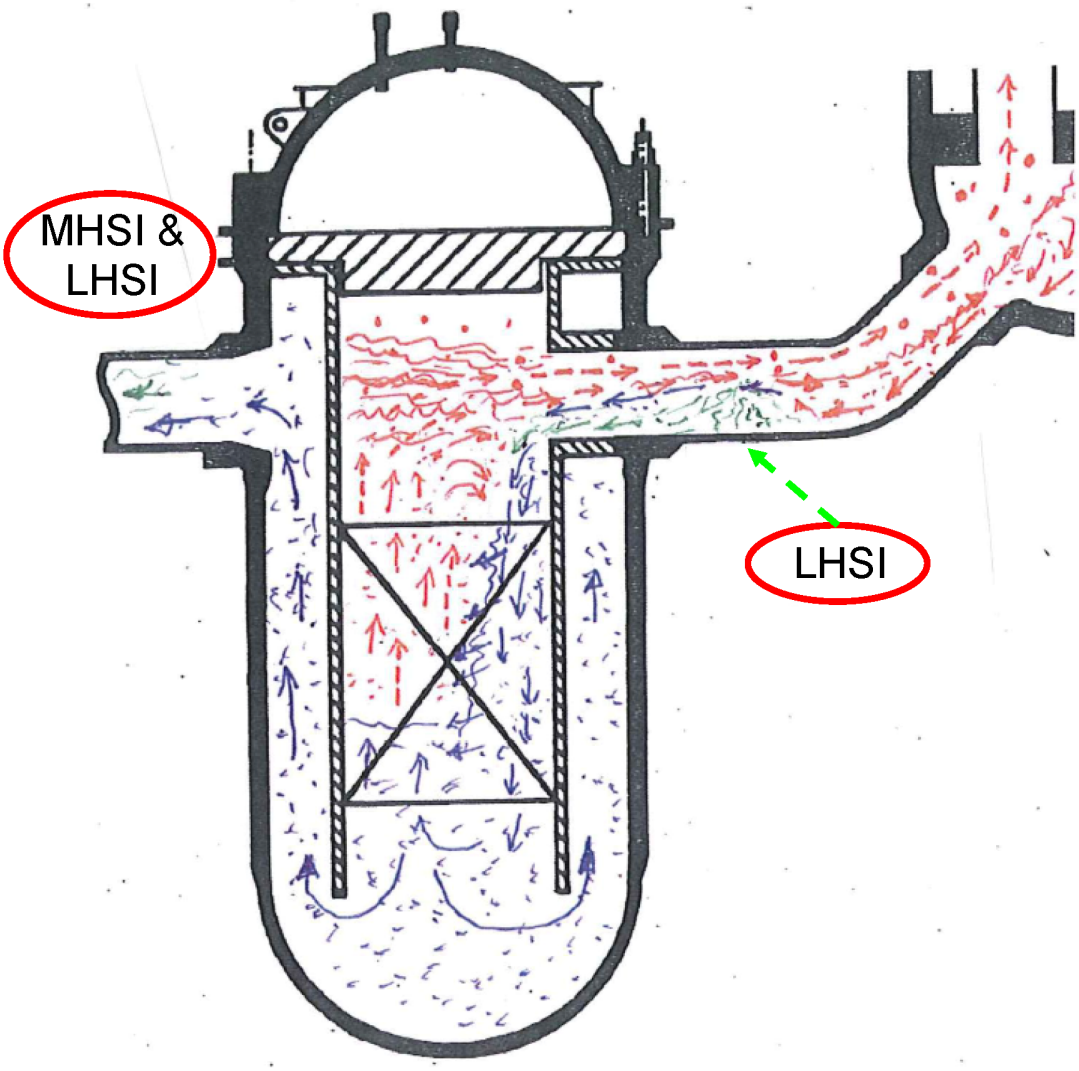

F.3 Debris Accumulation at Core Inlet or Intermediate Spacer Grids

Fuel assembly (FA) testing was performed to address the collection of debris in the fuel assembly bottom nozzle or at the spacer grids. The purpose of this testing was to justify an acceptance criteria for the mass of debris that can be deposited at the core entrance or spacer grids and not impede long-term core cooling flows to the core. These acceptance criteria will be used in part to demonstrate adequate flow for long-term decay heat removal.

F.3.1 Assumptions

The following assumptions were used in developing the inputs and boundary conditions for the FA testing.

1. For the cold leg break cases with cold side injection, the available driving head at the core inlet is calculated as though the core mixture level was fixed at the top of the core and all flow at the core exit is steam with an enthalpy no higher than that of saturated steam (i.e., not superheated). These are the limiting conditions to maintain core cooling with a core inlet blockage.

2. The ECCS liquid density is based on the IRWST liquid conditions. This density is used as the liquid density in the downcomer for calculating the available driving head for breaks with cold side injection. This density is also used as the liquid density in the hot legs for calculating the available driving head for breaks with HLI. Since density is inversely proportional to liquid temperature and a lower density will reduce the driving head from the downcomer, a conservatively high sump liquid temperature is selected. The maximum IRWST liquid temperature following a LOCA was calculated to be 230ºF. The liquid density is also a function of the containment pressure. As the pressure increases, the density increases. Consequently, a low containment pressure will produce a lower density. The containment pressure may be as low as 25 psia (see Assumption #7 below). The density corresponding to 230ºF and 25 psia is 59.4 lbm/ft^3. Accounting for the possibility of downcomer boiling (see Assumption #11 below), the density corresponding to a saturated pressure of 25 psia will be used, which further reduces the density to 59.1 lbm/ft^3.

3. The core decay heat used in this evaluation is based on 1.2 times the ANS 1971 standard plus B&W heavy actinides. The decay heat used in the LOCA analyses of record to establish the core operating limits and show compliance with the first three criteria of 10 CFR 50.46 is the 1979 ANS standard. The ANS 1971 standard produces a higher decay heat rate compared to the ANS 1979 standard. The decay heat rate is used to determine the core flow rate for a cold leg break. Since a maximum flow rate is conservative (see Section F.3.4), the higher decay heat rate is conservative.

4. It assumed that the debris is homogeneously mixed with the ECCS fluid such that the fraction of debris reaching the core is proportional to the fraction of flow reaching the core to the total ECCS flow rate. In order for the debris to transport through the RCS, it must be fairly well mixed in the ECCS fluid. Further, the transport of debris is dependent on the ECCS injection configuration, break location, and debris buoyancy. For cold side injection, breaks between the RCP and the vessel inlet (cold leg pump discharge, or CLPD) will bypass water directly to the break, supplying the core with only the water required to make up for boiloff. Debris that is positive in buoyancy will stay within the flow field at the top of the downcomer and proceed out the break. Debris that is negative in buoyancy will sink to the bottom of the vessel and accumulate. For this debris accumulation to be a problem, there must be enough of it to fill the lower head/lower plenum. Most of the neutrally buoyant debris will flow to the break because the dominant flow is toward the break. Some of it, however, could migrate to the lower plenum. The behavior of breaks within the pump suction piping is similar to cold leg pump discharge breaks except that the driving head for ECCS liquid is slightly greater. For breaks in the hot leg, all of the ECCS flow will proceed through the downcomer and the core to the break. The velocities in the downcomer correspond to the ECCS charging rate. Again, debris that is negative in buoyancy will tend to sink to the bottom of the vessel and accumulate. Debris with neutral or slightly positive buoyancy will be carried with the ECCS flow to the lower head. Debris that is positive in buoyancy will tend to remain in the upper downcomer but, after accumulation, will be dragged to the lower plenum/lower head. Similar behavior can be expected in the upper plenum during HLI. This assumption is used to determine the quantity of debris that reaches the core.

5. At the time in the transient when the fuel downstream analyses are performed, the liquid entering the bottom of the core is subcooled. However, ECCS subcooling is neglected to provide conservative liquid properties as explained in #2 above. This assumption is used in calculating the core boiloff rate and is consistent with Assumption #2 above.

6. Following a hot leg break with ECCS injection into the cold legs only, the ECCS liquid will remove core decay heat by liquid convection (if enough flow is present to suppress core boiling). If a blockage occurs at the core inlet, core boiling may result and the core mixture level may decrease to just above the top of the core and all flow at the core exit is steam, with an enthalpy no higher than that of saturated steam (i.e., not superheated) so as to preclude cladding heatup. Similar to a cold leg break with cold side injection, this condition is limiting for maintaining core cooling with a core inlet blockage (see #1 above). For the calculation of the available driving head for this break scenario, core voiding is neglected and the liquid level is assumed to be at the bottom of the hot leg (i.e., the break location). This assumption will increase the liquid head in the core for core decay heat removal flow rates. A top-side break would increase the level by the diameter of the hot leg pipe. However, this additional conservatism is not necessary given the limiting condition assumed.

7. In the calculation of the loop pressure drop and flow losses for the cold leg break scenario with cold side injection, a minimum containment pressure of 25 psia is assumed. Typically, a minimum pressure is not calculated for times past initial core recovery; therefore, a specific value is not readily available. The containment pressure response is calculated as an integral part of the RLBLOCA analysis. At the end of the S-RELAP5 RLBLOCA run for the highest peak clad temperature (PCT) case, the containment pressure is at or above 30 psia and relatively flat or slightly increasing. The containment pressure is reduced from 30 psia to 25 psia to account for variations in the initial containment volume and temperature based on a sensitivity study on the variation in containment pressure done in response to RAIs on the RLBLOCA containment response. When the containment response was calculated using the maximum containment volume and minimum initial temperature, the containment pressure was up to 5 psi lower than when using the best-estimate containment volume and nominal containment temperature. Finally, the U.S. EPR design does not credit containment

spray in the licensing basis, nor is actuation included in the emergency operating procedures. Containment spray is used only for severe accident scenarios. Therefore, there is no mechanism for rapidly reducing the containment pressure. Thus, a value of 25 psia is a conservative lower bound for the containment pressure up to 60 minutes.

In the calculation of the loop pressure drop and flow losses for the cold leg break scenario with cold side injection, a SG secondary side liquid temperature is needed. This value is used in combination with the containment pressure to determine the superheated steam density through the loops. A higher temperature produces a lower density, which ultimately increases the pressure drop through the loops and further reduces the allowed pressure drop due to the debris buildup at the core inlet. U.S. EPR S-RELAP5 analyses that represent a cold leg break scenario provide an estimate of the SG secondary side liquid temperature. The liquid temperatures from the S-RELAP5 control volumes representing the steam generator boiler region from one of the intact loops in the examined transient are extracted at 1000, 1500, and 3500 seconds.

For each time, the highest of the liquid temperatures in the S-RELAP5 control volumes representing the SG boiler region is used as the primary side temperature to calculate the RCS steam density.

8. For cold side injection, the core steaming following a cold leg break is vented through the loops. Following a break in the CLPS piping, the steam exiting the core will traverse the hot legs, SGs, and cold leg pump suction piping to the break. Shortly after the LOCA, the steaming rate will be sufficient to keep all of the loops open (i.e., a loop seal in the intact legs cold leg suction piping will not reform). As the core boiloff rate decreases, the steam velocities through the loops will decrease such that the loops seals may begin to re-form. A conservative, early estimate of loop seal re-formation following a CLPS break was determined to be 30 minutes. However, a less conservative analysis may indicate that loop seals re-form later in the event. Since simultaneous injection (i.e., HLI) begins within 60 minutes, it is assumed that steam venting through all four loops following a CLPS break will occur for up to 60 minutes. Following a break in the CLPD piping, steam exiting the core will traverse the hot legs, SGs, and cold legs to the break. The pump spillover elevation is 27.68 inches above the bottom of the CLPD piping. This

elevation increase will preclude liquid from falling back over the pump into the CLPS piping in the intact loops. Therefore, the loop seals will not re-form, and all four loops will be available to vent steam. Therefore, loop seal re-formation is not considered in the calculation of the available driving head for breaks with cold side injection.

9. The core liquid density is used to calculate the available driving head for breaks with cold side injection and is based on the containment pressure. As the pressure decreases, the saturation temperature decreases at a faster rate. Consequently, the net effect is that the fluid density increases. The containment pressure may be as low as 25 psia (see #7 above). While the core exit pressure may be higher than the containment pressure due to flow losses in the RCS loops, this increase will be conservatively neglected. The effect of this assumption is to increase the pressure in the core due to the liquid column, thereby minimizing the available driving head. Therefore, a density corresponding to a saturated pressure of 25 psia will be selected. This value is 59.1 lbm/ft^3.

10. The core latent heat of vaporization is used to calculate the core boiloff rate. As discussed in Section F.3.4, a maximum flow rate will maximize the pressure drop through a debris bed. Therefore, the latent heat of vaporization is based on the maximum containment pressure. As the pressure increases, the latent heat of vaporization decreases. The containment pressure may be as high as 67 psia. While the core exit pressure may be higher than the containment pressure due to flow losses in the RCS loops, the peak containment pressure occurs before 100 seconds into the transient. Beyond 15 minutes, the containment pressure is well below the maximum. Therefore, a latent heat of vaporization corresponding to a saturated pressure of 67 psia is used. This value is 910 BTU/lbm.

11. It is possible that all of the energy in the thick metal of the RV may not have been removed by this point in the transient, which can lead to boiling in the downcomer. Therefore, a void fraction of 20 percent in the downcomer is assumed in the calculation of the available driving head for a cold leg break with cold side injection. The effect of this assumption is to decrease the pressure in the downcomer due to the liquid column, thereby minimizing the available driving head.

12. Steam condensation on the cold ECCS injection is considered in the loop pressure drop calculation used to determine the available driving head for a cold leg break with cold side injection. A constant pressure drop of 0.5 psi in each intact loop is assumed. This is consistent with or bounds the values used during the reflooding portion of deterministic LOCA analyses with pumped injection (Reference [2, Vol. 1, p. 4-33] and Reference [3, Vol. 1, p. 4-25]). The effect of this assumption is to increase the loop pressure drop and decrease the available driving head.

13. All debris that passes through the sump screens over 30 days is treated as if it arrives in the RCS at the first opportunity. It takes a finite time for debris to transport from the break location to the RCS. Further, the mixing of fluid and debris on the heavy floor and the filtration of the retention baskets and strainers will cause the debris to arrive in the RCS over time. Therefore, testing the maximum, 30-day debris load is conservative.

14. Because the test loop continually recirculates debris, there are multiple opportunities to catch debris on an obstruction and block flow. Depending on the break location and ECCS configuration, this is not likely to occur in the core. For example, following a hot leg break with cold side injection, the fluid passes through the core once and returns to containment where it must be re-filtered by the retention baskets and strainers before it will reenter the RCS.

F.3.2 Sump Transport Delay

The time that debris reaches the RCS must be defined. The IRWST is initially full of clean water. Shortly after the LOCA, the ECCS pumps begin to draw suction from the bottom of the IRWST. The debris that is generated by the jet from the pipe break will fall to the heavy floor. The fluid discharged from the RCS will collect on the heavy floor (along with the debris) until the level is high enough to flow over the weirs surrounding the openings in the floor above the retaining baskets. Once this flow begins, debris will be transported with the fluid and fall into the retaining baskets, which are partially submerged in the IRWST. Any debris that is not captured in the baskets will continue through the IRWST and to the sump screens. Once debris reaches the sump screens, it may pass through and be introduced to the RCS. The debris laden fluid flows through the ECCS to the RCS and back through the break to the heavy floor.

The time for debris to reach the RCS is estimated by the time it takes to turn over the liquid in the IRWST one time. While some amount of mixing may occur in the IRWST, assuming that no mixing occurs and that all the fluid in the initial IRWST volume must pass through the system before debris arrives, gives a reasonable estimate of the debris arrival time to the RCS, because:

1. Debris and fluid must accumulate on the heavy floor to a certain level before debris is introduced to the retaining baskets.

2. As the debris falls into the retaining baskets, it is only drawn through the basket screens by the suction of the ECCS pumps.

3. The distance from the retaining baskets to the sump screens is 12 to 20 feet and there is little mechanism for mixing in this region.

The minimum liquid volume of the IRWST is 500,342 gal. The maximum ECCS flow rate, assuming all pumps and trains are operating, is 17,200 gpm. The shortest sump turn-over time is then

$$t = \frac{500{,}342\ \text{gal}}{17{,}200\ \text{gal}/\text{min}} = 29\ \text{min}$$

At the minimum assumed flow rate, it will take longer for debris to reach the core. The minimum assured ECCS flow rate is 442.3 lbm/s. At the maximum RHR exit temperature of 150 ºF, the ECCS fluid density will be 61 lbm/ft^3. The minimum assumed volumetric flow rate is then ~3250 gpm. At this flow rate, the sump turn-over time is then

$$t = \frac{500{,}342\ \text{gal}}{3250\ \text{gal}/\text{min}} = 154\ \text{min}$$

The actual sump turn-over time will be longer, for a number of reasons.

1. The ECCS flow rate is dependent on the available NPSH. At the minimum IRWST level, the NPSH is at a minimum, which would produce a flow rates from the ECCS pumps that is less than the maximum used above.

2. The ECCS flow rate is also dependent on the RCS and containment pressure. The maximum flow rate is achieved for low pressures. Following a LOCA, the containment pressure is well above atmospheric pressure for the 24 hours after the event. Consequently, the ECCS flow rate will be less than the maximum used above.

3. The IRWST liquid volume used is based on the minimum allowed level. It is expected that the volume will be controlled to a higher level.

4. The time that it takes fluid and debris to transport from the sump screen to the RCS is neglected.

Therefore, if no mixing in the IRWST is assumed, debris generated following a LOCA will not reach the RCS or core until between 29 and 154 minutes following break opening. While the above calculation is conservative, additional conservatism is applied by assuming that the earliest time that debris can reach the core is half of this time, or 15 minutes. This reduction in time accounts for unknowns (including mixing) in the transport process. Further, this time will only be used to determine the core boiloff rate following a cold leg break with cold side injection. An earlier time will produce a higher boiloff rate and a higher flow rate through the core. Together with the conservative assumptions listed in Section F.3.1, assuming that debris reaches the core no earlier than 15 minutes is reasonably conservative.

F.3.3 Core Void Fraction

The available driving head for each break location during cold side injection is dependent on the manometric balance between fluid in the RV downcomer and fluid in the core. The core voiding is conservatively minimized for each break location during this injection period. By reducing the core void fraction, more liquid resides in the core, which minimizes the head difference between the downcomer and core region. Consequently, the available driving head is minimized.

Estimates for core voiding for a 15x15 fuel assembly based on a core power of 1.02 times 2772 MWt using FOAM2 [4] are first presented:

P/P_0	Pressure, psia	Core Collapsed Liquid Level, ft	Core Void Fraction (12.0 – level)/12.0
0.02	25	4.304	0.64
0.01	14.7	5.626	0.53
0.001	14.7	9.746	0.19

The P/P_0 values above correspond to approximately 2500, 27000, and 2.40×10^7 sec, respectively, for 1.2 * 1971 ANS DH with B&W heavy actinides. These times are approximately 36 minutes, 7.5 hours, and 277 days, respectively. These calculations assumed a core inlet power shape to minimize the liquid volume in the core. Sensitivity studies using the Wilson/Shaw bubble rise model investigated the effect of the power shape on the core void fraction at a core pressure of 13 psia and a P/P0 of 0.012. The following results were obtained:

Peak Power	Core Void Fraction
18 kW/ft, 1.7 axial (9.75 ft), Outlet Peak	0.59
18 kW/ft, 1.7 axial (2.25 ft) Inlet Peak	0.72
15.9 kW/ft 1.5axial (3.25 ft) Somewhat Normal Peak	0.67

The variation in the core void fraction with P/P_0 of 0.012 (~ 4 hr) for the above results is approximately 20 percent. Therefore, for these calculations, the core void fractions at 36 minutes and 7.5 hours will be reduced by at least 20 percent to ensure conservative results associated with a core exit power peak. The time associated with a P/P_0 of 0.001 is approximately 277 days. Therefore, a 20 percent void fraction at 30 days is conservative. These void fractions are conservative considering that the U.S. EPR core power is 4612 MWt, which would increase the void fraction over the values reported here.

To summarize, the following core void fractions will be used in this analysis of cold leg breaks with cold side injection with linear interpolation between points. The void fraction for times before 36 minutes will be set to the value at 36 minutes. While these same void fractions could be used for hot leg breaks with cold side injection, core voiding in the core for this scenario is conservatively neglected as described in Assumption #6.

Time after LOCA	Core Void Fraction
36 minutes	0.5
7.5 hours	0.3
30 days	0.2

F.3.4 Flow Rates

The pressure drop varies as a function of flow rate through the debris bed. Darcy's Law suggests a linear relationship between pressure drop through a porous medium and the flow rate.

$$Q = \frac{\kappa \cdot A \cdot \Delta P}{\mu \cdot L}$$

Where Q = volumetric flow rate (ft^3/s)

κ = permeability (ft^2)

A = area (ft^2)

μ = dynamic viscosity ($lbf\text{-}s/in^2$)

L = length of porous bed (ft)

ΔP = differential pressure drop across bed (psid)

Similarly, Darcy's equation (also known as the Darcy-Weisbach equation) suggests a flow squared relationship between the pressure drop and the flow rate for flow through or around an obstruction in the flow field.

$$\Delta P = \frac{k}{A^2} \cdot \frac{\omega^2}{288 \cdot \rho \cdot g_c} \qquad \text{[Equation F-1]}$$

where ΔP = differential pressure (psid)

k = form-loss coefficient,

A = area upon which the form-loss coefficient is based (ft^2),

ω = flow rate (lbm/s),

ρ = density (lbm/ft^3), and

g_c = gravitational constant (32.2 lbm-ft/lbf-s^2).

In either case, the pressure drop will decrease as flow decreases. Therefore, the maximum pressure drop through a debris bed will be obtained when the flow rate is maximized. The following sub-sections determine the maximum flow rates for testing each break location during the two ECCS injection phases. A summary is provided in Section F.3.4.5.

F.3.4.1 *Cold Leg Break with Cold Side Injection*

As described in Section F.2.1, debris will be introduced to the core inlet. The net ECCS flow rate to the core is the core boiloff rate. By the time debris reaches the core, the RCS has refilled to the break elevation and quenched all of the metal in contact with liquid. Further, the control rods have been inserted and the ECCS liquid that is injected contains sufficient boron to maintain the reactor in a shutdown condition. Therefore, the only source of energy that needs to be removed from the system is the core decay heat.

For this analysis, 120 percent of the 1971 ANS standard decay heat with actinides is used. The decay heat power with respect to the initial core power is shown at certain time points in Table F.3-1. The total core power is calculated considering a steady-state core power of 4612 MWt, which includes measurement uncertainty.

The ECCS flow required to remove the decay heat energy can be determined by

$$\omega_{boiloff} = \frac{Q_{DH}}{\Delta h}$$

where $\omega_{boiloff}$ = core boiloff rate, lbm/s

Q_{DH} = core power due to decay heat, BTU/s and

Δh = enthalpy rise in the core, BTU/lbm.

At this point in the transient, the liquid entering the bottom of the core is subcooled. In the process of removing the decay heat, the liquid boils such that it is essentially saturated steam at the core exit. Neglecting core inlet subcooling, the enthalpy rise in the core is represented by the latent heat of vaporization, or h_{fg}. With subcooling, the enthalpy change increases,

which would decrease the core boiloff rate. Therefore, using h_{fg} is conservative. The above equation then becomes

$$\omega_{boiloff} = \frac{Q_{DH}}{h_{fg}} \qquad \text{[Equation F-2]}$$

h_{fg} is determined using the core exit pressure, which is based on the containment pressure plus an increase for flow losses through the loops.

$$h_{fg} = f(P_{core}) \Rightarrow P_{core} = P_{cont} + \Delta P_{loops}$$

As pressure increases h_{fg} decreases, which will produce a larger boiloff rate. Using the maximum containment pressure after the LOCA will ensure that a bounding boiloff rate is calculated (see Assumption #10). This value is 67 psia. At this pressure, h_{fg} is 910 BTU/lbm. The decay heat generated is calculated by

$$Q_{DH} = \text{SS Core Power} \cdot \frac{P}{P_0} \cdot 947.817 \frac{\text{BTU/s}}{\text{MWt}}$$

Where:

SS Core Power = 4612 MWt

P_{core} = 67 psia

Hfg = 910 BTU/lbm

The boiloff rate with time calculated using Equation F-2 is shown in Table F.3-1

Table F.3-1 Minimum Flow Required for DHR with Time

Time After Rx Trip			Q_{DH}		$\omega_{boiloff}$
(hrs)	(min)	P/P_o	(MWt)	(BTU/s)	(lbm/s)
0.25	15	0.02606	120.19	113917	125.2
0.5	30	0.02210	101.93	96606	106.2
0.67	40	0.02024	93035	88476	97.2
1	60	0.01766	81.45	77198	84.8
2	120	0.01425	65.72	62291	68.5
10	600	0.00909	41.92	39735	43.7
24	1433	0.00704	32.47	30774	33.82
720	43200	0.00238	10.98	10404	11.43

The maximum flow through the core for a cold leg break is then the maximum boiloff rate, or 125.2 lbm/s. The core for the U.S. EPR plant design has 241 fuel assemblies. The flow rate through each FA is then

$$w = \frac{125.2}{241\,\mathrm{FA}} = 0.52\,\mathrm{lbm/s/FA}$$

At room temperature (temperature at which the tests are run), the flow rate is 3.8 gpm/FA.

F.3.4.2 *Hot Leg Break Flow with Cold Side Injection*

As described in Section F.2.1, debris will be introduced to the core inlet. All of the ECCS will pass through the core to reach the break. The maximum flow through the core is then the maximum ECCS flow rate, or 17,200 gpm. The core for the U.S. EPR plant design has 241 fuel assemblies. The flow rate through each FA is then

$$w = \frac{17{,}200\,\mathrm{gpm}}{241\,\mathrm{FA}} = 71.4\,\mathrm{gpm/FA}$$

F.3.4.3 *Cold Leg Break with Simultaneous Injection*

Within one hour after the LOCA, the operators will take action to initiate hot leg injection (HLI) for boric acid precipitation control. The HLI flow rate is 1997 gpm per hot leg, which is based on the IRWST at Technical Specification maximum temperature with the RCS at 14.7 psia. Following a cold leg break, the HLI will condense core steam and flow back into the reactor vessel upper plenum and to the top of the core. Further, the HLI induces a reverse flow in the downcomer such that the ECCS injected into the cold legs flows directly to the break (see Section F.2.2). Consequently, debris is only introduced to the core exit.

In the U.S. EPR design, the two pairs of hot legs are next to each other such that the hot legs in Loop 1 and Loop 2 straddle 270^{o} and the hot legs in Loop 3 and Loop 4 straddle 90^{o}. For this arrangement, the HLI flow may not spread to cover the entire top of the core. Furthermore, it is expected that hot side injected ECCS water will penetrate into the core in front of the injecting hot legs [2]. Further, core boiling will continue following the LOCA such that there will be steam upflow in the higher power fuel assemblies. Consequently, the HLI flows into the lower power periphery assemblies near the hot legs. Since head loss increases

with flow rate, minimizing the number of fuel assemblies that receive HLI will maximize the head loss due to debris. As described in Section F.2.2, it is estimated that between 15 and 20 percent of the fuel assemblies per HLI location have flow into the top from the upper plenum at the start of HLI.

Fifteen percent of 241 fuel assemblies is ~36 assemblies. Twenty percent of 241 fuel assemblies is ~48 assemblies. For two ECCS train injection (assuming one train of pumped SI fails with another train unavailable due to maintenance), the number of fuel assemblies receiving flow is between 72 and 96. For four ECCS train injection, the number of fuel assemblies receiving flow is between 144 and 192.

For a minimum of two ECCS train injection, the total HLI flow is (2*1997 gpm =) 3994 gpm. The total flow per FA just considering the HLI flow is then between (3994 gpm / 72 FA =) 55 gpm/FA and (3994 gpm / 96 FA =) 42 gpm/FA. However, the condensation of the core steam production and subsequent liquid recirculation will increase this flow rate. Using a method for estimating the flow rate in the downflow bundles at mixing efficiencies of between 50 and 60 percent, the flow rates through these bundles ranges from 480 to 580 kg/s (1058 to 1279 lbm/s), which is approximately 5.0 to 8.1 kg/s per assembly.

For four ECCS train injection, the total HLI flow is (4*1997 gpm =) 7988 gpm. The total flow per FA just considering the HLI flow is then between (7988 gpm / 144 FA =) 55 gpm/FA and (7998 gpm / 192 FA =) 42 gpm/FA. However, the condensation of the core steam production and subsequent liquid recirculation will increase this flow rate. Using a method for estimating the flow rate in the downflow bundles at a mixing efficiency of 40 percent, the flow rate through these bundles is approximately 800 kg/s, which is approximately 4.2 to 5.6 kg/s per assembly.

These calculations, demonstrate that the HLI ranges from 4.2 to 8.1 kg/s per assembly. At a liquid density of 59.1 lbm/ft^3 (see Assumption #2), the volumetric flow rate ranges from

$$w = \frac{4.2\,{}^{kg}/_{s} \cdot 2.2046\,{}^{lbm}/_{kg} \cdot 7.481\,{}^{gal}/_{ft^3} \cdot 60\,{}^{s}/_{min}}{59.1\,{}^{lbm}/_{ft^3}} = 70.3\,\text{gpm/FA}$$

to

$$w = \frac{8.1\,{}^{kg}/_{s} \cdot 2.2046\,{}^{lbm}/_{kg} \cdot 7.481\,{}^{gal}/_{ft^3} \cdot 60\,{}^{s}/_{min}}{59.1\,{}^{lbm}/_{ft^3}} = 135.6\ \text{gpm/FA}$$

F.3.4.4 *Hot Leg Break with Simultaneous Injection*

Within one hour after the LOCA, the operators will take action to initiate hot leg injection (HLI) for boric acid precipitation control. The HLI flow rate is 1997 gpm per hot leg. Following a hot leg break, the LHSI from the intact hot leg(s) will mix with steam and flow into the core as described in Section F.2.2. The flow in the broken loop will exit the break before reaching the core. Therefore, the net LHSI flow to the top of the core will be less than that for the cold leg break described in Section F.3.4.3, where all of the HLI will reach the top of the core. The flow rate to the top of the core is therefore bounded by the cold leg break scenario with simultaneous injection.

The ECCS injected to the cold legs can enter the core in the usual core flow direction. The flow rate to the core inlet will then be the sum of the cold-side ECCS injection flow and any HLI flow that reaches the RV lower plenum through the heavy reflector region or guide tubes. However, since some of the HLI flow will enter the lower power fuel assemblies on the periphery of the core and then cross-flow to the higher power assemblies before reaching the RV lower plenum, the flow rate at the core inlet will be bounded by the maximum ECCS flow to the core inlet following a hot leg break with cold side injection (see Section F.3.4.2). That is, since an increased core inlet flow rate increases the measured pressure drop across a debris bed, this scenario is bounded by a hot leg break with cold side injection.

F.3.4.5 *Summary*

The pressure drop varies as a function of flow rate through the debris bed. Darcy's Law and Darcy's equation both suggest that the pressure drop increases as the flow rate increases. Therefore, the maximum pressure drop through a debris bed will be obtained when the flow rate is maximized. Maximum flow rates following a cold leg break and a hot leg break for both cold side and simultaneous injection are summarized on Table F.3-2. These flow rates are targeted during the testing to simulate the various ECCS injection configurations.

Table F.3-2 Maximum Core Flow Rates

Injection Configuration	Flow Rate/FA, gpm	Comments
Cold Leg Break, cold side injection	3.8	Delivered to core inlet. Decreases with time can be simulated if desired
Hot Leg Break, cold side injection	71.4	Delivered to core inlet
Cold Leg Break, simultaneous injection	70 – 136	Delivered to top of FA
Hot Leg Break, simultaneous injection	Bounded by other breaks	Flow to top of FA bounded by CL break with simultaneous injection Flow to core inlet bounded by HL break with cold side injection

F.3.5 Available Driving Head

The available driving head for each ECCS injection configuration defines the acceptance criteria for each test. That is, if the pressure drop through the debris bed exceeds the available driving head, then it is assumed that the core will begin to uncover and heat up (also see Assumption #1). As described in Section F.2, the available driving head is dependent on the break location and ECCS configuration.

F.3.5.1 *Cold Leg Break with Cold Side Injection*

Following a cold leg break with ECCS injection into the cold legs only, core flow is possible only if the manometric balance between the downcomer and the core is sufficient to overcome the flow losses in the downcomer (DC), RV LP, core, and loops at the core boiloff rate.

$$\Delta P_{avail} = \Delta P_{dz} - \Delta P_{flow} \qquad \text{[Equation F-3]}$$

The manometric balance between the downcomer and the bottom of the core is defined as

$$\Delta P_{dz} = \Delta P_{DC} - \Delta P_{core} \qquad \text{[Equation F-4]}$$

where ΔP_{DC} is elevation head due to liquid in the DC, and ΔP_{core} is the elevation head due to liquid in the core. To minimize the driving head, the lowest elevation in the cold leg will be used, which corresponds to the bottom of the pipe in the horizontal run. In this case, the

downcomer coolant level is at least at the bottom of the cold leg pipe.[1] So, the elevation head in the downcomer can be calculated by

$$\Delta P_{DC} = (Z_{DC} - Z_{core\text{-}in})\, \rho_{DC} / 144 \quad \text{(psi)}$$

where Z_{DC} = Elevation of the bottom of the cold leg pipe, ft

$Z_{core\text{-}in}$ = Elevation of bottom of core, ft

ρ_{DC} = downcomer liquid density, lbm/ft^3

The distance from the centerline of the cold leg to the top of the active fuel is 85.04 in. The inside diameter of the cold leg is 30.71 in. The length of active fuel is 165.35 in. The density of the liquid in the downcomer and core is ~59.1 lbm/ft^3 based on the sump conditions (see Assumption #2). It is possible that all of the energy in the thick metal of the RV may not have been removed by this point in the transient which can lead to boiling in the downcomer. A void fraction of 20 percent is used to account for this possibility (see Assumption #11). The elevation head in the downcomer is then

$$\Delta P_{DC} = \frac{(1-0.2)(85.04 - 30.71/2 + 165.35)/12 * (59.1)}{144} = 6.43 \text{ psi}$$

The downcomer elevation head will remain essentially constant through to the end of the evaluation at 30 days. The coolant temperature may decrease, which will increase the density and the driving head. Further, the boiling in the downcomer will continue to decrease and eventually cease, which will further increase the available driving head. However, these increases will be conservatively neglected.

The liquid level in the core and the flow losses through the loops will change with time. However, cold side injection occurs only for a short period of time after the break opens. Within one hour after the LOCA, the operators will take action to initiate hot leg injection (HLI) for boric acid precipitation control. Therefore, the available driving head for this break and ECCS configuration need only be calculated for a limited time. The following approach will be used to determine the resistance to the downcomer driving head at 15 minutes (the time that

[1] Note that this calculation neglects the additional DC height that is needed to push liquid out of the break. In reality, the DC liquid level will be higher by ~0.5 feet or more due to the liquid weir height.

debris might first arrive in the core, Section F.3.2), 30 minutes, and 60 minutes (time of HLI initiation).

In the process of removing the decay heat, the liquid boils such that it is essentially saturated steam at the core exit (see Assumption #1). The core elevation head at bottom of the core due to the liquid column is calculated by

$$\Delta P_{core} = (1 - \alpha)(Z_{core\text{-}out} - Z_{core\text{-}in})\, \rho_{core} / 144 \quad (psi) \qquad \text{[Equation F-5]}$$

where $Z_{core\text{-}out}$ = Elevation of the top of the core, ft

$Z_{core\text{-}in}$ = Elevation of bottom of core, ft

α = Core void fraction

ρ_{core} = Core liquid density, lbm/ft^3

The core average void fraction with time was calculated in Section F.3.3. Before 36 minutes, the core void fraction is 0.5. The density of pure liquid in the core is 59.1 lbm/ft^3 based on the sump conditions (see Assumption #9). However, as core boiling continues, boron may concentrate in the core, which will increase the fluid density. The boron concentration in the core at 15, 30, and 60 minutes is shown on Table F.3-3. These results reflect a core mixing volume of 542 ft^3. The increase in fluid density in the core as a consequence of boric acid concentration can be calculated using Equation 1.6 from [5].

$$\rho_s = \rho_{W,S}\left(1 + 5.72\text{Cx}10^{-6}\right)$$

where $\rho_{W,S}$ is the pure water density at the temperature of the solution, or 59.1 lbm/ft^3. The resulting core densities are shown on Table F.3-3.

Table F.3-3 Core Boron for Cold Leg Breaks with Cold Side Injection

	15 min	30 min	60 min
Boron Concentration, ppm	10,000	15,500	25,000
ρ_{core}, lbm/ft^3	62.5	64.3	67.6

Using this information and Equation F-5, ΔP_{core} is calculated at 15 and 30 minutes. The results are:

$$\Delta P_{core}\big|_{15\,min} = \frac{(1-0.5)(165.35/12)(62.5)}{144} = 2.99\,psi$$

$$\Delta P_{core}\big|_{30\,min} = \frac{(1-0.5)(165.35/12)(64.3)}{144} = 3.08\,psi$$

Similarly, at 60 minutes, the core void fraction is approximately 0.49 (based on linear interpolation from the data in Section F.3.3). The pressure drop in the core at 60 minutes using the same conditions as above is then:

$$\Delta P_{core}\big|_{60\,min} = \frac{(1-0.49)(165.35/12)(67.6)}{144} = 3.30\,psi$$

The elevation head must overcome the flow losses through the downcomer, lower plenum, core, and loops before adequate flow will enter the core to remove the decay heat. The pressure drop (in psi) due to the flow can be calculated using Darcy's formula (Equation F-1).

$$\Delta P_{flow} = \frac{k}{A^2} \cdot \frac{\omega^2}{288 \cdot \rho_g \cdot g_c}$$

In the downcomer, lower plenum, and core the k/A^2 is quite small (typically <0.1). Further, the liquid density is fairly large (~59 lbm/ft^3, see above). Therefore, the flow losses in these regions will be negligible and are therefore ignored.

$\Delta P_{flow\text{-}DC} = \Delta P_{flow\text{-}LP} = \Delta P_{flow\text{-}core} \sim 0$ psi

The steam exiting the core will traverse the loops to the break. To support the available driving head for this scenario, the flow losses for breaks in the cold leg pump suction (CLPS) and cold leg pump discharge (CLPD) were determined. Since all four loops are open and available for steam venting (see Assumption #8), the losses for a CLPS break and a CLPD break will be similar. Therefore, only one of them needs to be calculated. For this calculation, the CLPD break will be considered.

The losses through the loops are a combination of two parallel flow paths. The flow network is shown in Figure F.3-1. The two parallel flow paths are the three intact loops and the broken loop.

Figure F.3-1 Flow Loss Network for a CLPD Break

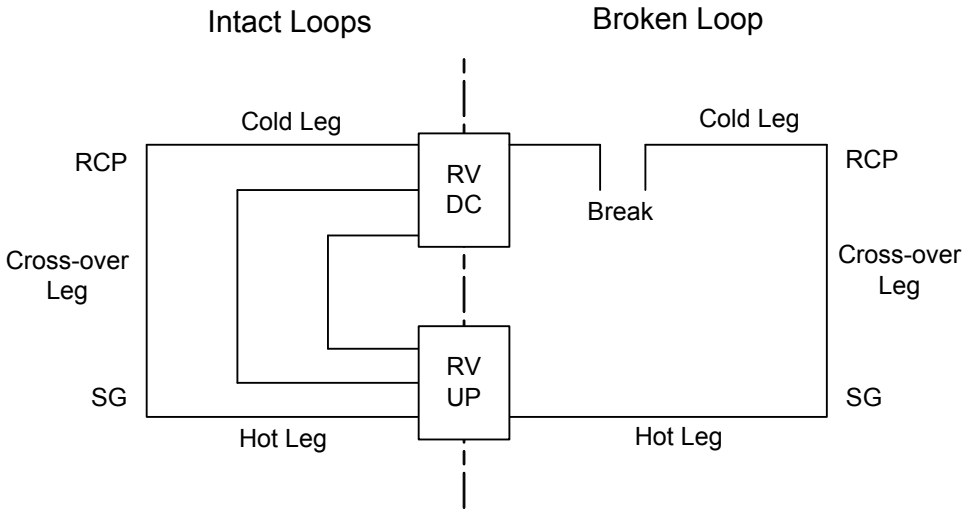

Within each path, the losses area a summation of the losses due to form (including RCP locked rotor in the broken loop), friction, and condensation on the ECCS injection.

$$\left.\frac{k}{A^2}\right|_{loops} = \left.\frac{k}{A^2}\right|_{form} + \left.\frac{k}{A^2}\right|_{friction} + \left.\frac{k}{A^2}\right|_{cond} + \left.\frac{k}{A^2}\right|_{break}$$

Each loop includes form losses from the RV upper plenum, through the hot leg and steam generator to the CL pump discharge. The equivalent k/A^2 due to form for the loops was determined using the large break LOCA model. The flow through the broken loop pump will cause it to overspeed and may lock the rotor. Therefore, the broken loop form-loss coefficient is further adjusted by adding in an RC pump locked rotor configuration.

The losses due to friction and condensation are a function of the core boiloff rate, which are a function of the core exit pressure, which is a function of the loop losses. This relationship requires an iterative solution. The process is as follows:

1. Assume a core exit pressure;

2. Calculate a core boil-off rate at this pressure (i.e. steam flow rate through the loops);

3. Calculate the friction and condensation losses based on this flow rate;

4. Calculate the loop pressure drop using the Darcy equation based on this flow rate;

5. Add the loop pressure drop to the containment pressure to obtain a new core exit pressure;

6. Compare the new core exit pressure with the value assumed in Step 1. If the pressures are the same, the solution is converged. If they are not, use the pressure calculated in Step 5 and repeat the calculation.

Between fifteen and thirty minutes following the LOCA, the containment pressure ranges from 25 psia on the low side (see Assumption #7) to 58 psia on the high side. There are competing effects associated with the pressure. In the core boiloff calculation, the latent heat of vaporization increases with decreasing pressure, which results in a lower core boiloff rate and lower loop losses (see Equation F-2 and Equation F-1). However, as pressure decreases, the steam density decreases, which increases the loop pressure drop (see Equation F-1). To ensure that a conservative result is obtained, calculations will be performed at both of these containment pressures.

Friction in the hot and cold legs and larger volumes will be negligible. However, the SG tubes have a small hydraulic diameter such that friction must be considered. The friction losses can be calculated by

$$k_{friction} = \frac{f \cdot \ell}{d} \qquad \text{[Equation F-6]}$$

where f = friction factor for the SG tubes

ℓ = tube length, and

d = hydraulic diameter of the SG tubes.

The diagrams in Appendix A of Crane Technical Paper No. 410 [6] were used to determine the appropriate friction factor as a function of Reynolds number. The viscosity in the Reynolds number was determined considering superheated steam at the containment pressure and the secondary side liquid temperature (see Assumption #7). These conditions produce a higher viscosity than considering a lower secondary side temperature or saturated steam conditions. The area of the unplugged steam generator was used to maximize the friction losses. Finally, the flow rate through the loops is dependent on the core boiloff rate. Since all four loops are open, each loop will have one fourth of the boiloff rate.

As the steam traverses the loop to the break, it will encounter the ECCS injection into the cold leg. Condensation will occur, which will produce a local pressure drop. Darcy's equation can be used to estimate the equivalent losses associated with a given ΔP. The Darcy equation is

$$\Delta P_{cond} = \frac{k}{A^2} \cdot \frac{\omega^2}{288 \cdot \rho \cdot g_c}$$

Rearranging,

$$\left.\frac{k}{A^2}\right|_{cond} = \frac{\Delta P_{cond} \cdot 288 \cdot \rho \cdot g_c}{\omega^2}$$

The form-loss associated with the steam condensation is a function of core boiloff rate and steam density in the loops. As discussed above, the steam density is determined from the containment pressure and secondary side liquid temperature. The flow rate through each loop is approximated as one fourth of the core boiloff rate. The boiloff rate is dependent on the time following the LOCA. Therefore, the losses due to condensation will be calculated based on the flow rate at the appropriate time. That same density will be used here. A condensation penalty of 0.5 psid will be assumed (see Assumption #12).

Finally, the pressure drop through the break was estimated used an abrupt expansion with a form-loss coefficient of 1.0.

The above information was used to determine the total losses through each loop considering the parallel flow path scenario. The pressure drop (ΔP_{flow}) for three times (15, 30, and 60

minutes) and two containment pressures (min and max) were calculated. The limiting results are summarized on Table F.3-4.

The available pressure drops at 15, 30, and 60 minutes are summarized on Table F.3-4. The minimum available driving head for a cold leg break with cold side injection is 1.33 psi.

Table F.3-4 Available Driving Head for Cold Leg Breaks with Cold Side Injection

	15 min	30 min	60 min
ΔP_{DC}	6.43	6.43	6.43
ΔP_{core}	2.99	3.08	3.30
ΔP_{flow}	2.11	1.63	1.19
ΔP_{avail}	**1.33**	**1.72**	**1.94**

F.3.5.2 *Hot Leg Break with Cold Side Injection*

Following a hot leg break with ECCS injection into the cold legs only, the ECCS must pass through the core to reach the break. The driving force is the manometric balance between the liquid in the downcomer and core. Should a debris bed begin to build up in the core, the liquid level will begin to build in the cold legs and SG. As the level begins to rise in the SG tubes, the elevation head to drive the flow through the core increases as well. The driving head reaches its peak at the shortest SG tube spillover elevation.

In the process of removing the decay heat, the ECCS liquid boils such that it is essentially saturated steam at the core exit. There will be a core average void fraction for a hot leg break if a blockage at the core inlet occurs. For this calculation, core voiding will be neglected and the liquid level will be assumed to be at the bottom of the hot leg (i.e., the break location, see Assumption #6). This assumption will maximize the liquid head in the core for core decay heat removal flow rates.

Using these assumptions, the available driving head at the core inlet can be calculated using Equation F-3.

$$\Delta P_{avail\_HLB\_cold} = \Delta P_{dz} - \Delta P_{flow}$$

The manometric balance between the downcomer and the bottom of the core is calculated by Equation F-4.

$$\Delta P_{dz} = \Delta P_{DC} - \Delta P_{core}$$

In equation form, the delta pressures are

$$\Delta P_{DC} = (Z_{SO} - Z_{core\text{-}in})\ \rho_{DC} / 144 \ \text{(psi)}$$

$$\Delta P_{core} = (Z_{Brk} - Z_{core\text{-}in})\ \rho_{core} / 144 \ \text{(psi)}$$

where Z_{SO} = SG spillover elevation, ft

$Z_{core\text{-}in}$ = Elevation of bottom of core, ft

Z_{brk} = Elevation of break, ft

ρ_{DC} = downcomer liquid density, lbm/ft^3

ρ_{core} = core liquid density, lbm/ft^3.

The distance from the centerline of the cold leg to the top of the active fuel is 85.04 in. The inside diameter of the cold leg is 30.71 in. The length of active fuel is 165.35 in. The density of the liquid in the core is 59.1 lbm/ft^3 based on the sump conditions (see Assumption #9).

The elevation head in the core is then

$$\Delta P_{Core} = \frac{(85.04 - 30.71/2 + 165.35)/12 * (59.1)}{144} = 8.04 \text{ psi}$$

To calculate the elevation head in the downcomer, the SG spillover elevation with respect to the cold leg centerline needs to be calculated. This distance was determined to be 11.37 ft. The elevation head in the downcomer and cold legs is then

$$\Delta P_{DC} = \frac{((85.04 + 165.35)/12 + 11.37 + 32.8) * (59.1)}{144} = 26.7 \text{ psi}$$

The available elevation head for a hot leg break is then

ΔP_{dz} = 26.7 – 8.04 = 18.7 psi

This elevation head must overcome the flow losses through the downcomer, lower plenum, core, and hot legs. In the downcomer, lower plenum, core, and hot leg the k/A^2 is quite small (typically <0.1). Further, the liquid density is fairly large (~60 lbm/ft^3, see below). Therefore, the flow losses in these regions will be negligible and are therefore ignored.

$$\Delta P_{flow\text{-}DC} = \Delta P_{flow\text{-}LP} = \Delta P_{flow\text{-}core} \sim 0 \text{ psi}$$

The allowed pressure drop due to debris buildup at the core inlet is then the difference between the driving head and the flow losses, or simply the available driving head as calculated above.

$$\Delta P_{avail\_HLB\_cold} = 18.7 - 0 = 18.7 \text{ psi}$$

F.3.5.3 *Cold Leg Break with Simultaneous Injection*

Within one hour after the LOCA, the operators will take action to initiate hot leg injection (HLI) for boric acid precipitation control. Following a cold leg break, the HLI will condense core steam and flow back into the reactor vessel upper plenum and to the top of the core introducing debris at the core exit. Debris that is introduced via the HLI will likely be captured at the uppermost spacer grid, which is at approximately the location of the top of active fuel. If sufficient debris accumulates to retard flow, the liquid level above the debris bed will begin to build, which increases the driving head. If the blockage is substantial enough, flow will either (1) be diverted through the heavy reflector region and flow to the core inlet or (2) the liquid level will begin to build into the upper plenum and hot leg. If flow is diverted to the heavy reflector region, debris build up may occur at the core inlet. Testing for cold and hot leg breaks with cold side injection will bound this situation. If liquid begins to build into the hot legs, the maximum driving head will be achieved at the shortest SG tube spillover elevation. The available driving head would then be the elevation difference between the top of the active fuel and the spillover elevation.

$$\Delta P_{avail\_CLB\_simultaneous} = \frac{(85.04/12 + 11.37 + 32.8) * (59.1)}{144} = 21.0 \text{ psi}$$

F.3.5.4 *Hot Leg Break with Simultaneous Injection*

Within one hour after the LOCA, the operators will take action to initiate hot leg injection (HLI) for boric acid precipitation control. Following a hot leg break, the HLI will condense core steam and flow back into the reactor vessel upper plenum and to the top of the core introducing debris at the core exit. The debris build-up will follow the same pattern described for the cold leg break with simultaneous injection in Section F.3.5.3. If sufficient debris accumulates to retard flow, the liquid level above the debris bed will begin to build, which increases the driving head. The available driving head is the elevation difference between the top of the core and the bottom of the hot leg. If debris builds up to increase the level to this point, then flow to the top of the core will likely cease. However, the MHSI injected to the cold legs would provide sufficient flow for core cooling such that the scenario of a hot leg break with flow to the top of the core during HLI need not be addressed.

The MHSI injected to the cold legs can enter the core in the usual core flow direction. The driving force is the manometric balance between the liquid in the downcomer and core. Should a debris bed begin to build up at the core inlet, the liquid level will begin to build in the cold legs and SG. As the level begins to rise in the SG tubes, the elevation head to drive the flow through the core increases as well. The driving head reaches its peak when the shortest SG tube has been filled. Once the ECCS flow reaches this elevation, no increase in water level to the higher tubes is achieved. This is the same situation described for the hot leg break with cold side injection in Section F.3.5.2. Consequently, the available driving head at the core inlet will be the same, 18.7 psi.

F.3.5.5 *Summary*

The available driving head for each ECCS injection configuration defines the acceptance criteria for each test. That is, if the pressure drop through the debris bed exceeds the available driving head, then it is assumed that the core will begin to uncover and heat up (also see Assumption #1). This conservatively calculated condition is used as the acceptance criterion. As described in Section F.2, the available driving head is dependent on the break location and ECCS configuration. Each combination was analyzed above. The results are summarized on Table F.3-5. These acceptance criteria are used during the testing to assess success.

Table F.3-5 Available Driving Head

Injection Configuration	Available Driving Head, psi	Comments
Cold Leg Break, cold side injection	>1.33	At core inlet.
Hot Leg Break, cold side injection	>18.7	At core inlet.
Cold Leg Break, simultaneous injection	>21.0	At top of FA
Hot Leg Break, simultaneous injection	Bounded by other breaks	dP at top of core not required per discussion in Section F.3.5.4. dP at core inlet bounded by HL break with cold side injection

F.3.6 Quantity of Debris

The quantity of debris generated following a LOCA was investigated for a number of break locations. The results are presented in Appendix C and summarized on Table F.3-6. The amount of debris that is generated on a per fuel assembly basis, considering 241 fuel assemblies, is also shown on Table F.3-6. A test was performed to determine the amount of fiber that passes through the retaining baskets and strainers and might reach the RCS and core. The results of this test showed that 34.4 percent of the fiber passes through the sump strainer over a 30 day period (Appendix E). Therefore, 34.5 percent fiber bypass will be used. All particulate (including Microtherm) is assumed to pass through the sump screen and reach the core. The amount of debris reaching the RCS considering these bypass fractions is also shown on Table F.3-6.

It should be noted that the debris quantities listed on Table F.3-6 and calculated in the following sub-sections represent the total amount of debris that will reach the RCS and core over a 30 day period. For testing, it is assumed that this quantity of debris reaches the core instantaneously (see Assumption #13). This conservatism was used to provide bounding results.

Table F.3-6 Summary of Maximum Debris Generated from All Break Locations

Debris Description	Total Amount Generated	Total Amount per FA assuming 100% Bypass of Baskets & Strainers	Total Amount per FA assuming 34.5% Bypass of Baskets & Strainers
Fiber (Nukon + latent debris + miscellaneous)	53.4 lbm	0.22 lbm	0.076 lbm (34.5% bypasss)
Particulates (qualified coatings + unqualified coatings + latent debris + miscellaneous)	1547.5 lbm	6.42 lbm	6.42 lbm (100% bypass)
Microtherm	12 lbm	0.05 lbm	0.05 lbm (100 % bypass)

F.3.6.1 *Hot Leg Break with Cold Side Injection*

As described in Section F.2.1, debris will be introduced to the core inlet. All of the ECCS will pass through the core to reach the break. Assuming that the debris is homogenously mixed in the ECCS fluid and that it is near neutrally buoyant (see Assumption #4), all debris that passes through the sump screens will be assumed to reach the core following a hot leg break. Therefore, the limits identified in the last column of Table F.3-6 are targeted for fuel assembly testing for this break and ECCS scenario.

F.3.6.2 *Cold Leg Break with Cold Side Injection*

The debris that reaches the RCS lower plenum and core inlet should be much lower than the debris that reaches the core for a hot leg break with cold side injection. As described in Section F.2.1, the ECCS flow that reaches the core is only that necessary to make up for core boil-off. This boil-off rate is a function of time after trip as a result of the LOCA, the core exit pressure, and the amount of subcooling at the core inlet. As time progresses, the decay heat decreases such that the core boil-off rate decreases. Any ECCS flow over and above the boil-off rate is returned to the containment via the break. Once in the IRWST, the debris may settle or be refiltered through the baskets or sump screens before it can return to the RCS.

In order for the debris to transport through the RCS, it must be fairly well mixed in the ECCS fluid and be near neutrally buoyant (see Assumption #4). Therefore, it is assumed that the debris is homogeneously mixed with the ECCS fluid such that the fraction of debris that reaches the RV lower plenum is proportional to the fraction of ECCS flow that reaches the RV lower plenum.

If no failures occur in the ECCS system, the total ECCS flow to the RCS may be as high as 17,200 gpm. At the maximum flow rates, the earliest time that debris will reach the RCS was assumed to be 15 minutes after the LOCA (Section F.3.2). At this time, the core boil-off rate is 125.2 lbm/s (Table F.3-1), or approximately 950 gpm assuming a core density of 59.1 lbm/ft^3. The amount of debris reaching the RV lower plenum is then estimated to be (950 / 17200) ~ 6%.

The minimum ECCS flow that reaches the RCS is 442.3 lbm/s, or approximately 3250 gpm. At the minimum flow rates, the time that debris reaches the core will be approximately 154 minutes (Section F.3.2). Using the core boiloff rate at 120 minutes produces a conservative estimate of the debris that reaches the reactor vessel lower plenum and core. At this time, the core boil-off rate is 68.7 lbm/s (Table F.3-1), or approximately 525 gpm assuming a core density of 59.1 lbm/ft^3. The amount of debris reaching the RV lower plenum is then estimated to be (525 / 3250) ~ 16%.

Based on the well mixed assumption and the core to break flow split evaluations, significantly less debris reaches the RV lower plenum for the cold leg break than for the hot leg break. As shown above, it is expected that between 5 and 16 percent of the debris will reach the RV lower plenum. Therefore, testing to 20 percent of the limits identified in the last column of Table F.3-6 is conservative for this break and ECCS scenario.

F.3.6.3 *Cold Leg Break with Simultaneous Injection*

The debris that reaches the RCS upper plenum and core exit should also be much lower than the debris that reaches the core inlet for either a hot or cold leg break. Within one hour after the LOCA, the operators will take action to initiate hot leg injection (HLI) for boric acid precipitation control. The HLI flow rate is 1997 gpm per hot leg. Following a cold leg break,

the HLI will condense core steam and flow back into the reactor vessel upper plenum and to the top of the core.

In order for the debris to transport through the RCS, it must be fairly well mixed in the ECCS fluid and be near neutrally buoyant (see Assumption #4). Therefore, it is assumed that the debris is homogeneously mixed with the ECCS fluid such that the fraction of debris that reaches the RV upper plenum is proportional to the fraction of ECCS flow that reaches the RV upper plenum.

If no failures occur in the ECCS system, the total HLI flow to the RCS may be as high as 4*(1997 gpm) = 7988 gpm. The total ECCS flow is 17,200 gpm. The amount of debris reaching the RV upper plenum is then estimated to be (7988 / 17200) ~ 46%. The minimum ECCS flow that reaches the RCS is 442.3 lbm/s, or approximately 3250 gpm. The HLI flow to the RCS will be to one hot leg, or 1997 gpm. The amount of debris reaching the RV upper plenum is then estimated to be (1997 / 3250) ~ 61%. Based on the well mixed assumption and the core to break flow split evaluations, it is expected that between 46 and 61 percent of the debris will reach the RV upper plenum.

The number of fuel assemblies receiving HLI is dependent on the ECCS flow rate. If no failures occur in the ECCS system, flow to all four legs will occur. As described in Section F.3.4.3 for this situation, between 144 and 192 fuel assemblies will receive flow. For this calculation, an average of 168 fuel assemblies will be used. This number is reasonable, because a lower number of FAs will receive flow close to the time of HLI actuation. As time progresses, more FAs will receive flow. Further, it takes time for debris to transport through the IRWST and reach the RCS. The amount of debris per fuel assembly can then be calculated using the total mass generated, an assumed bypass rate (34.5 percent for fiber and 100% for all other debris as discussed above), and the flow fraction of 46% calculated above.

$$m_{\text{fiber,max ECCS}} = \left(\frac{53.4\,\text{lbm}}{168\,\text{FA}}\right)\cdot(0.345)\cdot(0.46) = 0.050\,\text{lbm/FA}$$

$$m_{\text{particulate,max ECCS}} = \left(\frac{1547.5\,\text{lbm}}{168\,\text{FA}}\right)\cdot(1.0)\cdot(0.46) = 4.2\,\text{lbm/FA}$$

$$m_{microtherm,max\ ECCS} = \left(\frac{12\ lbm}{168\ FA}\right)\cdot(1.0)\cdot(0.46) = 0.033\ lbm/FA$$

If a single failure occurs in the ECCS system (assuming one train of pumped SI fails with another train unavailable due to maintenance), only two hot legs will receive ECCS. As described in Section F.3.4.3 for this situation, between 72 and 96 fuel assemblies will receive flow. For this calculation, an average of 84 fuel assemblies will be used. This number is reasonable, because a lower number of FAs will receive flow close to the time of HLI actuation. As time progresses, more FAs will receive flow. Further, it takes time for debris to transport through the IRWST and reach the RCS. The amount of debris per fuel assembly can then be calculated using the total mass generated, an assumed bypass rate (34.5 percent for fiber and 100% for all other debris as discussed above), and the flow fraction of 61% calculated above.

$$m_{fiber,min\ ECCS} = \left(\frac{53.4\ lbm}{84\ FA}\right)\cdot(0.345)\cdot(0.61) = 0.13\ lbm/FA$$

$$m_{particulate,min\ ECCS} = \left(\frac{1547.5\ lbm}{84\ FA}\right)\cdot(1.0)\cdot(0.61) = 11.2\ lbm/FA$$

$$m_{microtherm,min\ ECCS} = \left(\frac{12\ lbm}{84\ FA}\right)\cdot(1.0)\cdot(0.61) = 0.09\ lbm/FA$$

F.3.6.4 *Hot Leg Break with Simultaneous Injection*

Within one hour after the LOCA, the operators will take action to initiate hot leg injection (HLI) for boric acid precipitation control. The HLI flow rate is 1997 gpm per hot leg. Following a hot leg break, the HLI from the intact hot leg(s) will mix with steam and flow into the core as described in Section F.2.2. The flow in the broken loop will exit the break before reaching the core. Therefore, the net HLI flow to the top of the core will be less than that for the cold leg break with simultaneous injection described in Section F.3.6.3, where all of the HLI will reach the top of the core. Assuming that the debris is homogenously mixed in the ECCS fluid, the amount of debris deposited at the top of the core is bounded by the cold leg break scenario with simultaneous injection.

The ECCS injected to the cold legs can enter the core in the usual core flow direction. The flow rate to the core inlet will then be the sum of the cold-side ECCS flow and any HLI flow that reaches the RV lower plenum through the heavy reflector region or guide tubes. However, since some of the HLI flow will enter the lower power fuel assemblies on the periphery of the core and then cross-flow to the higher power assemblies before reaching the RV lower plenum, the flow rate at the core inlet will be bounded by the maximum ECCS flow to the core inlet following a hot leg break for cold side injection (see Section F.3.6.2). Assuming that the debris is homogenously mixed in the ECCS fluid, the amount of debris deposited at the core inlet is bounded by the hot leg break scenario with cold side injection.

F.3.6.5 *Chemical Precipitates*

Following the LOCA, the chemistry of the fluid in the IRWST and the core could produce chemical precipitates which could affect the pressure drop in a debris bed. The testing used aluminum oxyhyroxide (AlOOH) consistent with the testing summarized in [7].

Studies were performed to identify the specific compounds and quantities of materials that may precipitate within the U.S. EPR reactor containment pool following a LOCA (Appendix D). The precipitates that are predicted include sodium aluminum silicate, calcium phosphate, and aluminum hydroxide. Sodium aluminum silicate is a hazardous material and not available for testing. AlOOH has been shown to be conservative compared to actual precipitates that might

form [8]. Therefore, testing with AlOOH is appropriate. The quantities of precipitate that can be tolerated should be determined by testing.

F.3.6.6 *Summary*

The maximum quantity of debris that would bound each break and injection location as calculated in the preceding sections is summarized on Table F.3-7. These debris masses represent the upper bound on debris expected to reach the core.

Table F.3-7 Summary of Debris For Testing (per FA)

Debris Description	HL Break – Cold Side Injection	CL Break – Cold Side Injection	CL Break – Simultaneous Injection	HL Break – Simultaneous Injection
Fiber (Nukon + latent debris + miscellaneous), lbm (g)	0.076 (34.5)	0.015 (6.8)	0.13 (59)	Bounded by other breaks as described in Section F.3.6.4
Particulates (qualified coatings + unqualified coatings + latent debris + miscellaneous) lbm (g)	6.42 (2914)	1.28 (581)	11.2 (5080)	
Microtherm, lbm (g)	0.05 (22.7)	0.01 (4.5)	0.09 (40.8)	
AlOOH	TBD	TBD	TBD	

F.3.7 Cold Side Injection – Testing and Results

This section will be provided in a subsequent revision to this report.

F.3.8 Simultaneous Injection – Testing and Results

This section will be provided in a subsequent revision to this report.

F.3.9 Conclusion

Determining sufficient long-term core cooling is dependent on the break location and ECCS injection configuration postulated. Maximum flow rates following a cold leg break and a hot leg break and the minimum available driving head for both cold side and simultaneous injection were calculated. To demonstrate success, the pressure drop induced at the maximum volumetric flow rates must be less than the available driving head for all combinations of debris.

The maximum quantities of debris that would bound each break and injection location were identified and represent the upper bound on debris expected to reach the core within 30 days.

A series of experiments using fuel assemblies representative of the U.S. EPR fuel design will be performed to measure the pressure drop response to various quantities of fiber, particulate, and chemical surrogate. The assemblies used in these experiments each have a FUELGUARD™ filter. An evaluation of 1) the effect of the number of spacer grids on the results and 2) the geometric differences between the U.S. EPR fuel assembly and the tested assembly will be performed to demonstrate applicability to the U.S. EPR design. An evaluation of these experiments will be added in a subsequent revision to this report.

F.4 Deposition of Chemical Precipitates and Debris on Fuel Rods (EPRDM)

Analysis and testing provides insight into the chemical processes that may occur in post-accident containment sump fluids (see Appendix D). This work used the results of OLI StreamAnalyzer™ analyses as validated by autoclave testing to identify the chemical reactions expected to generate the most precipitate, through the application of more simplified configurations of individual insulation types, buffer solutions, and post-accident temperatures.

Two specific chemical compounds precipitated during this testing dependent upon the debris mixture and test parameters. The results of the analysis and test program indicated that the predominant chemical precipitates for the U.S. EPR plant design were sodium aluminum silicate ($NaAlSi_3O_8$) and calcium phosphate ($Ca_3(PO_4)_2$). Therefore, the chemical model considers only the release rates of the principal elements guiding the formation of these precipitate compounds: aluminum, calcium and silicon. Some aluminum oxyhydroxide (AlOOH) was formed, but the mass was small compared to sodium aluminum silicate and calcium phosphate and will be considered negligible for this calculation.

In order to perform analyses that will provide information on chemical or physical deposition on fuel rods and the subsequent effect on core cooling once ECCS flow is established, a method based on the OLI StreamAnalyzer™ output and test results is required. This calculation provides a conservative evaluation of (1) deposition thicknesses on fuel rod surfaces due to chemical and debris deposition and (2) to determine the cladding temperatures under the buildup for up to 30 days following a LOCA.

F.4.1 Acceptance Criteria

The following measures were developed to demonstrate compliance with the long-term core cooling acceptance criteria defined in 10 CFR 50.46(b)(5).

F.4.1.1 *Decay Heat Removal*

Cladding temperatures at or below 800°F maintain the cladding within the temperature range where additional corrosion and hydrogen pickup over a 30 day period will not have a significant effect on cladding properties. At temperatures greater than 800°F, rapid nodular corrosion and higher hydrogen pickup rates that can reduce cladding mechanical performance. Long-term autoclave testing has been performed to demonstrate that no significant degradation in cladding mechanical properties would be expected due to a localized hot spot. This testing demonstrated that the increase in oxide thickness and hydrogen loading was limited at temperatures of less than 800°F for periods of 30 days. With limited corrosion and hydrogen pickup, the impact on cladding mechanical performance is not significant. Therefore, no significant degradation in cladding properties would occur due to 30-day exposure at 800°F, and there would not be any adverse impact on core cooling ability. Based on the autoclave

results, maintenance of a maximum cladding temperature below 800°F is one measure to demonstrate long-term core cooling capability.

F.4.1.2 *Deposition Thickness*

If the calculation using plant-specific conditions results in a total deposition thickness (including existing oxide and crud layers) below 50 mils (1270 microns), the acceptance criteria within 10 CFR 50.46(b)(5) is satisfied.

The spacing between fuel rods is calculated by subtracting the fuel rod outside diameter from the fuel rod pitch. The fuel rod OD is 0.374 inches. The fuel rod pitch is 0.496 inches. The spacing between fuel rods is then 0.122 in, or 122 mils. Complete blockage in this space constitutes half the spacing between fuel rods: 61 mils. Restricting the total deposition buildup on any rod (including existing oxide and crud layers) to 50 mils will maintain an open rod-to-rod gap. Therefore, for the purposes of this evaluation, this deposition limit is considered an acceptance criterion.

F.4.2 Analytical Methodology

The U.S. EPR LOCA deposition model (EPRDM) incorporates deposition and heat transfer calculations to determine the effect of fibrous, particulate, and chemical debris that passes through the IRWST baskets and/or sump screens, enters the reactor vessel, and deposits on the fuel rods. Figure F.4-1 shows the basic layout of the U.S. EPR reactor section in the vicinity of a typical LOCA break. Materials upstream of the sump strainer are affected by the liquid in the sump and are subject to degradation effects. Once the ECCS is actuated and suction begins from the IRWST, bypassed materials and ions freed by dissociation of materials upstream of the strainer may reach the reactor vessel. In the presence of boiling in the core, these materials may be deposited on the fuel rods and build up an insulating layer that could inhibit core cooling by (1) degrading the heat transfer from the fuel rod or (2) closing the gap between fuel rods.

The EPRDM assumes that oxide and crud layers exist on fuel surfaces prior to the initiation of a LOCA. The model also conservatively assumes that all deposition occurs through the boiling process if conditions at each node predict that boiling will occur. The rate of deposition is governed by the steaming rate as all impurities are assumed to transport into the deposit

through large pores (i.e., boiling chimneys) in the crud deposit at this rate (see Figure F.4-2). Deposition occurs as impurities transport into the crud deposit with the flow of reactor coolant. Certain resultant chemical species will be forced to precipitate as they cannot exit through the top of the chimney with the newly converted steam phase. Small particulates and already formed precipitates are also assumed to be drawn into and merge with the growing deposit scale.

Since the deposition process is driven by boiling, increasing the boiling rate will increase the deposition thickness. As discussed in Section F.2, the break/ECCS configuration that presents the most boiling is a cold leg break with cold side injection. However, as discussed in Section F.2, the boiling in this break/ECCS configuration will decrease and eventually stop after Hot Leg Injection (HLI) initiates at 60 minutes. While it is not credible that this break/ECCS configuration will continue during the long-term cooling period of 30 days, assuming so provides conservative results and therefore will provide the basis for this analysis.

The EPRDM allows division of the core into specific region and elevation locations with various parameters including relative power, number of rods, initial cladding and crud thicknesses, and average depth within the core. The final deposition thickness is predicted for each core location using the overall core thermal power and the relative power and area for each specific core location. The cladding temperature is then calculated based on heat transfer through the final determined scale and deposition thickness. This is not a finite difference type of analysis; the relative factors of each core location are simply used to modify the numbers that would be calculated if all core locations are assumed equivalent.

The methodology assumes that fluid in the IRWST and reactor is well mixed, and that the dissolution of calcium, aluminum or silicon from one material will not inhibit the dissolution of calcium, aluminum or silicon from another material by the common ion effect. No species-specific interactions that could potentially influence crystal nucleation and growth are considered. As a result, reactions that inhibit precipitation are not replicated, thereby making the calculation results conservative. In reality, the presence of other ions in the solution would reduce the dissolution rate compared to the dissolution rate of a single ion solution. Credit is not taken for local corrosion inhibition effects by any materials present following the accident.

Figure F.4-1 Flows During a LOCA Cold Leg Break

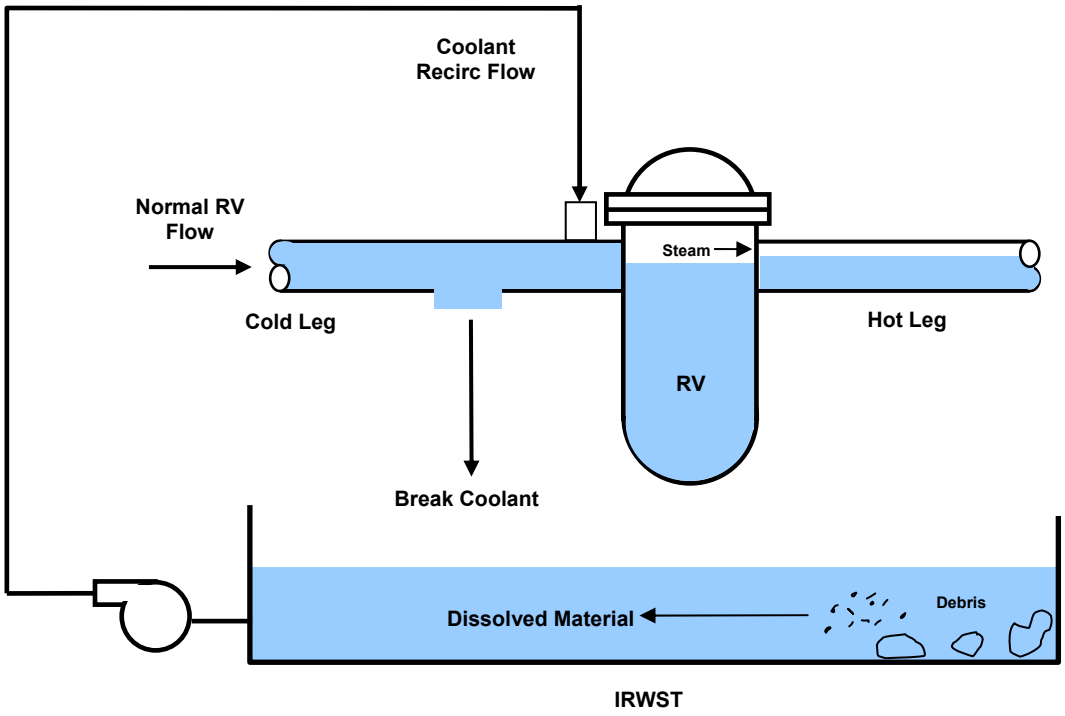

Figure F.4-2 Boiling Chimney Deposition Effect

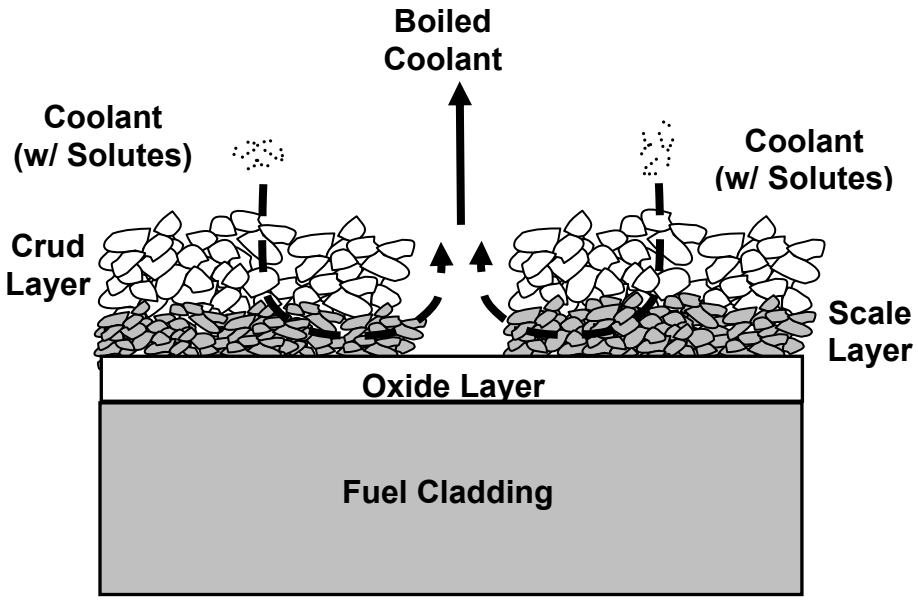

F.4.3 Assumptions

The following assumptions are made in the calculation methodology to provide a conservative estimate of the fuel rod cladding temperature and the amount of scale deposits formed within the core.

1. All large debris is trapped upstream of the reactor vessel and only material dissolved in the coolant or small enough to transport (i.e., small fibers and small particulates) is assumed to form deposits within the core.

2. The types of reactive elements assumed to be within the containment are: Aluminum, Calcium, Silicon, Fiber, and Miscellaneous Particulates.

3. Scale distribution within the core will be proportional to the relative power of each core section.

4. Coolant saturation pressure is the same as pure water. Impurities present in the coolant are non-volatile and will have the effect of raising the boiling point above pure water. Thus, the amount of boiling will be overestimated and provide a conservative estimate of scale thickness.

5. All dissolved elements for the entire coolant volume are deposited only on the fuel rod cladding and are not reduced or redistributed due to possible flow effects within the core. This is conservative since deposits will form on all of the surfaces exposed to coolant, which would distribute the scale deposits over a larger area and reduce the fuel rod cladding scale thickness.

6. All dissolved material will be deposited at a rate equal to a deposition rate multiplied by the dissolved material concentration. When the temperature at the oxide/crud interface is below the boiling point, deposition is assumed to occur via convective deposition rather than by boiling. The non-boiling rate of deposit build-up is proportional to heat flux and is 1/80th of that of boiling deposition at the same heat flux. This ratio is based on empirical data for mixed calcium salts under boiling and non-boiling conditions [9].

7. Fluid exiting the RV is assumed to be pure steam. In an actual accident scenario, this steam would carry some of the dissolved material out of the coolant steam and reduce the amount of deposited material and scale thickness thus giving conservative results.

8. The calculations assume an increase in deposit volume (or indirectly, mass) during precipitation due to the incorporation of species, such as the waters of hydration or boric acid. However, specific compounds are not assumed. This is done by specifying a deposit density that is sufficiently low to bound possible hydrates and adsorbed species (e.g., 12.5 lbm/ft^3 – See Section F.4.4.3).

9. Flow is not modeled explicitly. Instead, a generic heat transfer coefficient of 400 W/m^2-K (70 BTU/ft^2-°F) was assumed for the transfer of heat between bulk coolant within the fuel channels and the surface of the deposits. This is an appropriate heat transfer coefficient for convective flow within natural circulation systems.

10. The methodology assumes that fluid in the IRWST and reactor is well mixed, and that the dissolution of calcium, aluminum or silicon from one material will not inhibit the dissolution of calcium, aluminum or silicon from another material by the common ion effect.

11. The fiber transport rate is set so that all fiber that is not trapped by the sump strainers is deposited into the core within an hour. Early deposition of fiber will increase the overall deposition thickness which reduces the heat transfer away from the rod and increase the oxide/crud layer boundary temperature. The saturation pressure used to predict boiling rate is based on this temperature and will increase. The boiling rate will be overpredicted resulting in conservative output results. Fiber is treated as an element in solution for deposition purposes.

12. Particulates in the coolant are treated as a uniformly distributed solute and deposited in the same manner as dissolved elements.

13. All heat emanates radially from the fuel rods; the top and bottom inactive surfaces of the fuel rods do not add heat to the coolant and do not need to be added to the effective surface area of the rod. This is conservative because the full thermal power of the rod is confined to the active rod surface area resulting in a higher cladding temperature.

14. Fuel rod cladding is treated as a linear wall for heat transfer purposes instead of as a radial heat transfer surface. This gives conservative results because the thermal resistance of a radial wall is less than that of a flat wall.

15. For the purposes of calculating density used to determine pressure at depth, the coolant in the core will be assumed to be vapor which gives a lower density and pressure in the coolant column and will conservatively overpredict boiling and scale deposition.

16. For purposes of calculating pressure at depth used to determine if boiling is occurring, the depth will be calculated to the top of each elevation section which will be conservative by giving the lowest elevation section pressure.

17. Element solubility in the coolant solution is assumed to be zero to provide additional conservatism by allowing the total amount of the elements in solution to be deposited as scale instead of only the amount above the solubility limit.

18. Section F.4 states that some aluminum oxyhydroxide (AlOOH) was formed as a precipitate compound but that the mass was small compared to sodium aluminum silicate and calcium phosphate. Hence, aluminum hydroxide is assumed to be negligible in this calculation.

F.4.4 Inputs

F.4.4.1 *Liquid Volumes*

In the EPRDM calculation, the mass of two liquid volumes are important: (1) the reactor vessel core region liquid volume and (2) the IRWST volume during recirculation. While suction from the IRWST begins immediately upon ECCS initiation, debris is not expected to reach the core before approximately 30 minutes following the LOCA (Section F.3.2). To provide additional conservatism, this time was reduced to 15 minutes, which is consistent with the time assumed in Section F.3.2. At this time, the RCS fluid has been expelled and the accumulators and ECCS have refilled the core. Parameters calculated before the initial coolant recirculation time (< 15 minutes) are not considered to be accurate due to an expected transient time where the coolant is transitioning to a boiling state.

The input in EPRDM for the initial reactor vessel core region liquid volume (or mass) is not directly related to any specific transient analysis. If EPRDM was purely mechanistic, this input would be defined as the steady-state reactor vessel core region volume. However, this volume is actually the reactor vessel core region volume that is reached after the initial blowdown and refill phase of the LOCA when the core has been recovered. This quasi-steady volume is commonly known as the long-term core mixing volume and is consistent with the mixing volume used for boric acid precipitation analyses.

This volume is important for determining the concentration of chemicals in the core. From the boric acid precipitation analysis, the Core Region Mixing Volume is 542 ft^3. This is the volume consistent with the scenario described in Section F.2.1 for a cold leg break with cold side injection.

Since the core is boiling, the mass is calculated based on the density at saturation conditions. The average core liquid density is 60.495 lbm/ft^3. However, since a smaller density leads to smaller liquid mass which increases the chemical concentration the smaller density value of 57 lbm/ft^3 will be used. Therefore:

$$\textit{Reactor Vessel Core Region Liquid Mass} = 542\ ft^3 * 57\ lbm/ft^3$$

$$= 30{,}894\ lbm\ (14{,}013.3\ kg)$$

The input in EPRDM for the initial volume of the IRWST, represents the IRWST volume in the post-accident period when SI is operating in recirculation mode. This volume is important for determining the concentration of chemicals in the IRWST. Choosing a smaller liquid volume will result in a higher chemical concentration and provide a conservative result. The minimum initial IRWST liquid volume (based on the minimum IRWST level for SIS NPSH during LOCA recirculation) is 57,916 ft^3 (433,242 gal). (Note that this value is below the Technical Specification minimum value of 500,342 gallons. The smaller volume increases the concentration of the liquid transported to the core, and is therefore conservative for the deposition model.)

The liquid density is based on the IRWST liquid conditions following the LOCA. A lower liquid density will reduce the mass of liquid for a given liquid volume, which will increase the chemical concentration. Since density is inversely proportional to liquid temperature, a conservatively high IRWST liquid temperature is selected. The highest IRWST liquid temperature following a LOCA was calculated to be 230.0°F. Therefore, a density corresponding to a liquid temperature of 230.0°F will be the maximum density for the IRWST liquid following a LOCA.

Since density is directly proportional to the surface pressure, a conservatively low containment pressure is selected. The lowest density that would correspond to a temperature of 230.0°F would be the liquid density at saturation. The saturation density corresponding at 230.0°F is 59.52 lbm/ft^3. This equates to a mass of:

$$m_{IRWST} = \rho V = 59.52 \frac{lbm}{ft^3} \cdot 57{,}916\, ft^3 = 3{,}447{,}160.3\ lbm\ (1{,}563.607.5\, kg)$$

F.4.4.2 *Fiber and Particulate Quantities and Densities*

The elemental quantities reported in Appendix D were determined based on 257 ft^2 exposed concrete on the heavy floor following a LOCA. Further, all debris is assumed to be available for dissociation immediately following the break. The only elements assumed to be released in the IRWST are aluminum, calcium, and silicon.

The EPRDM provides an optional input to add an additional amount of aluminum to the debris in the IRWST to provide conservatism in the analysis. However, debris composed of

aluminum alloys (as opposed to the aluminum released from debris such as concrete) was not included in the list of predicted debris so this input was not used in the calculation of the maximum deposit thickness.

A total of 0.076 lbm of fiber per fuel assembly (241 fuel assemblies total) may bypass the strainers and reach the RCS. This fiber mass is only 34.4% of the total fiber debris generated in containment. However, to add conservatism, this calculation assumes that 100% of the fiber debris generated, 53.4 lbm, is able to pass through the screens. This approach is consistent with the approach described in Section F.3.6. The fiber transport rate is set so that all fiber that is not trapped by the sump strainers is deposited into the core within an hour. Since 100% bypass is assumed, this translates to 53.4 lbm of fiber debris. Thus, this rate can be calculated as: 53.4 lbm / 3600 s = 0.015 lbm/s. The as-fabricated density of Nukon fiber is 2.4 lbm/ft^3 [10, Vol. 1, Table 3-2]. However, the material density of fibrous material may be as high as 162 lbm/ft^3. A lower fiber density leads to a higher deposit thickness. A higher deposit thickness leads to a higher surface temperature. Thus, using the smaller, as-fabricated fiber density for Nukon is appropriate for this evaluation.

A total of 100% or 6.4 lbm of generated particulate and 0.05 lbm of generated Microtherm per fuel assembly (241 fuel assemblies total) may bypass the strainers. Microtherm is treated as a particulate [10, Vol. 1, p 3-66]. Summing the total amounts generated for microtherm and particulates gives a total mass of particulates of 1559.5 lbm. Particulates in containment comprise various material types with densities ranging from 94 lbm/ft^3 to 457 lbm/ft^3 [10, Vol.1, Table 3-3]. A value of 100 lbm/ft^3 is selected to represent particulates.

The fiber and particulate densities are used to determine the thickness of the fiber layer and the particulate debris deposit layer. Table F.4-1 shows a summary of these mass and density inputs.

F.4.4.3 *Scale Density*

The densities for the calcium carbonate and calcium hydroxide deposits formed under boiling conditions are approximated based on reported densities for calcium carbonate, magnesium hydroxide, and calcium hydroxide deposits. Densities of 147 to 155 lb/ft^3 (2350 to 2640 kg/m^3) have been reported for calcium carbonate, magnesium hydroxide, and calcium hydroxide

deposits formed under boiling conditions [11, p. 231]. Since calcium, aluminum, and silicon may bond with other RCS chemicals such as phosphate and borate, this number should be reduced significantly to introduce conservatism into the prediction of LOCA scale thickness.

A lower density leads to a thicker deposit thickness, which is conservative for this evaluation, because it results in a higher surface temperature. Measurements on cross-sectioned calcium sulfate scale have shown that the density varies from 12.5 to 106 lbm/ft^3 (200 to 1700 kg/m^3) across the thickness of the deposit [12, Fig. 11]. Using the lowest density in this range, 12.5 lbm/ft^3 (200 kg/m^3), introduces conservatism to the calculation.

F.4.4.4 *Mission Time*

To address the extended time period required in 10 CFR50.46(b)(5), [10, Volume 2, Section 2.0, paragraph 2] states: "For this evaluation of PWR recirculation performance, the staff considers this extended time to be 30 days, and requires cooling by recirculation of coolant using the ECCS sump."

Therefore, this evaluation assumes that the mission time for the ECCS operation is thirty (30) days and that only the quantity of precipitate that is generated up to that point must be calculated for use in head loss and downstream analyses.

F.4.4.5 *IRWST Liquid Temperature*

Use of a higher value for the IRWST liquid temperature increases the boiling and deposition on the fuel rods. Therefore, the fluid temperature as a function of time was taken from the maximum IRWST liquid temperature calculation. The IRWST temperature profile used for this evaluation is provided in Table F.4-2.

F.4.4.6 *Reactor Coolant Temperature*

Reactor coolant temperatures were obtained by increasing the IRWST liquid temperatures by 5°F. This temperature is used to determine the core pressure and the core boiling rate. The RV upper plenum pressure is higher than containment pressure, because the steam must travel through the loops to the break during the cold leg injection period. Increasing the RV coolant temperature by 5°F effectively increases the core region pressure by approximately 5 psi, which bounds the expected pressure drop through the loops (see Section F.3.5.1). The

IRWST temperature profile used for this evaluation to calculate the RV temperature profile is provided in Table F.4-2.

F.4.4.7 *Coolant Flow Balance*

The coolant flows of concern for this analysis are the IRWST recirculation flow and the core reactor vessel steam boiloff rate. As coolant in the reactor boils and condenses into the coolant stream, it is conservatively assumed that all impurities remain in the reactor vessel. In actual operation, some of the impurities would be carried out of the reactor vessel, thus reducing the amount of scale deposited in the reactor vessel. As a consequence of this conservative approach, the pure steam generated in the core condenses in the RCS coolant, returns to the IRWST through the break, and adds to the IRWST coolant volume, which reduces the impurity concentration in the IRWST.

F.4.4.8 *Total Mass of Released Elements Dissolved in the IRWST*

The total amount of released elements dissolved in the IRWST was obtained by analysis. The results from Appendix D, Table D.3-10 used in the EPRDM analysis are summarized in Table F.4-2.

F.4.4.9 *Core Data*

To calculate the amount of chemical precipitation in the core, specific core design parameters must be defined. These input parameters are discussed in this section.

The initial core power is selected to maximize boiling in the core. The value used in this calculation is 4,612 MWt (4,590 MWt + 22 MWt uncertainty). The core decay power fraction defines how the power output of the reactor is reduced over time. The model used is based on a curve-fit to the ANS 1971 standard plus 20 percent and includes actinides.

The fuel is represented by five radial regions: a hot rod, hot assembly, surrounding assemblies, average-core assembly and lower powered, outer assemblies. This is consistent with the LOCA linear heat rate limit analyses. Axially, each radial region is divided into 52 nodes. The relative power for 52 positions along the length of the fuel rods (i.e., axial power shape is consistent with that used in the highest PCT case in the 124 case RLBLOCA analysis (Reference [13, Appendix A].

A nominal fuel rod OD, 0.374 inches, is used in all cases. The total active fuel rod length is 165.354 inches.

Oxidation and crud formation during normal operation are also considered in the analysis. The model assumes a limiting oxide thickness of 35 microns (1.38 mils). This thickness includes the crud layer thickness. Because the crud and oxide thickness reference input is combined with no indication of relative amounts of each, the thermal conductivity used for the oxide/crud layer will be set to the lowest value of thermal conductivity present. A lower value will give less heat transfer and conservatively higher temperature predictions. The thermal conductivity of zirconium oxide (ZrO_2) expected to be present on fuel surfaces at the time of the accident is taken as 1.6 W/m-K [14, p. 435]. The thermal conductivity of the crud layer can be as low as 0.17 W/m-K [15]. This value assumes that the surrounding fluid is saturated steam. If the surrounding fluid is liquid water, as is expected for the accident, the thermal conductivity is higher and ranges between 0.46 BTU/h-ft-ºF (0.80 W/m-k) and 0.50 BTU/h-ft-ºF (0.87 W/m-K). Therefore, use of the saturated steam value is conservative since a lower value will result in less heat transfer and a higher surface temperature. Since this value is lower than the actual oxide layer thermal conductivity, 0.17 W/m-K will be used for the combined oxide-crud layer in this calculation. The oxide and crud thickness at any location in the core is dependent on the temperature achieved during a LOCA, which, in turn, is partly dependent on the time that the fuel rod has been in service and the axial and radial power. These variations result in oxide thicknesses that are less than the maximum value. EPRDM has the capability to model these variations. However, the analyses conservatively set the relative oxide and crud thickness fraction at each core location to 1.0 such that all locations start with the maximum oxide and crud thickness.

F.4.4.10 *Scale Deposit*

The two types of precipitates predicted to form out of solution are calcium phosphate, $Ca_5(PO_4)_2$, and sodium aluminum silicate, $NaAlSi_3O_8$ (Appendix D). Of these, sodium aluminum silicate is more insulating with thermal conductivity values as low as 0.2 W/m-K [16]. Thus, for a bounding calculation, choosing sodium aluminum silicate is appropriate. However, for conservatism, a value of 0.1 W/m-K has been used in this evaluation for the thermal conductivity of any LOCA scale in all cases.

F.4.4.11 *Distance from Hot Leg Inlet to Top of Pellet Stack*

The distance between the hot leg centerline to the top of the pellet stack in the U.S. EPR design is 85.04 inches or 2160 mm. The hot leg inner diameter is 30.71 inches or 780 mm. Subtracting the hot leg radius from this distance gives the distance from the hot leg inlet to the top of the pellet stack as 69.685 inches.

Table F.4-1 Debris Inputs

Debris Material	Density (lb/ft^3)	Mass (lbm)	Mass (kg)	Section
Additional Aluminum Debris	0	0	0.0	F.4.4.2
Bypassed Fiber	2.40	53.4	24.2	F.4.4.2
Bypassed Particulate (includes Microtherm)	100.00	1559.5	707.4	F.4.4.2
Scale Deposit Density	12.5			F.4.4.10

Table F.4-2 Inputs for IRWST Temp and Mass Releases

Time - hr (total)	IRWST Temp. (ºF)	Total Released Al (kg)	Total Released Ca (kg)	Total Released Si (kg)
0.00	122.000	0.00	0.00	0.00
0.25	168.926	0.57	6.78	4.77
0.58	189.334	0.66	6.80	5.95
0.92	202.049	0.76	6.82	5.97
1.25	210.196	0.84	6.84	6.02
1.58	214.915	0.93	6.86	6.05
1.92	218.989	1.03	6.89	6.09
2.25	224.220	1.12	6.91	6.15
4.50	227.974	1.74	7.16	6.58
6.50	220.208	2.29	7.34	6.91
9.50	208.701	3.10	7.57	7.32
13.50	197.296	4.20	7.87	7.80
20.00	186.159	5.96	8.28	8.40
31.50	177.092	6.04	8.97	9.28
37.50	174.462	6.08	9.19	9.64
49.50	170.447	6.14	9.64	10.15
60.00	167.511	6.18	10.04	10.61
80.00	167.511	6.28	10.81	11.48
120.00	167.511	6.36	12.02	11.71
240.00	167.511	6.61	15.69	12.41
360.00	167.511	6.85	19.36	13.13
480.00	167.511	7.10	22.97	13.84
600.00	167.511	7.35	26.75	14.54
720.00	167.511	7.59	30.36	15.25

Table F.4-3 Coolant/Miscellaneous Material Inputs

Parameter	Units	Value	Section
IRWST Coolant Density	lbm/ft^3	59.52	F.4.4.1
Initial IRWST Coolant Volume	ft^3	57,916.0	F.4.4.1
Initial IRWST Coolant Mass	lbm	3,447,160.3	F.4.4.1
Initial IRWST Coolant Mass	kg	1,563,607.5	F.4.4.1
RV Core Region Coolant Density	lbm/ft^3	57.00	F.4.4.1
Initial RV Core Region Coolant Volume	ft^3	542.0	F.4.4.1
Initial RV Core Region Coolant Mass	lbm	30,894.0	F.4.4.1
Initial RV Core Region Coolant Mass	kg	14,013.3	F.4.4.1
Fiber Screen Bypass Rate	lbm/s	0.015	F.4.4.2
Initial Recirculation Time	min	15	F.3.2

Table F.4-4 Reactor Core Parameters

Variable	Value	Units	Section
Reactor Power	4,612	MWt	0
Oxide/Crud Thermal Conductivity	0.17	W/m-K	0
Scale Deposit Thermal Conductivity	0.1	W/m-K	F.4.4.10
Fuel Rod OD	0.374	Inches	0
Fuel Rod Height	165.354	Inches	0
Distance from Hot Leg Inlet to Top of Pellet Stack	69.685	Inches	F.4.4.11
Average Initial Cladding Oxide/Crud Thickness	35	Microns	0
Number of Regions	5	Regions	0
Number of Elevation Sections	52	Elevations	0

F.4.5 Results

The methodology and assumptions for the deposition of chemical precipitates and debris on fuel rods are applied to calculate peak cladding temperatures throughout the core, and the final magnitude of LOCA scale thickness predicted for each analyzed node.

Table F.4-5 through Table F.4-9 show the results of the EPRDM calculation. The final amount of material deposition thickness predicted for each analyzed node post-LOCA is shown in Table F.4-6 through Table F.4-9. The maximum total deposit thickness is 29.99 mils. For each node the acceptance criteria were met throughout the calculation.

The EPRDM calculation with U.S. EPR-specific information calculates a peak cladding temperature of 427.8°F (refer to Table F.4-5 at 1.58 hours). This peak temperature is well below 800°F. All final total deposit thicknesses were calculated to be well below 50 mils (1270 1270 microns).

Therefore, the results of this calculation, applying conservative assumptions, shows that chemical precipitation and deposition will not prevent adequate removal of core decay heat and the long-term core cooling criterion of 10 CFR 50.46(b)(5) is met.

Table F.4-5 EPRDM Output For Each Time Step

Time	Al Conc (ppm)		Ca Conc (ppm)		Si Conc (ppm)		Fiber Conc (ppm)		Particulate Conc (ppm)		Region of Max Scale Thk	Elev. of Max Scale Thk	Max Scale Thk (microns)	Max Fuel Cladding Temp (°F)
Hours	RV	IRWST	RV	IRWST	RV	IRWST	RV	IRWST	RV	IRWST				
0.00	0.00	0.00	0.00	0.00	0.00	0.00	0.00	15.49	0.00	452.39				
0.25	0.00	0.36	0.00	4.34	0.00	3.05	0.00	15.49	0.00	452.39				
0.58	0.39	0.41	4.16	4.19	3.48	3.68	142.20	10.38	432.71	435.83	1	43	54.68	386.0
0.92	0.46	0.47	4.25	4.22	3.72	3.70	167.35	5.11	425.53	421.90	1	43	125.53	407.7
1.25	0.51	0.52	4.28	4.25	3.76	3.74	185.93	0.00	413.97	410.27	1	43	194.35	427.7
1.58	0.56	0.58	4.30	4.28	3.79	3.77	10.48	0.00	403.46	399.84	1	43	218.67	427.8
1.92	0.62	0.64	4.32	4.30	3.82	3.80	0.64	0.00	393.51	389.98	1	43	223.48	422.8
2.25	0.68	0.70	4.34	4.32	3.86	3.84	0.05	0.00	384.48	381.04	1	43	226.89	421.4
4.50	0.97	0.99	4.01	3.98	3.68	3.67	0.00	0.00	333.54	330.55	1	43	246.00	402.1
6.50	1.31	1.33	4.24	4.21	3.98	3.97	0.00	0.00	298.51	295.83	1	43	259.65	381.8
9.50	1.73	1.75	4.21	4.19	4.08	4.06	0.00	0.00	257.48	255.17	1	43	276.29	357.1
13.50	2.29	2.31	4.27	4.24	4.24	4.21	0.00	0.00	216.27	214.33	1	43	294.04	334.9
20.00	3.07	3.09	4.17	4.15	4.24	4.22	0.00	0.00	168.16	166.66	1	43	316.68	314.6
31.50	2.63	2.61	3.96	3.93	4.11	4.08	0.00	0.00	113.23	112.22	1	43	346.20	297.8
37.50	3.24	3.22	4.91	4.87	5.15	5.12	0.00	0.00	93.59	92.75	1	43	359.13	292.3
49.50	2.78	2.75	4.39	4.36	4.62	4.59	0.00	0.00	65.50	64.91	1	43	380.21	283.1
60.00	2.99	2.96	4.87	4.83	5.15	5.11	0.00	0.00	49.00	48.56	1	43	396.00	276.0
80.00	2.45	2.43	4.28	4.25	4.55	4.52	0.00	0.00	29.50	29.23	1	43	419.85	269.1
120.00	1.70	1.69	3.39	3.37	3.15	3.12	0.00	0.00	12.15	12.04	1	43	453.07	258.8
240.00	0.55	0.55	1.92	1.92	1.08	1.08	0.00	0.00	1.44	1.42	1	43	503.28	244.0
360.00	0.79	0.78	2.81	2.80	1.56	1.55	0.00	0.00	0.24	0.24	1	43	553.78	239.4
480.00	0.97	0.97	3.69	3.67	1.94	1.93	0.00	0.00	0.05	0.05	1	43	607.74	237.4
600.00	1.14	1.13	4.69	4.66	2.29	2.28	0.00	0.00	0.01	0.01	1	43	665.43	236.4
720.00	1.30	1.29	5.68	5.64	2.65	2.63	0.00	0.00	0.00	0.00	1	43	726.72	236.1

Table F.4-6 EPRDM Output For Core Elevations 1-13

Elevation	1	2	3	4	5	6	7	8	9	10	11	12	13
Region (Scale Thickness in microns)													
1	48.71	139.31	211.75	260.89	288.79	302.59	310.98	320.14	331.31	341.90	349.10	352.98	356.62
2	46.70	133.58	203.03	250.14	276.90	290.13	298.18	306.96	317.67	327.83	334.72	338.44	341.94
3	34.67	99.16	150.72	185.69	205.55	215.38	221.35	227.86	235.81	243.36	248.47	251.24	253.83
4	31.52	90.14	137.01	168.81	186.86	195.80	201.22	207.15	214.38	221.23	225.89	228.40	230.76
5	16.90	48.35	73.49	90.54	100.23	105.02	107.93	111.11	114.98	118.66	121.16	122.50	123.77
Region (Scale Thickness in mils)													
1	1.92	5.48	8.34	10.27	11.37	11.91	12.24	12.60	13.04	13.46	13.74	13.90	14.04
2	1.84	5.26	7.99	9.85	10.90	11.42	11.74	12.08	12.51	12.91	13.18	13.32	13.46
3	1.36	3.90	5.93	7.31	8.09	8.48	8.71	8.97	9.28	9.58	9.78	9.89	9.99
4	1.24	3.55	5.39	6.65	7.36	7.71	7.92	8.16	8.44	8.71	8.89	8.99	9.08
5	0.67	1.90	2.89	3.56	3.95	4.13	4.25	4.37	4.53	4.67	4.77	4.82	4.87
Region (Total Deposit Thickness in mils)													
1	3.30	6.86	9.71	11.65	12.75	13.29	13.62	13.98	14.42	14.84	15.12	15.27	15.42
2	3.22	6.64	9.37	11.23	12.28	12.80	13.12	13.46	13.88	14.28	14.56	14.70	14.84
3	2.74	5.28	7.31	8.69	9.47	9.86	10.09	10.35	10.66	10.96	11.16	11.27	11.37
4	2.62	4.93	6.77	8.02	8.73	9.09	9.30	9.53	9.82	10.09	10.27	10.37	10.46
5	2.04	3.28	4.27	4.94	5.32	5.51	5.63	5.75	5.90	6.05	6.15	6.20	6.25
Region (Final Fuel Cladding Temp (deg. F))													
1	173.88	177.52	181.48	184.68	186.69	187.73	188.39	189.11	190.01	190.89	191.50	191.83	192.14
2	173.81	177.25	180.95	183.94	185.82	186.79	187.40	188.07	188.91	189.73	190.29	190.60	190.89
3	173.44	175.73	178.08	179.95	181.10	181.70	182.07	182.48	182.99	183.49	183.83	184.02	184.19
4	173.35	175.37	177.41	179.02	180.01	180.53	180.84	181.20	181.64	182.06	182.35	182.51	182.67
5	172.94	173.86	174.73	175.38	175.77	175.97	176.10	176.23	176.40	176.57	176.68	176.74	176.80
Region: Boiling at node at end?													
1	Y	Y	Y	Y	Y	Y	Y	Y	Y	Y	Y	Y	Y
2	Y	Y	Y	Y	Y	Y	Y	Y	Y	Y	Y	Y	Y
3	Y	Y	Y	Y	Y	Y	Y	Y	Y	Y	Y	Y	Y
4	Y	Y	Y	Y	Y	Y	Y	Y	Y	Y	Y	Y	Y
5	Y	Y	Y	Y	Y	Y	Y	Y	Y	Y	Y	Y	Y

Table F.4-7 EPRDM Output For Core Elevations 14-26

Elevation	14	15	16	17	18	19	20	21	22	23	24	25	26
Region (Scale Thickness in microns)													
1	363.53	374.65	387.83	400.10	410.12	419.47	431.02	446.22	463.62	480.11	493.92	506.00	519.28
2	348.56	359.22	371.86	383.63	393.24	402.20	413.28	427.85	444.53	460.35	473.58	485.17	497.90
3	258.74	266.66	276.04	284.78	291.91	298.56	306.79	317.60	329.99	341.73	351.56	360.15	369.61
4	235.22	242.42	250.95	258.89	265.37	271.42	278.90	288.73	299.99	310.66	319.60	327.41	336.01
5	126.16	130.02	134.60	138.86	142.34	145.58	149.59	154.87	160.90	166.63	171.42	175.61	180.22
Region (Scale Thickness in mils)													
1	14.31	14.75	15.27	15.75	16.15	16.51	16.97	17.57	18.25	18.90	19.45	19.92	20.44
2	13.72	14.14	14.64	15.10	15.48	15.83	16.27	16.84	17.50	18.12	18.65	19.10	19.60
3	10.19	10.50	10.87	11.21	11.49	11.75	12.08	12.50	12.99	13.45	13.84	14.18	14.55
4	9.26	9.54	9.88	10.19	10.45	10.69	10.98	11.37	11.81	12.23	12.58	12.89	13.23
5	4.97	5.12	5.30	5.47	5.60	5.73	5.89	6.10	6.33	6.56	6.75	6.91	7.10
Region (Total Deposit Thickness in mils)													
1	15.69	16.13	16.65	17.13	17.52	17.89	18.35	18.95	19.63	20.28	20.82	21.30	21.82
2	15.10	15.52	16.02	16.48	16.86	17.21	17.65	18.22	18.88	19.50	20.02	20.48	20.98
3	11.56	11.88	12.25	12.59	12.87	13.13	13.46	13.88	14.37	14.83	15.22	15.56	15.93
4	10.64	10.92	11.26	11.57	11.83	12.06	12.36	12.75	13.19	13.61	13.96	14.27	14.61
5	6.35	6.50	6.68	6.84	6.98	7.11	7.27	7.48	7.71	7.94	8.13	8.29	8.47
Region (Final Fuel Cladding Temp (deg. F))													
1	192.74	193.73	194.92	196.06	197.02	197.92	199.05	200.59	202.39	204.15	205.65	207.00	208.51
2	191.45	192.37	193.48	194.54	195.42	196.26	197.32	198.74	200.41	202.05	203.44	204.69	206.10
3	184.53	185.09	185.76	186.39	186.92	187.43	188.06	188.91	189.91	190.88	191.71	192.45	193.28
4	182.95	183.43	184.00	184.54	185.00	185.42	185.96	186.69	187.54	188.36	189.07	189.70	190.40
5	176.90	177.08	177.30	177.50	177.67	177.83	178.03	178.29	178.61	178.91	179.16	179.39	179.64
Region: Boiling at node at end?													
1	Y	Y	Y	Y	Y	Y	Y	Y	Y	Y	Y	Y	Y
2	Y	Y	Y	Y	Y	Y	Y	Y	Y	Y	Y	Y	Y
3	Y	Y	Y	Y	Y	Y	Y	Y	Y	Y	Y	Y	Y
4	Y	Y	Y	Y	Y	Y	Y	Y	Y	Y	Y	Y	Y
5	Y	Y	Y	Y	Y	Y	Y	Y	Y	Y	Y	Y	Y

Table F.4-8 EPRDM Output For Core Elevations 27-39

Elevation	27	28	29	30	31	32	33	34	35	36	37	38	39
Region (Scale Thickness in microns)													
1	535.87	554.80	572.88	587.55	598.91	609.89	623.45	639.75	656.44	670.05	679.26	685.73	693.01
2	513.80	531.96	549.29	563.35	574.25	584.77	597.78	613.41	629.41	642.46	651.29	657.49	664.48
3	381.41	394.89	407.75	418.20	426.28	434.10	443.75	455.35	467.23	476.92	483.47	488.08	493.26
4	346.74	358.99	370.69	380.18	387.53	394.63	403.41	413.96	424.75	433.56	439.52	443.71	448.42
5	185.98	192.55	198.82	203.91	207.86	211.67	216.38	222.03	227.82	232.55	235.74	237.99	240.52
Region (Scale Thickness in mils)													
1	21.10	21.84	22.55	23.13	23.58	24.01	24.55	25.19	25.84	26.38	26.74	27.00	27.28
2	20.23	20.94	21.63	22.18	22.61	23.02	23.53	24.15	24.78	25.29	25.64	25.89	26.16
3	15.02	15.55	16.05	16.46	16.78	17.09	17.47	17.93	18.39	18.78	19.03	19.22	19.42
4	13.65	14.13	14.59	14.97	15.26	15.54	15.88	16.30	16.72	17.07	17.30	17.47	17.65
5	7.32	7.58	7.83	8.03	8.18	8.33	8.52	8.74	8.97	9.16	9.28	9.37	9.47
Region (Total Deposit Thickness in mils)													
1	22.48	23.22	23.93	24.51	24.96	25.39	25.92	26.57	27.22	27.76	28.12	28.38	28.66
2	21.61	22.32	23.00	23.56	23.99	24.40	24.91	25.53	26.16	26.67	27.02	27.26	27.54
3	16.39	16.92	17.43	17.84	18.16	18.47	18.85	19.31	19.77	20.15	20.41	20.59	20.80
4	15.03	15.51	15.97	16.35	16.64	16.91	17.26	17.68	18.10	18.45	18.68	18.85	19.03
5	8.70	8.96	9.21	9.41	9.56	9.71	9.90	10.12	10.35	10.53	10.66	10.75	10.85
Region (Final Fuel Cladding Temp (deg. F))													
1	210.44	212.71	214.92	216.77	218.22	219.64	221.44	223.63	225.92	227.83	229.14	230.07	231.13
2	207.89	209.98	212.04	213.75	215.09	216.41	218.07	220.11	222.23	224.00	225.21	226.07	227.05
3	194.34	195.58	196.79	197.79	198.59	199.36	200.33	201.53	202.77	203.80	204.51	205.01	205.58
4	191.30	192.35	193.38	194.23	194.90	195.55	196.38	197.38	198.43	199.31	199.91	200.33	200.81
5	179.96	180.34	180.70	181.00	181.24	181.47	181.76	182.11	182.48	182.78	182.99	183.13	183.30
Region: Boiling at node at end?													
1	Y	Y	Y	Y	Y	Y	Y	Y	Y	Y	Y	Y	Y
2	Y	Y	Y	Y	Y	Y	Y	Y	Y	Y	Y	Y	Y
3	Y	Y	Y	Y	Y	Y	Y	Y	Y	Y	Y	Y	Y
4	Y	Y	Y	Y	Y	Y	Y	Y	Y	Y	Y	Y	Y
5	Y	Y	Y	Y	Y	Y	Y	Y	Y	Y	Y	Y	Y

Table F.4-9 EPRDM Output For Core Elevations 40-52

Elevation	40	41	42	43	44	45	46	47	48	49	50	51	52
Region (Scale Thickness in microns)													
1	703.61	716.07	725.57	726.72	717.27	699.20	675.71	646.08	602.12	531.70	424.79	276.71	96.31
2	674.64	686.59	695.69	696.79	687.74	670.41	647.88	619.48	577.33	509.80	407.30	265.31	92.34
3	500.80	509.68	516.43	517.25	510.53	497.66	480.95	459.86	428.57	378.44	302.35	196.95	68.55
4	455.28	463.34	469.48	470.23	464.12	452.42	437.22	418.05	389.61	344.04	274.87	179.05	62.32
5	244.19	248.52	251.81	252.21	248.94	242.66	234.51	224.23	208.97	184.53	147.43	96.03	33.43
Region (Scale Thickness in mils)													
1	27.70	28.19	28.57	28.61	28.24	27.53	26.60	25.44	23.71	20.93	16.72	10.89	3.79
2	26.56	27.03	27.39	27.43	27.08	26.39	25.51	24.39	22.73	20.07	16.04	10.45	3.64
3	19.72	20.07	20.33	20.36	20.10	19.59	18.93	18.10	16.87	14.90	11.90	7.75	2.70
4	17.92	18.24	18.48	18.51	18.27	17.81	17.21	16.46	15.34	13.54	10.82	7.05	2.45
5	9.61	9.78	9.91	9.93	9.80	9.55	9.23	8.83	8.23	7.26	5.80	3.78	1.32
Region (Total Deposit Thickness in mils)													
1	29.08	29.57	29.94	29.99	29.62	28.91	27.98	26.81	25.08	22.31	18.10	12.27	5.17
2	27.94	28.41	28.77	28.81	28.45	27.77	26.89	25.77	24.11	21.45	17.41	11.82	5.01
3	21.09	21.44	21.71	21.74	21.48	20.97	20.31	19.48	18.25	16.28	13.28	9.13	4.08
4	19.30	19.62	19.86	19.89	19.65	19.19	18.59	17.84	16.72	14.92	12.20	8.43	3.83
5	10.99	11.16	11.29	11.31	11.18	10.93	10.61	10.21	9.61	8.64	7.18	5.16	2.69
Region (Final Fuel Cladding Temp (deg. F))													
1	232.68	234.52	235.95	236.13	234.70	232.03	228.64	224.49	218.63	209.95	198.44	185.80	175.61
2	228.48	230.19	231.51	231.68	230.36	227.88	224.74	220.91	215.48	207.43	196.75	184.99	175.45
3	206.42	207.42	208.19	208.28	207.51	206.07	204.24	201.99	198.81	194.07	187.72	180.59	174.55
4	201.52	202.36	203.01	203.09	202.44	201.22	199.67	197.78	195.09	191.07	185.67	179.58	174.33
5	183.54	183.83	184.06	184.08	183.86	183.44	182.91	182.25	181.31	179.88	177.92	175.60	173.40
Region: Boiling at node at end?													
1	Y	Y	Y	Y	Y	Y	Y	Y	Y	Y	Y	Y	Y
2	Y	Y	Y	Y	Y	Y	Y	Y	Y	Y	Y	Y	Y
3	Y	Y	Y	Y	Y	Y	Y	Y	Y	Y	Y	Y	Y
4	Y	Y	Y	Y	Y	Y	Y	Y	Y	Y	Y	Y	Y
5	Y	Y	Y	Y	Y	Y	Y	Y	Y	Y	Y	Y	Y

F.4.6 Conclusion

The purpose of this analysis was to perform a conservative evaluation of the core chemical effects associated with the long term core cooling capability of the U.S. EPR design. This analysis considers the presence of fibrous, particulate and chemical debris in the recirculating fluid following a postulated design basis LOCA. This evaluation was performed based on conservative assumptions using the EPRDM to evaluate the final deposit thicknesses and peak cladding temperatures expected for a single postulated condition.

The results of this calculation show that the acceptance criteria were met for each location in the core throughout the accident. The EPRDM calculation with U.S. EPR-specific information calculated a peak cladding temperature of 427.8°F (refer to Table F.4-5 at 1.58 hours). From the total deposit thickness results presented in Table F.4-6 through Table F.4-9, the maximum total deposit thickness is 29.99 mils.

Therefore, the results of this calculation show that chemical precipitation and deposition will not prevent adequate removal of core decay heat and the long-term core cooling criterion of 10 CFR 50.46(b)(5) is met.

F.5 Summary and Conclusion

Analyses and testing were performed to evaluate the effect of debris and chemical products on core cooling for the U.S. EPR design when the ECCS is actuated. The objective of the program was to demonstrate sufficient LTCC to comply with the requirements of 10 CFR 50.46 (b)(5), considering debris and chemical products that might be transported to the reactor vessel and core by coolant recirculating from the IRWST. The debris composition includes particulate and fiber debris, as well as post-accident chemical products. This evaluation considered the design of the U.S. EPR plant, the design of the open-lattice fuel, the design and tested performance of the strainer baskets and sump screens, the tested performance of materials inside containment, and the tested performance of fuel assemblies in the presence of debris. Specific areas addressed in this evaluation include:

- Collection of debris on fuel assembly bottom nozzle or intermediate spacer grids,
- Production and deposition of chemical precipitants and debris on the fuel rod cladding.

To address the collection of debris in the fuel assembly bottom nozzle or at the spacer grids, fuel assembly testing will be performed. The purpose of this testing is to quantify the mass of debris that can be deposited at the core entrance or spacer grids and not impede long-term core cooling flows to the core. This report provides the inputs and boundary conditions to support the testing process and to define the success criteria. The results of the testing will be provided in a subsequent revision to this report.

An evaluation of the deposition of chemical precipitates and debris on the fuel rods was performed by applying U.S. EPR-specific design parameters to the U.S. EPR LOCA Deposition Analysis Model (EPRDM). This calculation provides a conservative evaluation of (1) deposition thicknesses on fuel rod surfaces due to chemical and debris deposition and (2) to determine the cladding temperatures under the buildup for up to

30 days following a LOCA. The results of this calculation demonstrate that long-term core cooling is maintained for each location in the core throughout the accident.

F.5.1 References

PLACE APPENDIX A TEXT ABOVE THIS LINE. DO NOT DELETE THIS BOOKMARK.

1. NRC GL 2004-02, "Potential Impact of Debris Blockage on Emergency Recirculation During Design Basis Accidents at Pressurized Water Reactors," September 13, 2004 (ML042360586).

2. AREVA NP Topical Report BAW-10192P-A, Rev. 2, "BWNT LOCA – BWNT Loss-of-Coolant Accident Evaluation Model for Once-Through Steam Generator Plants."

3. AREVA NP Topical Report BAW-10168P-A, Rev. 2, "RSG LOCA – BWNT Loss-of-Coolant Accident Evaluation Model for Recirculating Steam Generator Plants."

4. AREVA NP Topical Report BAW-10155A, "FOAM2 – Computer Program to Calculate Core Swell Level and Mass Flow Rate During Small Break LOCA," October 1987.

5. Palazov, Vesselin V., "Scaling Approach for Turbulent Mixing During Rapid Boron Dilution Transients in Pressurized Water Reactors," Master of Science Thesis from University of Maryland.

6. Crane Technical Paper No. 410, "Flow of Fluids Through Valves, Fittings, and Pipe," 1988.

7. WCAP-16793-NP, Rev. 1, "Evaluation of Long-Term Cooling Considering Particulate, Fibrous and Chemical Debris in the Recirculating Fluid," April 2009.

8. B. B. Banh, K. E. Kasza, and W. J. Shack, "Technical Letter Report on Follow-on Studies in Chemical Effects head-Loss Research; Studies on WCAP Surrogates and Sodium Tetraborate Solutions," Argonne National Laboratory, NRC Contract N6100.

9. A. Helalizadeh, H. Muller-Steinhagen, M. Jamialahmadi, "Crystallization Fouling of Mixed Salts During Convective Heat Transfer and Sub-Cooled Flow Boiling Conditions," 2003 ECI Conference on Heat Exchanger Fouling and Cleaning: Fundamentals and Applications, Paper 6, Santa Fe, New Mexico.

10. NEI 04-07, "Pressurized Water Reactor Sump Performance Evaluation Methodology," Volumes 1 (Methodology) and 2 (Safety Evaluation), December 2004.

11. V.N. Slesarenko, V.G. Dobrzansky, V.V. Slesarenko, "The account of heat exchange features when modelling scale formation at distillation plants," Desalination 152 (2002) 229–236, April 2002.

12. Fahmi Brahim, Wolfgang Augustin, Matthias Bohnet, "Numerical simulation of the fouling process," International Journal of Thermal Sciences 42 (2003) 323-334.

13. AREVA NP Topical Report ANP-10287P, Rev. 1, "U.S. EPR Realistic Large Break Loss of Coolant Accident, January 2010."

14. ASTM STP754-EB, “Zirconium in the Nuclear Industry,” American Society for Testing and Materials, January 1982.

15. Paul Cohen, “Water Coolant Technology of Power Reactors,” Gordon and Breach Science Publishers, New York, NY, p. 25-26, 1969.

16. Hans Muller-Steinhagen, “Heat Exchanger Fouling- Mitigation and Cleaning Technologies,” (Institution of Chemical Engineers, Rugby, UK, 2000) p. 4.